# PROCEEDINGS

OF THE

# 26th Czech-Japan Seminar on Data Analysis and Decision Making



Nový Jičín, Czech Republic, November 5-8, 2026

# Proceedings of the 26th Czech-Japan Seminar on Data Analysis and Decision Making *(CJS 2026)* Nový Jičín, Czech Republic

Masahiro Inuiguchi, Václav Kratochvíl, Yoshifumi Kusunoki,
Karel Mls, Shao-Chin Sung
(editors)

November 5-8, 2026

**Published by:**
ÚTIA - Institute of Information Theory and Automation,
Czech Academy of Sciences
Pod Vodárenskou věží 4, 182 00 Praha 8, Czech Republic

The text hasn't passed the review or lecturer control of the publishing house ÚTIA.
The publication has been issued for the purposes of the CJS 2026 conference.
The publishing house ÚTIA is not responsible for the quality and content of the text.

Printed in Prague — November 2026

**Organized by:**
Institute for Research and Applications of Fuzzy Modeling, University of Ostrava
Faculty of Informatics and Management, University of Hradec Králové
Institute of Information Theory and Automation, Czech Academy of Sciences

**Sponsors:**
Institute for Research and Applications of Fuzzy Modeling, University of Ostrava
Faculty of Informatics and Management, University of Hradec Králové
Institute of Information Theory and Automation, Czech Academy of Sciences

**Credits:**
Editors: Masahiro Inuiguchi, Václav Kratochvíl, Yoshifumi Kusunoki, Karel Mls, Shao-Chin Sung
LaTeXeditor: Václav Kratochvíl
Cover design: Václav Kratochvíl
using LaTeX's 'confproc' package, version 0.8 by V. Verfaille

© M. Inuiguchi, V. Kratochvíl, Y. Kusunoki, K. Mls, SC. Sung (Eds.), 2026
© ÚTIA - Institute of Information Theory and Automations
Czech Academy of Sciences, 2026

**ISBN: 978-80-905688-1-5**

# 26th CZECH-JAPAN SEMINAR ON DATA ANALYSIS AND DECISION MAKING



*Nový Jičín coat of arms*

**Organized by:**
Institute for Research and Applications of Fuzzy Modeling, University of Ostrava
Faculty of Informatics and Management, University of Hradec Králové
Institute of Information Theory and Automation, Czech Academy of Sciences

Nový Jičín

November 5-8, 2026

**Programme and Conference Committee:**
Karel Mls - Chair, *University of Hradec Králové, Czechia*
Masahiro Inuiguchi - Chair, *Osaka University, Japan*

Richard Cimler, *University of Hradec Králové, Czechia*
Ondřej Čepek, *Charles University, Czechia*
Radim Jiroušek, *Czech Academy of Sciences, Czechia*
Václav Kratochvíl, *Czech Academy of Sciences, Czechia*
Yoshifumi Kusunoki, *Osaka Metropolitan University, Japan*
Shinji Mochida, *University of Marketing and Distribution Sciences, Japan*
Vilém Novák, *University of Ostrava, Czechia*
Irina Perfilieva, *University of Ostrava, Czechia*
Shao Chin Sung, *Aoyama Gakuin University, Japan*
Martin Štěpnička, *University of Ostrava, Czechia*
Milan Vlach, *Charles University, Czechia*

**Organizing Committee:**
Jiří Kupka - chair, *University of Ostrava*
Karel Mls, *University of Hradec Králové*
Lenka Štěpničková, *University of Ostrava*

# Foreword

Dear Friends and Colleagues,

It is a great pleasure to welcome you to the 26th Czech-Japan Seminar on Data Analysis and Decision Making, held from November 5 to 8, 2026, in Nový Jičín, Czech Republic. For more than twenty-five years, our seminar has brought together researchers from the Czech Republic, Japan, and other countries, providing an opportunity not only to exchange scientific ideas but also to maintain friendships and establish new collaborations.

The organization of this year's seminar has been somewhat unusual. We originally planned to meet in Hradec Králové in September, but the number of registrations from Japan was lower than expected. We therefore decided to postpone the meeting until November and combine it with another traditional Czech scientific event, VŘSR. Since the two seminars share many participants and research interests, this seemed a natural solution.

This year's VŘSR is organized by our friends from the University of Ostrava, particularly Jiří Kupka and Lenka Štěpničková. We would like to express our sincere gratitude to both of them. When we approached them with the idea of joining the two meetings—and effectively placing much of the additional organizational burden on their shoulders—they agreed without hesitation. We truly appreciate their willingness and support.

The proceedings contain ten contributions covering a broad range of topics in data analysis, decision making, and artificial intelligence. They include theoretical studies on belief functions, entropy, knowledge representation, and rough sets, as well as contributions on machine learning, multi-agent systems, optimization, and cooperative games. One paper also explores the emerging role of generative AI in mathematical research. We hope that this diversity of topics will stimulate interesting discussions and encourage new collaborations.

Over the years, we have learned that some of the most valuable outcomes of our meetings arise not only during scientific presentations, but also in informal conversations over coffee, dinner, or simply while spending time together. We are therefore pleased that joining the two seminars has brought together a larger and somewhat different audience. We hope that this combination will bring fresh ideas and new energy to our meetings, while preserving the friendly and informal atmosphere that has always been an important part of the Czech-Japan Seminar.

We would like to thank all the authors for their contributions, as well as everyone who has helped to organize this year's meeting. Above all, we thank the participants for keeping the Czech-Japan Seminar tradition alive.

We wish you an enjoyable seminar, inspiring discussions, and many pleasant encounters with old and new friends. We look forward to meeting you again at future Czech-Japan Seminars.

Enjoy the seminar – and enjoy your reading!

In Prague, November 3, 2026

*Václav Kratochvíl, Karel Mls*

# List of Content

1 *Ondřej Čepek*
Recent developments in list-based knowledge representation languages

3 *Toshitaka Hayashi*
Meta learning for classification of datasets

11 *Masahiro Inuiguchi, Shigeaki Innan*
A Detailed Decision Analysis via Interval Priority Estimation from a Crisp Pairwise Comparison Matrix

14 *Radim Jiroušek, Václav Kratochvíl, Milan Daniel*
On Computation of Harmanec–Klir Entropy for Belief Functions

26 *Václav Kratochvíl, Milan Daniel, Radim Jiroušek*
On Geometry of Optimal Faces in Belief-Function Polytopes

36 *Yoshifumi Kusunoki*
Comparison of Parametric Models for Dominance-based Rough Set Approach

47 *Jakub Mestek*
Shared Verifiable Local Policies for Multi-Agent Pathfinding

50 *Karel Mls*
Human-AI Collaboration in Mathematical Problem Solving: Capabilities, Limitations, and a Worked Example

65 *Shao-Chin Sung*
On the Convergence of Relaxed Core Dynamics in Simple Symmetric Fractional Hedonic Games

77 *Xiaowen Zhao, Shao-Chin Sung*
Minimizing the Number of Late Jobs with Non-Renewable Resources

91 **List of Authors**

# Recent developments in list-based knowledge representation languages

**Ondřej Čepek**

Department of Theoretical Computer Science and Mathematical Logic
Faculty of Mathematics and Physics, Charles University
ondrej.cepek@mff.cuni.cz

**Abstract**

Boolean functions naturally appear and are extensively used in several areas of mathematics and computer science. There are many different ways in which a Boolean function may be represented. Common representations include truth table (TT), list of models (MODS), various types of Boolean formulas (including CNFs and DNFs), various types of binary decision diagrams (BDDs, FBDDs, OBDDs), and negational normal forms (NNF, DNNF, d-DNNF). The task of transforming one of the representations of a given function f into another representation of f (e.g. transforming a DNF representation into an OBDD or a DNNF into a CNF) is called knowledge compilation. A comprehensive review paper on knowledge compilation (3) appeared more than 20 years ago, and introduced a so called Knowledge Compilation Map (KCM). KCM systematically investigates different representation languages with respect to (1) their relative succinctness, (2) the complexity of common transformations, and (3) the complexity of common queries. Since the publication of (3) many interesting knowledge representation languages were added to KCM. These languages include pseudo-boolean and cardinality constraints (1), nearest neighbour representations (4), and switch-list representations (2).

In my talk I will concentrate on the continuation of research started in (4) and (2) which both deal with list-based knowledge representation languages. These languages represent Boolean functions by an ordered list of Boolean or real-valued vectors, where the dimension of the vectors is in all cases the number of variables of the represented Boolean function.

The Nearest Neighbor (NN) representation introduced in (4) uses real-valued vectors to represent a Boolean function. The real vectors are called prototypes and are of two kinds, positive prototypes and negative prototypes. The value $f(x)$ of a Boolean function $f$ at a Boolean vector $x$ is then determined as follows: the Euclidian distance of $x$ to all prototypes is computed, and if the closest prototype to $x$ is positive then $f(x) = 1$, while if the closest prototype to $x$ is negative then $f(x) = 0$. Ties are not allowed, i.e. there must not exist a vector $x$ such that there are both positive and negative prototypes at the minimum distance from $x$. In other words, if such a vector $x$ exists, then the set of prototypes does not form a valid representation.

A special case of the NN language called Boolean Nearest Neighbor (BNN) language was extensively studied in (5). In BNN also the prototypes are required to be Boolean vectors, which is of course a special case of real-valued ones, and hence any BNN representation is also an NN representation. The main goal of (5) was to include the BNN language in the Knowledge Compilation Map by establishing the complexity of standard queries and transformations and determining the succinctness relations of BNN to other standard knowledge representation languages. In my talk I will concentrate on the results from (5) and on the complexity of determining that a given set of prototypes is a valid BNN representation.

The language of Switch List Representations (SLR) was included in the Knowledge Compilation Map in (2). This language uses a natural lexicographic ordering of Boolean vectors (which is an ordering of natural numbers if the Boolean vectors are understood as binary numbers). Similar languages can be defined for different orders. An interesting ordering to consider is the following: first order the vectors by their norm (i.e. the number of ones) and then order lexicographically the vectors with the same norm. Surprisingly, the language defined in this way is strictly more succinct than the SLR language while maintaining the support for most standard queries and transformations. I will report some results concerning this new language (a joint work with Barbora Dohnalová) in the second part of my talk.

**Keywords:** knowledge representation languages; knowledge compilation; tractable queries and transformations

# References

[1] Daniel Le Berre, Pierre Marquis, Stefan Mengel, and Romain Wallon. Pseudo-Boolean Constraints from a Knowledge Representation Perspective. In *IJCAI*, pages 1891–1897. ijcai.org, 2018.

[2] Ondřej Čepek and Miloš Chromý. Properties of Switch-List Representations of Boolean Functions. *J. Artif. Intell. Res.*, 69:501–529, 2020.

[3] Adnan Darwiche and Pierre Marquis. A knowledge compilation map. *J. Artif. Intell. Res.*, 17:229–264, 2002.

[4] Péter Hajnal, Zhihao Liu, and György Turán. Nearest neighbor representations of Boolean functions. *Inf. Comput.*, 285(Part B):104879, 2022.

[5] Ondřej Čepek and Jelena Glišić. Boolean Nearest Neighbor Language in the Knowledge Compilation Map. In *Proceedings of KR 2025 - 22nd International Conference on Principles of Knowledge Representation and Reasoning*, pages 240–249, 2025.

# Meta Learning for classification of datasets

**Toshitaka Hayashi**

Faculty of Science
University of Hradec Kralove
toshitaka.hayashi@uhk.cz

**Abstract**

Traditional supervised classification has been considered for single samples. However, this does not apply to all problems. For example, classification of sleep regularity requires multiple sleep records, while classification of families must consider all family members. Roughly speaking, these problems are classifications of datasets containing multiple samples. To tackle this issue, this paper discusses a meta-classification approach. The idea is to train arbitrary ML models from datasets. These models act as representations of datasets. Subsequently, meta-classification of ML models is considered. The results correspond to dataset classification. The experiment is conducted on an X-ray image dataset, where an image is treated as a dataset containing patches.

**Keywords:** Meta Learning; Multi-instance Learning; One-class classification

## 1 Introduction

Traditional supervised classification has been considered for single samples. However, several cases require classifying multiple samples together. For example, classification of sleep regularity requires multiple sleep records.

Multi-instance learning (MIL)[9] is a learning paradigm where the input is a bag containing multiple instances. Annotation is made at the bag-level, while instances are unlabeled. There are several examples of MIL:

- An image is a bag of pixels/patches.
- Signal is a bag of sliding windows.
- Sleep schedule is a bag of sleep records.
- A human is a bag of cells.

MIL is categorized into 1) bag-level classification and 2) instance-level classification[9]. Bag-level classification classifies labeled bags, while instance-level classification classifies unlabeled instances within labeled bags. This paper focuses on bag-level classification, which is essentially dataset classification.

This paper considers meta-learning. The idea is to treat bags as datasets and train ML models. Subsequently, meta-classification is considered to classify ML models. In particular, this paper applies the one-class classification (OCC) algorithm to represent datasets because OCC can learn from unlabeled samples. Moreover, there is a meta-classification algorithm for OCC models[2].

The contribution of this paper is as follows:

- This paper applies meta-classification of OCC [2] to classify datasets.
- The experiment treats X-ray images as datasets containing patches.

The paper is organized as follows. Section 2 mentions related work, and Section 3 presents the methodology. Sections 4 and 5 show experimental results and discussions, respectively. Finally, Section 6 is the conclusion.

# 2 Related work

This paper is related to multi-instance learning, one-class classification, and meta-learning.

## 2.1 One-class classification

The definition of one-class classification (OCC) is as follows [2].

- **OCC** is a supervised classification problem where the training dataset contains solely one class. The goal is to classify inputs into one or other classes.
- **OCC algorithms** refer to the algorithms that "can" train the model from a single class. One can apply OCC algorithm to multiple classes by approximating that all training samples belong to a single class.
- **OCC models** refer to the models trained by OCC algorithms. The models might learn multiple classes if OCC algorithms are applied to such dataset.

OCC algorithm trains the model from a dataset.

$$OCC\ algorithm : dataset \rightarrow model \tag{1}$$

The OCC model contains a classification function, a score function, and a threshold value $\lambda$. The classification function classifies samples:

$$OCC : X \rightarrow class \tag{2}$$

where classes include one known class and the remaining unknown classes.

The general classification function is written as:

$$OCC(X) = \begin{cases} One(score(X) \geq \lambda) \\ Other(score(X) < \lambda) \end{cases}, \tag{3}$$

where the score function computes the normality of the sample:

$$score : X \rightarrow normality \tag{4}$$

Normality refers to the likelihood of belonging to one class. Note that the above equation is abstract, and every OCC algorithm has a different hypothesis for normality. The existing score functions are roughly categorized into boundary, distance, probability, fake, and subtask-based approaches [1].

This study applies the OCC algorithm for representing datasets as OCC models.OCC algorithm is a reasonable direction to represent datasets because it can train models from unlabeled samples.

### 2.2 Meta learning

Meta-learning[8] is a technique to learn learning process. Meta-learning was originally developed for accelarating hyperparameter tuning process. Vanschoren [8] categorized meta-learning into three types: 1) predicting the hyperparameters from the model errors and tasks, 2) predicting the model error from hyperparameters and tasks, and 3) using prior models as the starting point of new models.

Meta-classification is classification of ML models. Hayashi et al.[2] proposed meta-classification of OCC models as shown in Figure 1. The main idea is to represent OCC models as normality rankings, and consider the nearest neighbors for the rankings. Spearman correlation [7] was applied to compute the similarity between rankings.

## 3 Meta learning for classification of datasets

This section describes the problem setting and solution.

### 3.1 Problem setting

This study considers the following datasets. The training set contains N datasets.

$$Training\ set = [dataset_1, dataset_2, ..., dataset_N] \tag{5}$$

Dataset size can vary if non-zero and non-negative. On the other hand, samples in datasets should have the same size. The training stage creates the model from the training set and class.

$$Training : Training\ set,\ class \rightarrow model \tag{6}$$

The model should classify the dataset into classes.

$$model : dataset \rightarrow class \tag{7}$$

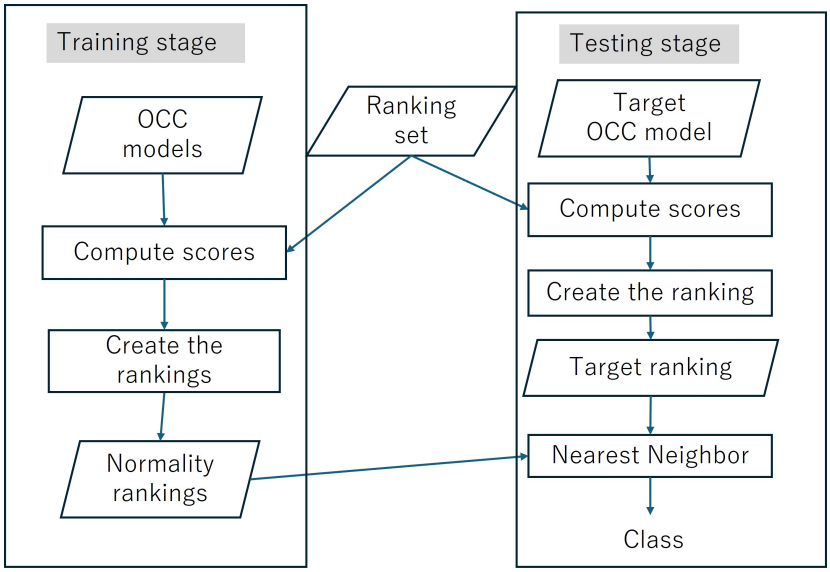



Figure 1: Meta-classification of OCC models[2]

### 3.2 The proposed solution

Figure 2 shows the meta-classification framework. The idea is to train OCC models on each dataset and then apply meta-classification to the OCC models. The result corresponds to the classification of datasets.




Figure 2: The processing image

In order to apply meta-classification of OCC models, an independent set, namely a ranking set, is required.

$$Ranking\ set = [X_1, X_2, ..., X_n] \tag{8}$$

where n is the number of samples. Moreover, samples have the same shape as in the datasets. Moreover, the ranking set should not contain duplicate samples to avoid ties.

Algorithm 1 shows the training stage, where the input is datasets and classes, and the output is rankings, which represent OCC models for the training sets. In particular, a single dataset is represented as a single OCC model. Moreover, hyperparameters include the choice of ranking set and OCC algorithm.

**Algorithm 1** Training stage

**Input:** training_set, classes
**Output:** rankings_train
models=[]
**For** dataset in training_set:
  model = an arbitrary OCC algorithm.
  model.fit(dataset)
  models.append(model)
//The following lines correspond to the training stage of Figure 1.
scores=[]
**For** model in models:
  score = model.score(ranking_set) //Compute scores.
  scores.append(score)
scores=np.array(scores)
rankings_train=scores.argsort(axis=1).argsort(axis=1) //Create normality rankings.

Algorithm 2 show testing stage, where input is single dataset and output is class.

**Algorithm 2** Testing stage

**Input:** dataset
**Output:** class
**Information from training stage:** Ranking_set, OCC algorithm, rankings_train, classes
model = an arbitrary OCC algorithm.
model.fit(dataset)
score = model.score(ranking_set) //Compute scores.
rank_test=score.argsort().argsort() //Create normality ranking.
similarity = []
**For** ranking in rankings_train:
  similarity.append( rank_correlation (rank_test, ranking))
similarity = np.array(similarity)
class = classes[similarity.argmax()]

# 4 Experiment

## 4.1 Dataset

The experiment uses X-ray image dataset for pneumonia classification [3, 5]. Table 1 shows class balance. The dataset contains unresized images; the height range is 127–2713, while the width range is 384-2916.

Table 1: Class balance of X-ray pneumonia dataset

| | normal | pneumonia | total |
|---|---|---|---|
| train | 1341 | 3875 | 5216 |
| test | 234 | 390 | 624 |
| total | 1575 | 4265 | 5840 |

This paper applies Isolation Forest(IF)[4] for representing images because IF is the fastest OCC algorithm in sklearn [6]. IF computes normal/abnormal scores using random trees, where processing time does not scale with dataset size. All experiments used random state = 0.

Figure 3 shows how to represent an image as an IF model. A single image contains multiple patches of size $d \times d$; These patches are reshaped into $d \times d$ dimensional vectors. IF model learns these vectors. The experiment creates 5840 IF models in total. Finally, meta-classification is considered for IF models. Note that pixel values were divided by 255.




Figure 3: How to represent an image as an IF model

## 4.2 Result

Table 2 reports classification results. The experiments were conducted on 1) unresized images and 2) images resized to 32 × 32. The experiment considered The evaluation metrics are accuracy and balanced accuracy (BA). The hyperparameters include patch size and step size, which are the same value. Therefore, patches do not overlap. In addition, the ranking set contains 100 randomly generated samples.

Table 2: Classification results

| unresized | | | resized to 32 × 32 | | |
|---|---|---|---|---|---|
| patch | Accuracy | BA | patch | Accuracy | BA |
| 2×2 | 68.2 | 63.8 | 2×2 | 68.7 | 64.7 |
| 3×3 | 64.7 | 61.2 | 3×3 | 70.0 | 67.1 |
| 5×5 | 60.7 | 56.3 | 5×5 | 68.4 | 64.0 |
| 7×7 | 60.8 | 56.2 | 8×8 | 70.8 | 65.2 |
| 10×10 | 63.1 | 58.1 | 16×16 | 67.7 | 61.6 |

Table 3 analyzes similarity between classes, using a resized experiment with a patch size of 8 × 8. Normal training images and normal testing images are similar. However,

the test-pneumonia set is more similar to the train-pneumonia set. One possible reason is that the pneumonia distribution surrounds the normal distribution. This may be the main reason for low classification accuracy.

Table 3: Average ranking correlation (resized, patch $8 \times 8$)

| | train-normal | train-pneumonia |
|---|---|---|
| test-normal | 0.469 | 0.434 |
| test-pneumonia | 0.449 | 0.437 |

# 5 Discussion

The proposed method has the following challenges.

- The previous paper [2] reported that meta-classification is successful when training datasets are dissimilar. However, X-ray images have a certain degree of structural similarity because all images have chests.
- The distribution of the dataset might not be suitable for OCC algorithms. Other unsupervised learning algorithms should be tried to represent the datasets. Moreover, meta-classification algorithms of these models should be developed.
- IF is the fastest OCC algorithm. However, training 5840 models is still time-consuming. It took 8 minutes for the resized experiment and 20 minutes for the unresized experiment.
- The method has a space complexity issue because the experiment represents a single image with a single model. 5216 IF models from 5216 unresized images require 7 GB.

# 6 Conclusion

This paper applied meta-learning to classify datasets. The proposed method is evaluated with an X-ray image dataset. The experiment treated images as datasets, represented datasets as IF models, and executed meta-classification on IF models. This is a new knowledge contribution. Future work should improve the details. In particular, processing speed and space complexity are important challenges.

# Acknowledgement

This study is supported by the research project “2200/04/2024-2026” as part of the "Competition for 2024-2026 Postdoctoral Job Positions at the University of Hradec Králové", at the Faculty of Science, University of Hradec Králové. This study is financially supported from the project "Research of Excellence on Digital Technologies and Wellbeing

CZ.02.01.01/00/22_008/0004583“, which is co-financed by the European Union. The author thanks Dr. Richard Cimler.

# References

[1] Toshitaka Hayashi, Dalibor Cimr, Hamido Fujita, and Richard Cimler. Critical review for one-class classification: Recent advances and reality behind them. *Wiley Interdisciplinary Reviews: Data Mining and Knowledge Discovery*, 16(1):e70058, 2026.

[2] Toshitaka Hayashi, Hamido Fujita, Dalibor Cimr, Richard Cimler, and Jitka Kühnová. Meta-classification of one-class classification models using ranking correlation and nearest neighbor. *Results in Engineering*, 32:113133, 2026.

[3] Daniel Kermany. Labeled optical coherence tomography (oct) and chest x-ray images for classification. *Mendeley data*, 2018.

[4] Fei Tony Liu, Kai Ming Ting, and Zhi-Hua Zhou. Isolation forest. In *2008 eighth ieee international conference on data mining*, pages 413–422. IEEE, 2008.

[5] P. Mooney. Chest x-ray images (pneumonia), 2018.

[6] Fabian Pedregosa, Gaël Varoquaux, Alexandre Gramfort, Vincent Michel, Bertrand Thirion, Olivier Grisel, Mathieu Blondel, Peter Prettenhofer, Ron Weiss, Vincent Dubourg, et al. Scikit-learn: Machine learning in python. *the Journal of machine Learning research*, 12:2825–2830, 2011.

[7] Charles Spearman. Correlation calculated from faulty data. *British journal of psychology*, 3(3):271, 1910.

[8] Joaquin Vanschoren. Meta-learning. In *Automated machine learning: methods, systems, challenges*, pages 35–61. Springer International Publishing, Cham, 2019.

[9] Muhammad Waqas, Syed Umaid Ahmed, Muhammad Atif Tahir, Jia Wu, and Rizwan Qureshi. Exploring multiple instance learning (mil): A brief survey. *Expert Systems with Applications*, 250:123893, 2024.

# A Detailed Decision Analysis via Interval Priority Estimation from a Crisp Pairwise Comparison Matrix

**Masahiro Inuiguchi**

Department of Systems Innovation
Graduate School of Engineering Science
The University of Osaka
inuiguti@sys.es.osaka-u.ac.jp

**Shigeaki Innan**

Department of Systems Innovation
Graduate School of Engineering Science
The University of Osaka
innan@sys.es.osaka-u.ac.jp

**Abstract**

The good performances of interval priority weight (IPW) estimation methods have been shown by numerical experiments assuming the decision maker's vague evaluation. We investigate a decision analysis via the IPW estimation from a crisp pairwise comparison matrix for multiple criteria decision problems. The IPW estimation problem has a nonunique solution, which is obtained as a line segment in the IPW vector space. We propose a decision analysis with the solution set using the Hurwicz rule. The proposed method provides an explainable and detailed analysis with the comprehension of the decision maker's hesitation.

**Keywords:** AHP; interval priority weight; Hurwicz rule

## 1 Introduction

Recently, the good performances of interval priority weight estimation methods have been shown by numerical experiments under the assumption that the decision maker's evaluation is vague (see [2, 4]). However, the decision analysis based on the estimated interval priority weights has not yet been studied comprehensively. In this paper, we investigate a method for decision analysis using the interval priority weight estimation from a crisp pairwise comparison matrix in the setting of multiple criteria decision problems.

## 2 Multiple Criteria Decision Problem and Hurwicz Rule Application

The scores of alternatives under criteria are assumed to be given in the decision problems. Then the priority weights of the criteria are estimated by intervals. The interval priority weight estimation problem has a nonunique solution such that the solution set is obtained as a line segment in the interval priority weight vector space (see [3]). Because the total scores of alternatives become intervals under each interval priority weight vector in the solution set, we apply a decision rule under total uncertainty to order the alternatives. We select the Hurwicz rule [1] with an optimism coefficient. It reduced the maximin rule when the coefficient is zero, and the maximax rule when the coefficient is one. As we have a solution set expressed by a line segment to the interval priority weight estimation problem, we have another parameter specifying an interval priority weight vector in the set. We demonstrate the advantage of using interval priority estimation by a few concrete examples where three alternatives take similar total scores in the classical priority weight estimation.

## 3 The Usefulness of the Proposed Decision Analysis

The alternatives are ordered by the total scores obtained from the estimated priority weights. However, we cannot have strong confidence in the obtained result when the differences between total scores are very small. By the proposed approach, we may analyze the hesitation of the decision maker by showing all potentially acceptable orders of alternatives on a map, i.e., a plane coordinate consisting of the parameter specifying an interval priority weight vector and the optimism coefficient. An interval priority weight indicates the range of weights that can be adjusted according to the evaluation attitude toward the intervals. It is composed of the minimum weight reserved for a criterion and its range of additional weight. When the optimism coefficient is large, the additional weight is assigned more to the criterion with a larger score. In the same way, when the optimism coefficient is small, the additional weight is assigned more to the criterion with a smaller score. On the other hand, when the parameter specifying an interval priority weight vector determines the ratio of the sum of minimum weights, which may reflect the evaluation policy. When it is large, all ranges of additional weights become small. Using the map of orders of alternatives, we can advise the decision maker to select a suitable alternative or to order alternatives according to her/his evaluation attitude and policy. The area size of an order of alternatives on the map may express its robustness against the parameter selection. When only one order of alternatives appears on the map, it can indicate that the order is robust and fully recommended for the decision maker.

## 4 Conclusion

Through the presentation, we demonstrate the usefulness of the interval priority estimation in the decision analysis.

# References

[1] Simon French. *Decision Theory: An Introduction to the Mathematics of Rationality*. Ellis Horwood, London, 1988.

[2] Shigeaki Innan and Masahiro Inuiguchi. Parameter-free interval priority weight estimation methods based on minimum conceivable ranges under a crisp pairwise comparison matrix. *Journal of Advanced Computational Intelligence and Intelligent Informatics*, 28(2):333–351, 2024.

[3] Masahiro Inuiguchi. Non-uniqueness of interval weight vector to consistent interval pairwise comparison matrix and logarithmic estimation methods. In Van-Nam Huynh, Masahiro Inuiguchi, Bac Le, Bao Nguyen Le, and Thierry Denoeux, editors, *Integrated Uncertainty in Knowledge Modelling and Decision Making*, pages 39–50, Cham, 2016. Springer International Publishing.

[4] Masahiro Inuiguchi, Yeyang Hong, and Shigeaki Innan. Modifying submodels in estimation methods using minimum possible ranges for interval priority weights under a crisp pairwise comparison matrix. In Van-Nam Huynh, Katsuhiro Honda, Bac Le, Masahiro Inuiguchi, and Hieu T. Huynh, editors, *Integrated Uncertainty in Knowledge Modelling and Decision Making*, pages 16–28, Singapore, 2025. Springer Nature Singapore.

# On Computation of Harmanec–Klir Entropy for Belief Functions

**Radim Jiroušek, Václav Kratochvíl, Milan Daniel**

Institute of Information Theory and Automation,
Czech Academy of Sciences, Prague, Czech Republic
[radim/velorex]@utia.cas.cz, daniel@cs.cas.cz

**Abstract**

Because of its several important theoretical properties, Shannon entropy is often used to control the learning processes of data-based probability models. When imprecise probabilities are considered, the learning of a belief function from data is usually considered. There is no equivalent to Shannon entropy in this theory. From a theoretical point of view, Maeda-Ichihashi entropy seems to be the best candidate for a model learning controller; however, it has one serious drawback: computational complexity. This is because evaluating Maeda-Ichihashi entropy requires solving an optimization problem related to Harmanec-Klir entropy evaluation. This paper explores bypassing the optimization process for a class of belief functions.

**Keywords:** imprecise probability; Shannon entropy; computational complexity

## 1 Introduction

Unlike probability, the process of learning belief functions from data cannot be grounded in mathematical statistics because no such data-based theory exists. Another drawback of learning belief functions arises from the fact that, despite the intensive efforts of researchers, an equivalent to probabilistic Shannon entropy has not been found for belief functions. Shannon entropy is often used as a criterion for controlling the process of probability model learning. Thus, a measure of the informativeness of belief functions is sought. More than a hundred of papers have been published studying different types of uncertainty, informativeness, and measures of conflict for belief functions. These papers suggest more than thirty different measures for this purpose. The key difficulty is that a belief function contains at least two types of uncertainty, not just one: One is randomness (as in probability theory) and the other is nonspecificity/imprecision (corresponding to mass on larger sets). In (5), we studied which of the twenty-five chosen characteristics could be considered a measure of the informativeness of belief functions. Though none met all the requirements we set down, some were recommended as useful heuristics to

control the belief function learning process. From a theoretical point of view, the best candidate seems to be the proposal by Maeda and Ichihashi (6). Formally, it is a sum of two other measures, measure of information proposed by Dubois and Prade (2) and measure of total uncertainty suggested by Harmanec and Klir (4). The computation of the former one is easy, but the evaluation of the latter is computationally hard. Evaluating its value requires computing the maximum entropy of probability measures from the corresponding credal set. Such optimization problems are generally of exponential complexity.

In this paper, we explore methods for evaluating the Harmanec-Klir entropy and demonstrate the limitations of the examined approaches. After introducing the notation used in this paper (Section 2), we present a simple characterization of probability measures that maximize the Shannon entropy. This characterization may simplify the computational process in some situations (see Section 3). Section 4 describes an algorithm for constructing a probability function that maximizes the Shannon entropy within a credal set of a belief function without employing nonlinear programming libraries. Results from pilot experiments presenting the time complexity of the described processes are in Section 5. The paper concludes with a brief section on future research directions (Section 6).

## 2 Notation and Basic Properties

Let $\Omega$ be a finite *frame of discernment*. We denote by $2^\Omega$ the power set of $\Omega$. A *belief function* on $\Omega$ is a function $f : 2^\Omega \to [0,1]$, such that $f(\emptyset) = 0$, and $f(\Omega) = 1$, which is *superadditive* in the sense that is often called *complete monotonicity*. It means that for any $k \geq 2$ and for any family $a_1, \ldots, a_k \subseteq \Omega$,

$$f\left(\bigcup_{i=1}^{k} a_i\right) \geq \sum_{\emptyset \neq I \subseteq \{1,\ldots,k\}} (-1)^{|I|+1} f\left(\bigcap_{i \in I} a_i\right).$$

This property guarantees that each belief function is uniquely defined by its *basic probability assignment*, which is a mapping $m_f : 2^\Omega \to [0,1]$ satisfying

$$f(a) = \sum_{b \subseteq a} m_f(b),$$

for each $a \subseteq \Omega$. Recall that the basic probability assignment $m_f$ can be computed from belief function $f$ by the famous Möbius transform:

$$m_f(a) \;=\; \sum_{b \subseteq a} (-1)^{|a \setminus b|} f(b) \quad \geq 0, \qquad \forall a \subseteq \Omega, a \neq \emptyset.$$

Subsets $a \subseteq \Omega$ such that $m_f(a) > 0$ are called *focal elements*. The set of all focal elements is in this text denoted

$$\mathcal{E}_f = \{a \subseteq \Omega : m_f(a) > 0\}.$$

If all focal elements of a basic probability assignment are singletons, then the corresponding belief function will be referred to as a *Bayesian belief function*. Note that such a belief function corresponds exactly to a classical probability measure on $\Omega$. Unlike probability functions, belief functions can also describe situations of ignorance. Total ignorance is represented by a belief function with a single focal element, which is the entire space $\Omega$. This belief function is called *vacuous*.

Note that in this proposal we adopt the generalized probability interpretation of belief functions in the sense of Fagin and Halpern (3). Thus, the following considerations are based on the fact that each belief function is also uniquely connected with its *credal set*, which is a convex set of probability measures $\pi : 2^\Omega \to [0, 1]$ for which

$$\pi(a) \geq f(a) \text{ for all } a \subseteq \Omega.$$

The set of all such probability measures is denoted by $\mathcal{C}(f)$. $\mathcal{C}(f)$ is always nonempty, and contains only one element if and only if $f$ is Bayesian.

**Remarks on testing whether $\pi \in \mathcal{C}(f)$.** In general, it is computationally hard to verify whether a given probability measure $\pi$ belongs to the credal set of the belief function $f$. However, there are properties that can simplify this process in certain situations. Recall that an algebra on $\Omega$ is a system of subsets of $\Omega$ that is closed under intersection and complementation. Consider the minimal algebra, denoted by $\mathcal{A}_f$, which contains all focal elements (it is an algebra *generated* by focal elements). Thus, $\mathcal{E}_f \subset \mathcal{A}_f$. An atom of an algebra is a nonempty set that does not contain any other nonempty set in the algebra as a proper subset. The set of all atoms will be denoted by $\mathcal{A}^\circ_f$.

From the relation $f(c) = \sum_{b \subseteq c} m_f(b)$, we can see that, in general,

$$f(c) = \max_{a \in \mathcal{A}_f : a \subseteq c} f(a),$$

for any $c \subseteq \Omega$. Thus, if the cardinality of $\mathcal{A}^\circ_f$ is much smaller than that of $\Omega$, some advantageous properties can be exploited. For example, it is evident that for any proper subset $c$ of an atom $a$, $f(c) = 0$. Another property is expressed by the following assertion.

**Lemma 1** *Consider a belief function $f$ on $\Omega$, and two probability functions $\pi_1$, $\pi_2$ such that $\pi_1(\omega) = \pi_2(\omega)$ for all $\omega \in \Omega \setminus \{\omega_1, \omega_2\}$. If $\{\omega_1, \omega_2\}$ is in one atom from $\mathcal{A}^\circ_f$, then*

$$\pi_1 \in \mathcal{C}(f) \implies \frac{\pi_1 + \pi_2}{2} \in \mathcal{C}(f).$$

*Proof.* First notice that for all sets $c \in \mathcal{A}_f$, $\pi_1(c) = \pi_2(c) = \frac{\pi_1+\pi_2}{2}(c)$ because $\pi_1(\omega_1) + \pi_1(\omega_2) = \pi_2(\omega_1) + \pi_2(\omega_2)$. Therefore, $\frac{\pi_1+\pi_2}{2}(c) \geq f(c)$ for all $c \in \mathcal{A}_f$. To finish the proof we have to show that this inequality holds also for all $c \notin \mathcal{A}_f$. From the monotonicity of the probability function $\frac{\pi_1+\pi_2}{2}$

$$\frac{\pi_1 + \pi_2}{2}(c) \geq \max_{a \in \mathcal{A}_f : a \subseteq c} \frac{\pi_1 + \pi_2}{2}(a) = \max_{a \in \mathcal{A}_f : a \subseteq c} \pi_1(a) \geq \max_{a \in \mathcal{A}_f : a \subseteq c} f(a) = f(c).$$

□

From the proof of Lemma 1 one can deduce that $\pi \in \mathcal{C}(f)$ if $f(c) \leq \pi(c)$ for all $c \in \mathcal{A}_f$. But, as shown in the following example, it is not enough to check whether $f(a) \leq \pi(a)$ only for focal elements $a \in \mathcal{E}_f$.

**Example 1:**

Consider $\Omega = \{\omega_1, \omega_2, \omega_3, \omega_4\}$, probability function $\pi = (0.1, 0.7, 0.1, 0.1)$, and a belief function $f$ with six focal elements:

$$
\begin{aligned}
&m_f(\{\omega_1, \omega_2\}) = 0.2,\\
&m_f(\{\omega_1, \omega_3\}) = 0.1,\\
&m_f(\{\omega_1, \omega_4\}) = 0.2,\\
&m_f(\{\omega_3, \omega_4\}) = 0.2,\\
&m_f(\{\omega_1, \omega_2, \omega_3\}) = 0.2,\\
&m_f(\{\Omega\}) = 0.1.
\end{aligned}
$$

In this case we get for focal elements

$$
\begin{aligned}
&f(\{\omega_1, \omega_2\}) = 0.2 \leq \pi(\{\omega_1, \omega_2\}) = 0.8,\\
&f(\{\omega_1, \omega_3\}) = 0.1 \leq \pi(\{\omega_1, \omega_3\}) = 0.2,\\
&f(\{\omega_1, \omega_4\}) = 0.2 \leq \pi(\{\omega_1, \omega_4\}) = 0.2,\\
&f(\{\omega_3, \omega_4\}) = 0.2 \leq \pi(\{\omega_3, \omega_4\}) = 0.2,\\
&f(\{\omega_1, \omega_2, \omega_3\}) = 0.5 \leq \pi(\{\omega_1, \omega_2, \omega_3\}) = 0.9,\\
&f(\{\Omega\}) = 1 \leq \pi(\{\Omega\}) = 1.
\end{aligned}
$$

However, for non-focal element $\{\omega_1, \omega_3, \omega_4\}$, we get $\pi(\{\omega_1, \omega_3, \omega_4\}) = 0.3$, and $f(\{\omega_1, \omega_3, \omega_4\}) = 0.5$. Thus, $\pi \notin \mathcal{C}(f)$.

Nevertheless, it does not mean that when testing whether $\pi$ belongs to $\mathcal{C}(f)$, one must test all non-focal elements from $\mathcal{A}_f$. It is easy to verify that one can avoid testing non-focal elements of cardinality one and two:

Assume that for all $a \in \mathcal{E}_f$, $\pi(a) \geq f(a)$ and consider the smallest $b \subseteq \Omega$ for which $\pi(b) < f(b)$. Clearly, $b$ cannot be a singleton because, if it were, then $\pi(b) < f(b) = m_f(b)$ would mean that $b$ must be a focal element of $f$, for which this inequality cannot hold. It cannot be even a two-element set. Assume that $b = \{\omega_1, \omega_2\}$ is not a focal element of $f$. Then, $m_f(b) = 0$, and therefore

$$f(b) = m_f(\{\omega_1\}) + m_f(\{\omega_2\}) + m_f(b) = m_f(\{\omega_1\}) + m_f(\{\omega_2\}) = f(\{\omega_1\}) + f(\{\omega_2\}).$$

In general, the following assertion states that one can avoid testing of a rather large number of non-focal elements.

**Lemma 2** *Consider a belief function $f$ on $\Omega$, and two nonempty disjoint subsets $a$ and $b$ of $\Omega$, for which $f(a\cup b) = f(a)+f(b)$. If a probability function $\pi$ is such that $\pi(c) \geq f(c)$ for all $c \subset \Omega : |c| < |a \cup b|$, then $\pi(a \cup b) \geq f(a \cup b)$.*

*Proof.* Assuming opposite, one gets

$$\pi(a \cup b) < f(a \cup b) = f(a) + f(b) \leq \pi(a) + \pi(b),$$

which contradicts with the additivity of probability functions. □

# 3 Shannon entropy of probability measures

As is the tradition, we denote the Shannon entropy of a probability measure with uppercase Greek eta:

$$\mathbf{H}(\pi) = \sum_{\omega\in\Omega:\pi(\omega)>0} \pi(\omega)\log\frac{1}{\pi(\omega)}.$$

It is perhaps not necessary to recall that its values are always within the interval $[0, \log|\Omega|]$ achieving its maximum value for (and only for) the uniform measure, and it equals 0 for degenerated probability measures that equals 1 for some singleton.

**Maximization of Shannon Entropy on credal sets.** Since a credal set is a closed and convex set of probability functions (measures), and since the Shannon entropy is a continuous concave function, it is evident that for each credal set, $\mathcal{C}(f)$, one can find the values $\min_{\pi\in\mathcal{C}(f)}\{\mathbf{H}(\pi)\}$, and $\max_{\pi\in\mathcal{C}(f)}\{\mathbf{H}(\pi)\}$. The latter is always achieved by a single probability measure from $\mathcal{C}(f)$. The subsequent assertion proves that the form of this extreme function is not arbitrary.

**Lemma 3** $\pi^\star_f = \arg\max_{\pi\in\mathcal{C}(f)}\{\mathbf{H}(\pi)\}$ *is measurable with respect to the minimal algebra $\mathcal{A}_f$ generated by focal elements of $f$.*

*Proof.* Consider maximum entropy probability function $\pi^\star_f$, and an atom $a$ from $\mathcal{A}^\circ_f$. Let us prove the assertion by contradiction. Assume $a$ contains two points $\omega_1, \omega_2 \in a$ such that $\pi^\star_f(\omega_1) \neq \pi^\star_f(\omega_2)$. This enables us to define probability function $\kappa$

$$\kappa(\omega) = \begin{cases} \frac{\pi^\star_f(\omega_1)+\pi^\star_f(\omega_2)}{2} & \text{for } \omega \in \{\omega_1, \omega_2\}, \\ \pi^\star_f(\omega) & \text{for } \omega \in \Omega \setminus \{\omega_1, \omega_2\}. \end{cases}$$

Evidently, $\kappa \neq \pi^\star_f$. $\kappa \in \mathcal{C}(f)$ due to Lemma 1.

Since $\pi^\star_f(\omega_1) \neq \pi^\star_f(\omega_2)$, it is clear that $(\pi^\star_f(\omega_1)+\pi^\star_f(\omega_2))/2 > 0$. Compute the relative entropy (Kullback-Leibler divergence) of $\pi^\star_f$ with respect to $\kappa$. Note that it is finite in

this case because $\pi^\star_f$ is dominated by $\kappa$.

$$\begin{aligned}
KL(\pi^\star_f||\kappa) &= \sum_{\omega\in\Omega:\kappa(\omega)>0} \pi^\star_f(\omega)\log\frac{\pi^\star_f(\omega)}{\kappa(\omega)} = \sum_{i=1,2}\pi^\star_f(\omega_i)\log\frac{\pi^\star_f(\omega_i)}{\kappa(\omega_i)}\\
&= \sum_{i=1,2:\pi^\star_f(\omega_i)>0}\pi^\star_f(\omega_i)\log\pi^\star_f(\omega_i) + \sum_{i=1,2}\pi^\star_f(\omega_i)\log\frac{1}{\kappa(\omega_i)}\\
&= \sum_{i=1,2:\pi^\star_f(\omega_i)>0}\pi^\star_f(\omega_i)\log\pi^\star_f(\omega_i) - \log\frac{\pi^\star_f(\omega_1)+\pi^\star_f(\omega_2)}{2}\sum_{i=1,2:\pi^\star_f(\omega_i)>0}\pi^\star_f(\omega_i)\\
&= \sum_{i=1,2:\pi^\star_f(\omega_i)>0}\pi^\star_f(\omega_i)\log\pi^\star_f(\omega_i) - (\pi^\star_f(\omega_1)+\pi^\star_f(\omega_2))\log\frac{\pi^\star_f(\omega_1)+\pi^\star_f(\omega_2)}{2}.
\end{aligned}$$

Now, compute

$$\begin{aligned}
\mathbf{H}(\kappa)-\mathbf{H}(\pi^\star_f) &= -\sum_{\omega\in\Omega:\kappa(\omega)>0}\kappa(\omega)\log\kappa(\omega) + \sum_{\omega\in\Omega:\pi^\star_f(\omega)>0}\pi^\star_f(\omega)\log\pi^\star_f(\omega)\\
&= -\sum_{i=1,2}\kappa(\omega_i)\log\kappa(\omega_i) + \sum_{i=1,2:\pi^\star_f(\omega_i)>0}\pi^\star_f(\omega_i)\log\pi^\star_f(\omega_i)\\
&= -(\pi^\star_f(\omega_1)+\pi^\star_f(\omega_2))\log\frac{\pi^\star_f(\omega_1)+\pi^\star_f(\omega_2)}{2} + \sum_{i=1,2:\pi^\star_f(\omega_i)>0}\pi^\star_f(\omega_i)\log\pi^\star_f(\omega_i)\\
&= KL(\pi^\star_f||\kappa),
\end{aligned}$$

which is known to be positive for two different probability measures. This finishes the proof because it contradicts our assumption that $\pi^\star$ maximizes the Shannon entropy in the respective credal set. □

**Transformation of an optimization problem.** Denote by $\mathcal{A}_f$ the minimal algebra of subsets of $\Omega$ that contains all focal elements of the belief function $f$. Denote the set of its atoms by $\mathcal{A}^\circ_f$. All elements $c \in \mathcal{A}^\circ_f$ are thus nonempty and mutually disjoint. Furthermore, the set of all atoms in $\mathcal{A}^\circ_f$ is a partition of $\Omega$, meaning that $\Omega$ equals the union of all atoms in $\mathcal{A}^\circ_f$. There is a one-to-one correspondence between $\mathcal{A}_f$-measurable probability functions $\pi$ on $\Omega$ and probability measures $p$ on $\mathcal{A}_f$:

$$\begin{aligned}
p(c) &= \sum_{\omega\in c}\pi(\omega),\\
\pi(\omega) &= \frac{p(c)}{|c|} \text{ for } \omega\in c.
\end{aligned}$$

Thus, instead of looking for $\mathcal{A}_f$-measurable probability function $\pi$ on $\Omega$ that maximizes

$$\mathbf{H}(\pi) = \sum_{\omega\in\Omega}\pi(\omega)\log\frac{1}{\pi(\omega)},$$

we can look for a probability measure $p$ on $\mathcal{A}_f$ that maximizes[1]

$$\mathbf{W}(p) = \mathbf{H}(p) + \sum_{c\in\mathcal{A}^\circ : p(c)>0} p(c)\log(|c|) = -\sum_{c\in\mathcal{A}^\circ : p(c)>0} p(c)\log\frac{p(c)}{|c|},$$
$$= -\sum_{c\in\mathcal{A}^\circ : p(c)>0} \log\frac{p(c)}{|c|}\sum_{\omega\in c}\pi(\omega) = -\sum_{\omega\in c}\pi(\omega)\log(\pi(\omega)).$$

Both tasks are nonlinear optimization problems, the only, but important, difference (from the viewpoint of computational complexity) is the dimension of the considered spaces. Naturally $|\mathcal{A}^\circ_f| \leq |\Omega|$. In many situations the difference can be substantial as $|\mathcal{A}^\circ_f| \leq 2^{|\mathcal{E}_f|}$. Therefore, if we restrict our considerations to belief functions with a limited number of focal elements (say 10), we can compute their Harmanec-Klir entropy (almost) regardless of the cardinality of $\Omega$.

**Example: 2**

Consider $\Omega = \{\omega_1, \omega_2, \ldots, \omega_{10}\}$, and the belief functions $f$ with three focal elements: $m_f(\{\omega_2, \omega_5, \omega_7\}) = 0.30$, $m_f(\{\omega_1, \omega_3, \omega_8\}) = 0.45$, $m_f(\{\omega_4, \omega_5, \omega_6, \omega_9\}) = 0.25$.
In this case,

$$\mathcal{A}^\circ_f = \big\{\{\omega_5\}, \{\omega_{10}\}, \{\omega_2, \omega_7\}, \{\omega_1, \omega_3, \omega_8\}, \{\omega_4, \omega_6, \omega_9\}\big\},$$

and the criterion $\mathbf{W}(p)$ is maximized for the probability measure $p^\star$

$p^\star(\{\omega_5\}) = 0.10$ $\quad p^\star(\{\omega_{10}\}) = 0$ $\quad p^\star(\{\omega_2, \omega_7\}) = 0.20$
$p^\star(\{\omega_1, \omega_3, \omega_8\}) = 0.45$ $\quad p^\star(\{\omega_4, \omega_6, \omega_9\}) = 0.25$

from which we get the required probability measure achieving the maximum entropy $\mathbf{H}(\pi^\star) = 2.1657$, where

$\pi^\star(\omega_1) = 0.15$ $\quad \pi^\star(\omega_2) = 0.10$ $\quad \pi^\star(\omega_3) = 0.15$ $\quad \pi^\star(\omega_4) = 0.0833$
$\pi^\star(\omega_5) = 0.10$ $\quad \pi^\star(\omega_6) = 0.0833$ $\quad \pi^\star(\omega_7) = 0.10$ $\quad \pi^\star(\omega_8) = 0.15$
$\pi^\star(\omega_9) = 0.0833$ $\quad \pi^\star(\omega_{10}) = 0$

# 4 An algorithm inspired by geomorphology

Imagine the optimal probability function $\pi^\star$ on $\Omega$ as hilly countryside. The altitude of each point $\omega$ in $\Omega$ is expressed by $\pi^\star(\omega)$. According to Lemma 3, each atom $a \in \mathcal{A}^\circ_f$ is actually a mesa, as its entire surface is at the same altitude. To achieve the optimal relief

[1] Notice the resemblance of the formula for $\mathbf{W}(p)$ to the Maeda-Ishibashi entropy for belief functions (6), which is

$$\mathbf{H}_{MI}(f) = \max_{\pi\in\mathcal{C}(f)} \mathbf{H}(\pi) + \sum_{a\subseteq\Omega} m_f(a)\log(|a|).$$

$\pi^\star$, we can start with a relief defined by the given belief function, $f$. This determines the basis of the relief created by volcanic activity. The total volume of this basic relief is given by

$$Vol(f) = \sum_{\omega\in\Omega} f(\omega).$$

Imagine that the remaining volume of the Earth's mass, $(1 - Vol(f))$, is in the form of vapor. When it begins to condense, it rains across the entire landscape $\Omega$. Water naturally flows down from the hills and fills the valleys. The water level throughout the countryside remains constant, forming seas and oceans. The same property can be proven for a model representing a probability function that maximizes the Shannon entropy. This proof is based on the same idea as the proof of Lemma 3. The following algorithm, which realizes the described geomorphological process, successively identifies all hills above sea level, starting with the highest peaks.

To keep the notation simple, we will omit the index $f$ when denoting the respective algebras in the following algorithm. We will use the following notation: $rest\Omega$ will denote the part of $\Omega$ that has not yet been mapped. The symbol $\mathcal{A}^\circ{}_{|rest\Omega}$ will denote the atoms from $rest\Omega$, i.e.,

$$\mathcal{A}^\circ{}_{|rest\Omega} = \{c \in \mathcal{A}^\circ : c \subseteq rest\Omega\},$$

and analogously,

$$\mathcal{A}_{|rest\Omega} = \{a \in \mathcal{A} : a \subseteq rest\Omega\}.$$

**ALGORITHM**

---

**Input:** A list of focal elements defining basic probability assignment $m_f$

**Output:** Optimal $p^* : \mathcal{A}^\circ \to [0,1]$, for which $\pi^\star(\omega) = \frac{p^\star(c)}{|c|}$ for all $\omega \in c$.

**Initialization:**

$rest\Omega := \Omega$; *# uncharted area*

$restW := 1$; *# remaining amount of water*

Generate algebra $\mathcal{A} = \mathcal{A}_{|rest\Omega}$, and the belief function $f(a)$ for all $a \in \mathcal{A}_{|rest\Omega}$.

**Repeated cycle:**

**If** $\max_{a\in\mathcal{A}_{|rest\Omega}} \frac{f(a)}{|a|} \leq \frac{restW}{|rest\Omega|}$

**Then** *# there are no more peaks above the sea level*

**For** $c \in \mathcal{A}^\circ{}_{|rest\Omega}$ $\{p^\star(c) := \frac{restW}{|rest\Omega|}\}$; **STOP**

**Otherwise** *# found new peaks above the sea level*

$\hat{a} := \arg\max_{a\in\mathcal{A}_{|rest\Omega}} \frac{f(a)}{|a|}$

**For** $c \in \mathcal{A}^\circ{}_{|\hat{a}}$ $\{p^\star(c) := \frac{|c|f(\hat{a})}{|\hat{a}|}\}$; *# mapping new peaks*

$rest\Omega := rest\Omega \setminus \hat{a}$; *# reconstruction of uncharted area*

$restW := restW - f(\hat{a})$;

**For** $a \in \mathcal{A}_{|rest\Omega}$ $\{f(a) := f(a \cup \hat{a}) - f(\hat{a})\}$;

This algorithm is practically identical to the one designed by Meyerowitz et al. in Theorem 15 (7). Their idea is formally formulated as Meyerowitz et al.'s Algorithm in (1), where a slight speed enhancement is also proposed. However, there is a difference between the algorithm defined here and those in (1). The latter algorithms do not simplify the considered structure to the algebra $\mathcal{A}_f$, but rather consider the full algebra $2^\Omega$.

The two examples below illustrate the behavior of the peak-seeking algorithm on belief functions from Examples 1 and 2. The second example shows the benefit of converting the problem from $2^\Omega$ to the minimal algebra generated by focal elements.

**Example:** Application of the Algorithm to belief function from Example 1

Consider $\Omega = \{\omega_1, \omega_2, \omega_3, \omega_4\}$, and a belief function $f$ with six focal elements: $m_f(\{\omega_1, \omega_2\}) = 0.2$, $m_f(\{\omega_1, \omega_3\}) = 0.1$, $m_f(\{\omega_1, \omega_4\}) = 0.2$, $m_f(\{\omega_3, \omega_4\}) = 0.2$, $m_f(\{\omega_1, \omega_2, \omega_3\}) = 0.2$, and $m_f(\{\Omega\}) = 0.1$. Notice that in this case $\mathcal{A} = 2^\Omega$, and that belief function $f$ is positive only for nine subsets of $\Omega$:

$$\begin{array}{lll} f(\{\omega_1, \omega_2\}) = 0.2, & f(\{\omega_1, \omega_3\}) = 0.1, & f(\{\omega_1, \omega_4\}) = 0.2, \\ f(\{\omega_3, \omega_4\}) = 0.2, & f(\{\omega_1, \omega_2, \omega_3\}) = 0.5, & f(\{\omega_1, \omega_2, \omega_4\}) = 0.4, \\ f(\{\omega_1, \omega_3, \omega_4\}) = 0.3, & f(\{\omega_2, \omega_3, \omega_4\}) = 0.2, & f(\{\Omega\}) = 1. \end{array}$$

When performing the first test, the algorithm compares

$$\max_{a \in \mathcal{A}} \frac{f(a)}{|a|} = \frac{f(\{\omega_1, \omega_2, \omega_3\})}{|\{\omega_1, \omega_2, \omega_3\}|} = \frac{0.5}{3} \quad \text{and} \quad \frac{restW}{|rest\Omega|} = \frac{1}{4}.$$

Because the ratio on the right-hand side is greater than the ratio on the left-hand side, the algorithm terminates immediately, yielding the uniform probability function as its result.

**Example:** Application of the Algorithm to the belief function from Example 2

There are 31 nonempty elements of the algebra $\mathcal{A}_f$, which must be considered when comparing $\max_{a\in\mathcal{A}_f} \frac{f(a)}{|a|}$ and $\frac{restW}{|rest\Omega|}$. The first ratio evidently maximizes for $a = \{\omega_1, \omega_3, \omega_8\}$, and since $\frac{0{,}45}{3} > \frac{1}{10}$, the algorithm assigns the value 0.45 to the atom $\{\omega_1, \omega_3, \omega_8\}$. When we recompute the belief function in preparation for the second cycle, we do not change the value of $f(\{\omega_2, \omega_5, \omega_7\})$, which maximizes the tested ratio in the second cycle when comparing $\max_{a\in\mathcal{A}_{|rest\Omega}} \frac{f(a)}{|a|} = \frac{0.3}{3}$ with $\frac{restW}{|rest\Omega|} = \frac{0.55}{7}$. The test result directs the algorithm to finish the second cycle by assigning $p^\star(\{\omega_5\} = 0.1$ and $p^\star(\{\omega_2, \omega_7\} = 0.2$.

At the beginning of the third cycle $\mathcal{A}^\circ{}_{|rest\Omega} = \{\{\omega_4, \omega_6, \omega_9\}, \{\omega_{10}\}\}$ with $f(\{\omega_4, \omega_6, \omega_9\}) = f(\{\omega_4, \omega_6, \omega_9, \omega_{10}\}) = 0.25$, and $f(\{\omega_{10}\}) = 0$. Thus,

$$\max_{a\in\mathcal{A}_{|rest\Omega}} \frac{f(a)}{|a|} = \frac{f(\{\omega_4, \omega_6, \omega_9\})}{|\{\omega_4, \omega_6, \omega_9\}|} = \frac{0.25}{3} > \frac{restW}{|rest\Omega|} = \frac{0.25}{4},$$

which means that the remaining mass is assigned to $\{\omega_4, \omega_6, \omega_9\}$: $p^\star(\{\omega_4, \omega_6, \omega_9\}) = 0.25$. At the beginning of the fourth cycle, $\mathcal{A}^\circ{}_{|rest\Omega} = \{\{\omega_{10}\}\}$, $f(\{\omega_{10}\}) = 0$, and $restW = 0$. The tested inequality holds, and before stopping, the algorithm assigns $p^\star(\{\omega_{10}\}) = 0$.

# 5 Results from the computational comparisons

To examine the time of processing of the above described methods, We carried out a pilot series of 30 experiments. We randomly generated basic probability assignments with 2 – 6 focal elements on $\Omega$ of cardinality 12. To each basic probability assignment we applied the following four processes, each yielding the probability functions on $\Omega$.

**Method 1**:
1. Upload of bpa $m$;
2. Derivation of the constrains for all subsets of $\Omega$;
3. Application of the optimization procedure CVXR.

**Method 2**:
1. Upload of bpa $m$;
2. Derivation of all atoms of the minimal algebra $\mathcal{A}_f$ generated by the focal elements of $m$;
3. Derivation of the constrains for all sets of algebra $\mathcal{A}_f$;
4. Application of the optimization procedure CVXR.

**Method 3**: 1. Upload of bpa $m$;
2. Derivation of all atoms of the minimal algebra $\mathcal{A}_f$ generated by the focal elements of $m$;
3. Upload of the reduced set of constrains for the selected sets of algebra $\mathcal{A}_f$ (recall that Lemma 2 makes constraint deletion possible);
4. Application of the optimization procedure CVXR.

**Method 4**: 1. Upload of bpa $m$;
2. Application of the seeking peaks algorithm.

| | | | Time of processing in seconds | | | |
|---|---|---|---|---|---|---|
| $\lvert\mathcal{E}_f\rvert$ | count | $\lvert\mathcal{A}^\circ{}_f\rvert$ | **Method 1**: | **Method 2**: | **Method 3**: | **Method 4**: |
| 2 | 7 | 4 | 0.18 – 0.70 | 0.28 – 0.55 | 0.14 – 0.39 | 0 |
| 3 | 7 | 5, 6 | 0.32 – 1.52 | 0.72 – 30.15 | 0.48 – 2.29 | 0 |
| 4 | 6 | 7 – 10 | 1.07 – 17.58 | 2.31 – 51.17 | 1.11 – 7.55 | 0 – 0.01 |
| 5 | 6 | 9 – 11 | 7.22 – 52.30 | 8.97 – 47.09 | 3.51 – 16.73 | 0 – 0.01 |
| 6 | 4 | 10 – 12 | 10.64 – 146.35 | 19.65 – 96.10 | 7.49 – 32.58 | 0.01 – 0.02 |

Table 1: Time demands in computational experiments with 30 bpas

**Method 2** differs from **Method 1** in that it introduces the aforementioned transformation of the optimization problem from $\Omega$ to the minimal algebra $\mathcal{A}_f$. Thus, **Method 2** has to construct the minimal algebra generated by focal elements, which takes time. However, the optimization process is then faster because in most cases $|\mathcal{A}_f| < |\Omega|$. Therefore, it is not surprising that, for some belief functions, **Method 1** was faster than **Method 2**, for some others it was the other way around.

As the results in Table 1 show, **Method 3** is the fastest optimization technique. It takes advantage of Lemma 2 and applies only the smaller set of constraints. For the 30 basic probability assignments considered, this property reduced the number of constraints to almost exactly one half. While the achieved times are promising, one must consider that **Method 3** uploaded the restricted set of constraints deduced separately. This fact completely devalues the idea. The brute force algorithm used to deduce the restricted set of constraints was extremely demanding. For the most complicated belief function, the computation took more than two hours.

As expected, the peak-seeking algorithm was the most efficient, incomparably faster than any of the other studied optimization techniques. It is, in fact, the Meyerowitz et al. algorithm enhanced by the transformation process. Since it operates within minimal algebra, it can be applied to belief functions with a limited number of focal elements, even when the discernment space under consideration has hundreds of elements.

# 6 Conclusions

Since all the programs were designed by OpenAI's ChatGPT, many questions remain unanswered. The main ones concern the efficiency of the processes used. One important

question is whether a system of non-redundant constraints could be generated to bypass the time-consuming process of eliminating redundant constraints. Other questions focus on designing efficient data structures for handling belief functions and related concepts. This contribution also emphasizes the importance of devoting more attention to studying classes of belief functions defined by a limited number of focal elements.

## Acknowledgment

The R/CVXR programs and other computational programs used in this paper were developed in collaboration with OpenAI's ChatGPT. ChatGPT assisted with implementation, debugging, and computational experimentation. The research questions, mathematical reasoning, algorithm inspired by geomorphology, experimental design, and interpretation of the results are the responsibility of the authors.

# References

[1] Joaquín Abellán, Alejandro Pérez-Lara, and Serafín Moral-García. A variation of the algorithm to achieve the maximum entropy for belief functions. *Entropy*, 25(6):867, 2023.

[2] Didier Dubois and Henri Prade. Properties of measures of information in evidence and possibility theories. *Fuzzy sets and systems*, 24(2):161–182, 1987.

[3] Ronald Fagin and Joseph Y Halpern. Uncertainty, belief, and probability 1. *Computational Intelligence*, 7(3):160–173, 1991.

[4] David Harmanec and George J Klir. Measuring total uncertainty in dempster-shafer theory: A novel approach. *International journal of general system*, 22(4):405–419, 1994.

[5] Radim Jiroušek and Václav Kratochvíl. About twenty-five naughty entropies in belief function theory: do they measure informativeness? *International Journal of Approximate Reasoning*, page 109454, 2025.

[6] Yutaka Maeda and Hidetomo Ichihashi. An uncertainty measure with monotonicity under the random set inclusion. *International Journal Of General System*, 21(4):379–392, 1993.

[7] Aaron Meyerowitz, Fred Richman, and Elbert Walker. Calculating maximum-entropy probability densities for belief functions. *International Journal of Uncertainty, Fuzziness and Knowledge-Based Systems*, 2(04):377–389, 1994.

# On Geometry of Optimal Faces in Belief-Function Polytopes

**Václav Kratochvíl** **Milan Daniel** **Radim Jiroušek**

Institute of Information Theory and Automation,
Czech Academy of Sciences, Prague, Czech Republic
[velorex/radim]@utia.cas.cz, daniel@cs.cas.cz

**Abstract**

Previous polyhedral work on learning belief functions from possibly imprecise data selected a single belief function from the set of admissible ones by linear optimization. In this paper, we study the complete sets of optimal solutions for three previously proposed selection criteria. Controlled experiments with synthetically generated observations show substantial changes in the relation between optimal sets as the proportion of ambiguous observations and the number of different ambiguous subsets are varied. The criteria also differ in how uniquely they determine a solution. A separate experiment with only precise observations shows that nontrivial differences between optimal solutions can remain even without observational ambiguity, because samples introduce an additional statistical source of imprecision. Thus, a single solution returned by linear optimization may conceal substantial structure arising from both the observed data and their finite-sample statistical treatment.

## 1 Introduction

Belief functions originate in Dempster's work on upper and lower probabilities and Shafer's theory of evidence (Dempster, 1967; Shafer, 1976); see also (Denoeux, 2019) for a recent overview. Let $\Omega = \{\omega_1, \ldots, \omega_n\}$ be a finite frame of discernment. A belief function is determined by a basic probability assignment (BPA) $m : 2^\Omega \to [0, 1]$, satisfying $m(\emptyset) = 0$ and

$$\sum_{A \subseteq \Omega} m(A) = 1.$$

Its belief values are

$$\mathrm{Bel}_m(A) = \sum_{B \subseteq A} m(B).$$

Under the lower-probability interpretation, a belief function can be viewed as the lower envelope of a family of compatible probability measures (Fagin and Halpern, 1991). This

interpretation is particularly useful when belief functions are constructed from possibly imprecise data.

In the data model considered here, an observation is a nonempty subset $X_i \subseteq \Omega$. A singleton $X_i = \{\omega_j\}$ is a precise observation, whereas $X_i$ represents an ambiguous observation when $|X_i| > 1$: the state is known only to belong to the reported subset. For an event $A \subseteq \Omega$, observations satisfying $X_i \subseteq A$ provide support for $A$.

Following the construction introduced in (Kratochvíl et al., 2026), the number of observations supporting $A$ is converted into a Jeffreys lower confidence bound for its unknown probability (Jeffreys, 1946; Brown et al., 2001). Denote this lower bound by $g(A)$, with $g(\Omega) = 1$. We call a belief function admissible if

$$\mathrm{Bel}_m(A) \geq g(A), \qquad A \subseteq \Omega.$$

The function $g$ is a normalized monotone set function derived from the data, but in general it is not a belief function. Thus, the admissible belief functions are precisely those that dominate $g$.

A representative belief function can then be selected by linear optimization. However, the optimal solution need not be unique. Reporting only one returned solution may therefore conceal other belief functions that are equally optimal for the same criterion. This leads to two questions that motivate the present study:

*What is the complete set of belief functions that are optimal for a given criterion?*

*How are the optimal sets obtained from different criteria related, and what can affect their relations?*

## 2 Optimal faces in the dominance polytope

The set of admissible belief functions introduced above is the dominance polytope

$$\mathcal{M}_g = \left\{ m \;\middle|\; m(\emptyset) = 0,\ \sum_{A \subseteq \Omega} m(A) = 1,\ \forall A \subseteq \Omega : \big(\mathrm{Bel}_m(A) \geq g(A)\ \&\ m(A) \geq 0\big) \right\}.$$

Each point of $\mathcal{M}_g$ is therefore a belief function compatible with the lower bounds derived from the data.

In this paper, we consider the same three linear criteria as in (Kratochvíl et al., 2026). The $L1$ criterion corresponds to minimizing the $L_1$ distance between the belief function $\mathrm{Bel}_m$ and the data-derived lower-bound function $g$. Expressed in terms of the basic probability assignment $m$, it takes the form

$$L1(m) = \sum_{\emptyset \neq A \subseteq \Omega} 2^{|\Omega|-|A|} m(A) \longrightarrow \min.$$

Thus, $L1$ favours belief functions that remain close to the lower bounds derived from the data.

The second criterion maximizes the Dubois–Prade nonspecificity measure (Dubois and Prade, 1987),

$$HD(m) = \sum_{\emptyset \neq A \subseteq \Omega} m(A) \log_2 |A| \longrightarrow \max .$$

It therefore favours mass assigned to larger subsets.

The third criterion is

$$CW(m) = \sum_{\emptyset \neq A \subseteq \Omega} \frac{1}{|A|} m(A) \longrightarrow \min .$$

It also favours larger focal sets, but uses inverse-cardinality weights rather than logarithmic cardinality.

For a unified notation, we minimize $L1$, $CW$, and $-HD$.

## 2.1 Optimal exposed faces

For a linear criterion optimized over a polytope, the complete set of optimal solutions forms an exposed face (Rockafellar, 1970). We now apply this observation to the three criteria considered above. Let

$$\mathcal{C} = \{L1, CW, -HD\}.$$

For every criterion $C \in \mathcal{C}$, let $S_C$ denote the set of optimal vertices

$$S_C = \left\{ v \in \mathrm{vert}(\mathcal{M}_g) \;\middle|\; C(v) = \min_{u \in \mathrm{vert}(\mathcal{M}_g)} C(u) \right\},$$

where $\mathrm{vert}(\mathcal{M}_g)$ denotes the set of vertices of $\mathcal{M}_g$. For simplicity, we write $S_{HD}$ for the set obtained by minimizing $-HD$.

Because the criteria are linear, the complete set of optimal solutions is the exposed face

$$\mathcal{F}_C = \mathrm{conv}(S_C).$$

Thus, $S_C$ contains precisely the vertices of the corresponding optimal face $\mathcal{F}_C$.

Since all optimal faces considered here are faces of the same dominance polytope $\mathcal{M}_g$, their mutual relations can be determined from their vertex sets. In particular,

$$\mathcal{F}_{C_1} \subseteq \mathcal{F}_{C_2} \quad \Longleftrightarrow \quad S_{C_1} \subseteq S_{C_2},$$

and

$$\mathcal{F}_{C_1} = \mathcal{F}_{C_2} \quad \Longleftrightarrow \quad S_{C_1} = S_{C_2}.$$

Moreover, the nonempty intersection of two faces of the same polytope is again a face and therefore contains a vertex of that polytope. Consequently,

$$\mathcal{F}_{C_1} \cap \mathcal{F}_{C_2} \neq \emptyset \quad \Longleftrightarrow \quad S_{C_1} \cap S_{C_2} \neq \emptyset.$$

Let us stress that these equivalences rely on the fact that all sets considered here are faces of one common polytope; they do not hold for arbitrary intersecting polytopes. In the computational experiments we therefore compare the vertex sets $S_C$, while interpreting the resulting relations as relations between the corresponding optimal faces $\mathcal{F}_C$.

$|S_C| = 1$ means that criterion $C$ has a unique optimal vertex, whereas $|S_C| > 1$ means that several distinct belief functions attain exactly the same optimal criterion value.

For

$$S_C = \{v_1, \ldots, v_r\},$$

the affine dimension of the corresponding optimal face is

$$\dim \mathcal{F}_C = \operatorname{rank} \begin{pmatrix} v_2 - v_1 \\ v_3 - v_1 \\ \vdots \\ v_r - v_1 \end{pmatrix}.$$

The number of optimal vertices and the affine dimension describe different properties of the face and need not determine one another.

For two criteria, their optimal faces may be disjoint, equal, one may be a proper subface of the other, or they may intersect without either one containing the other. We call the last situation a *crossing*.

## 2.2 The discriminating quaternary example

Preliminary experiments, particularly for four-element frames, frequently produced the inclusion $S_{HD} \subseteq S_{L1}$. Therefore, we find it interesting to present a small example from (Kratochvíl et al., 2026) showing that this inclusion does not generally hold.

Let

$$\Omega = \{\omega_1, \omega_2, \omega_3, \omega_4\}.$$

The observed subsets with nonzero counts are

| $X_i$ | $\{\omega_1\}$ | $\{\omega_2\}$ | $\{\omega_3\}$ | $\{\omega_4\}$ | $\{\omega_1, \omega_2, \omega_4\}$ | $\{\omega_2, \omega_3, \omega_4\}$ |
|---|---|---|---|---|---|---|
| count | 16 | 20 | 8 | 1 | 9 | 16 |

and all other nonsingleton subsets have zero counts. Using the confidence level ($1 - \alpha = 0.95$), the resulting dominance polytope has (11451) vertices.

The $L1$- and $HD$-optimal faces contain 10 and 4 vertices, respectively, and both have affine dimension 3. They share exactly one vertex, but neither face contains the other. Hence their relation is a crossing. The unique $CW$-optimal vertex belongs to neither of them.

The importance of the example is therefore not merely to show that generally $S_{HD} \not\subseteq S_{L1}$, bual also that the three criteria can return different representative solutions. This counterexample motivates the controlled experiments below, where we study when the $L1$- and $HD$-optimal faces coincide, overlap, become nested, or remain disjoint.

| quantity | value |
|---|---|
| vertices of $\mathcal{M}_g$ | 11451 |
| $\lvert S_{L1}\rvert$ | 10 |
| $\lvert S_{HD}\rvert$ | 4 |
| $\lvert S_{CW}\rvert$ | 1 |
| $\dim \mathcal{F}_{L1}$ | 3 |
| $\dim \mathcal{F}_{HD}$ | 3 |
| $\dim \mathcal{F}_{CW}$ | 0 |
| $\lvert S_{L1} \cap S_{HD}\rvert$ | 1 |
| $S_{L1} \cap S_{CW}$ | $\emptyset$ |
| $S_{HD} \cap S_{CW}$ | $\emptyset$ |

Table 1: Optimal faces for the discriminating quaternary example.

# 3 Experiments

Preliminary experiments, particularly for four-element frames, frequently suggested a strong relation between the $L1$- and $HD$-optimal faces. In many instances,

$$S_{HD} \subseteq S_{L1},$$

so that every $HD$-optimal vertex was also $L1$-optimal. The discriminating quaternary example in the previous section shows, however, that this inclusion does not hold in general.

This raises two related questions: under what conditions do the $L1$- and $HD$-optimal faces overlap or become nested, and which properties of the observed data influence their relation?

As a first hypothesis, we investigate the role of ambiguity in the observations. Ambiguity can differ in more than one way: datasets may contain different proportions of ambiguous observations, and the ambiguous observations may be concentrated on only a few subsets or distributed over many different subsets. To compare these aspects systematically across the generated datasets, we describe them by two quantities.

Let $N_{\text{amb}}$ denote the number of observations $X_i$ with $|X_i| > 1$, and let $N$ be the total number of observations. We define

$$q = \frac{N_{\text{amb}}}{N},$$

so that $q$ is the proportion of observations that are ambiguous.

The value of $q$ alone does not distinguish whether the ambiguous observations repeatedly involve the same subsets or occur across many different subsets. We therefore also define

$$\rho = \frac{\#\{A \subseteq \Omega : \ |A| \geq 2, \ A \text{ occurs among the observations}\}}{2^{|\Omega|} - |\Omega| - 1}.$$

The quantity $\rho$ describes the relative coverage of the possible nonempty nonsingleton subsets. Thus, two datasets may have the same proportion $q$ of ambiguous observations

but different values of $\rho$ if those observations are distributed over different numbers of distinct subsets.

We use $\rho$ only as a normalized experimental index that allows us to compare subset coverage across different frame sizes considered below. It is not intended as a general measure of imprecision.

## 3.1 Computation of the optimal faces

Complete vertex enumeration of $\mathcal{M}_g$ becomes computationally demanding as the cardinality of the frame increases. Since we need only the optimal face for a given criterion, we avoid enumerating the complete dominance polytope whenever possible.

For each criterion $C$, we first determine its optimal value

$$\min_{m \in \mathcal{M}_g} C(m).$$

We then restrict $\mathcal{M}_g$ to all points attaining this value

$$C(m) = \min_{u \in \mathcal{M}_g} C(u).$$

Together with the constraints defining $\mathcal{M}_g$, this equality defines exactly the optimal exposed face $\mathcal{F}_C$. We therefore enumerate only the vertices of $\mathcal{F}_C$.

## 3.2 Amount and coverage of ambiguous observations

The first controlled experiment separates the proportion of ambiguous observations from the number of different ambiguous subsets occurring in the data. We fix

$$N = 500$$

and

$$q \in \{0.25, 0.50, 0.75\},$$

and vary $\rho$ while keeping $q$ fixed. The experiment should therefore help answer whether the relation between the $L1$- and $HD$-optimal faces changes when the same number of ambiguous observations is distributed across different numbers of distinct subsets.

The numbers of possible nonempty nonsingleton subsets are 11, 26, and 57 for $|\Omega| = 4, 5$, and 6, respectively. Consequently, the attainable values of $\rho$ differ slightly between the three frame sizes, and approximately corresponding coverage levels are used.

All singleton subsets occur in every generated dataset. The precise observations are distributed as evenly as possible among them. For a chosen value of $\rho$, the corresponding number of distinct nonsingleton subsets is selected uniformly at random without replacement. Each selected subset first receives one observation, and the remaining ambiguous observations are then allocated among the selected subsets with equal probabilities.

In total, we generated 11130 datasets. For each dataset, we constructed the corresponding lower-bound function $g$, the dominance polytope $\mathcal{M}_g$, and the optimal faces for the three criteria. We then evaluated the mutual relation of the $L1$- and $HD$-optimal faces, together with the numbers of optimal vertices, affine dimensions, and uniqueness for all three criteria. These characteristics are analyzed in the following subsections.

| $\lvert\Omega\rvert$ | values of $\rho$ | runs per $(q, \rho)$ | total runs |
|---|---|---|---|
| 4 | $0.091, 0.182, 0.364, 0.545, 0.727, 0.909, 1$ | 300 | 6300 |
| 5 | $0.077, 0.192, 0.346, 0.538, 0.731, 0.923, 1$ | 200 | 4200 |
| 6 | $0.088, 0.175, 0.368, 0.544, 0.719, 0.912, 1$ | 30 | 630 |

Table 2: Design of the controlled experiment. For each frame size, the complete grid of $\rho$ values is evaluated separately for $q = 0.25, 0.50, 0.75$. The values of $\rho$ represent approximately corresponding levels of relative nonsingleton-subset coverage.

### 3.3 Mutual position of the optimal faces

We first examine how the relation between the $L1$- and $HD$-optimal faces changes with $q$ and $\rho$. As shown above, because both are faces of the same dominance polytope, their relations can be determined from the corresponding vertex sets $S_{L1}$ and $S_{HD}$.

Figure 1 shows the proportion of runs for which the two optimal faces intersect for $|\Omega| = 5$. Along each curve, the proportion $q$ of ambiguous observations is fixed and only the relative subset coverage $\rho$ changes.

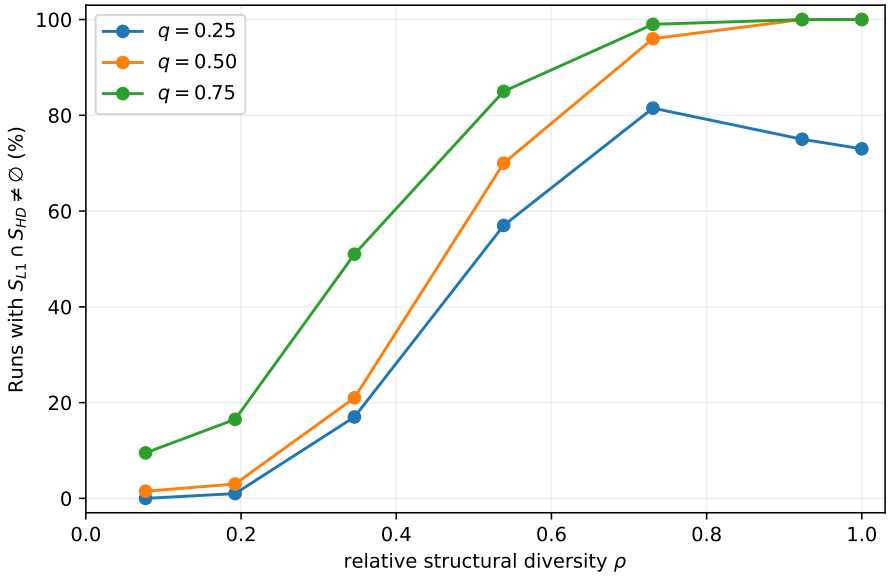



Figure 1: Percentage of runs with $S_{L1} \cap S_{HD} \neq \emptyset$ for $|\Omega| = 5$. The proportion $q$ of ambiguous observations is fixed along each curve, while the relative nonsingleton-subset coverage $\rho$ varies.

For example, for $q = 0.50$, the proportion of runs with intersecting optimal faces increases from 1.5% at $\rho \approx 0.077$ to 21% at $\rho \approx 0.346$, 70% at $\rho \approx 0.538$, and 100% at $\rho \approx 0.923$ and $\rho = 1$. Thus, for this frame size and fixed proportion of ambiguous observations, the $L1$–$HD$ overlap changes substantially with the number of distinct ambiguous subsets represented in the data.

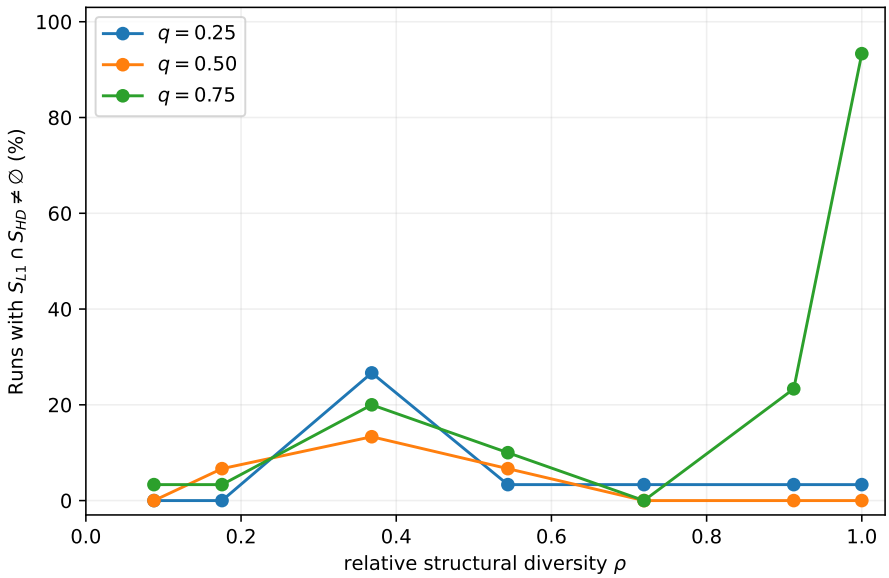



Figure 2: Percentage of runs with $S_{L1} \cap S_{HD} \neq \emptyset$ for $|\Omega| = 6$. The curves correspond to different fixed proportions $q$ of ambiguous observations.

As the overlap becomes more frequent, the previously observed inclusion

$$S_{HD} \subseteq S_{L1}$$

appears frequently, whereas crossing occurs only in a small fraction of the transition cases. The inclusion observed in the preliminary experiments is therefore visible again, although the discriminating example has already shown that it is not a general property.

The six-element case shows that $\rho$ alone is not sufficient to determine the relation; see Figure 2. In particular, even at full subset coverage, $\rho = 1$, the relation changes substantially with $q$.

Table 3 gives the relations observed at $\rho = 1$. The categories shown are mutually exclusive. No reverse proper inclusion $S_{L1} \subsetneq S_{HD}$ occurred at full coverage and is therefore omitted from the table.

The contrast is particularly clear for $|\Omega| = 6$. At $q = 0.50$, the two optimal faces are disjoint in all 30 runs, whereas at $q = 0.75$ they intersect in 28 of the 30 runs. Thus, even for the same frame and complete coverage of all nonsingleton subsets, changing the proportion of ambiguous observations can substantially change the relation between the optimal faces.

At $N = 500$ and $\rho = 1$, the values $q = 0.25, 0.50$, and $0.75$ correspond to 125, 250, and 375 ambiguous observations. For $|\Omega| = 6$, these observations are distributed over all 57 nonsingleton subsets, giving on average approximately 2.19, 4.39, and 6.58 observations per subset, respectively. The high overlap at $q = 0.75$ therefore cannot be attributed to a sparse allocation of observations over the ambiguous subsets.

| $\lvert\Omega\rvert$ | $q$ | disjoint | equal | $S_{HD} \subsetneq S_{L1}$ | crossing |
|---|---|---|---|---|---|
| 4 | 0.25 | 0 | 83.0 | 17.0 | 0 |
| 4 | 0.50 | 0 | 100 | 0 | 0 |
| 4 | 0.75 | 0 | 100 | 0 | 0 |
| 5 | 0.25 | 27.0 | 58.5 | 14.5 | 0 |
| 5 | 0.50 | 0 | 74.0 | 26.0 | 0 |
| 5 | 0.75 | 0 | 100 | 0 | 0 |
| 6 | 0.25 | 96.7 | 0 | 3.3 | 0 |
| 6 | 0.50 | 100 | 0 | 0 | 0 |
| 6 | 0.75 | 6.7 | 53.3 | 40.0 | 0 |

Table 3: Percentage of runs in each observed $HD$–$L1$ relation at full nonsingleton-subset coverage, $\rho = 1$.

Increasing $q$, however, simultaneously increases the number of ambiguous observations and reduces the number of precise singleton observations. The present experiment does not separate these two effects and therefore does not identify which of them is responsible for the observed change.

Taken together, the results show that neither $q$ nor $\rho$ alone is sufficient to characterize the relation between the $L1$- and $HD$-optimal faces. At fixed $q$, the relation changes with subset coverage, while at fixed full coverage it changes with $q$.

## 3.4 Size and uniqueness of the optimal faces

So far, we have compared the mutual position of the $L1$- and $HD$-optimal faces. A different question is how strongly each of the three criteria restricts the set of optimal belief functions. We describe this by the number of optimal vertices $|S_C|$ and the affine dimension $\dim \mathcal{F}_C$.

Table 4 gives representative results for $q = 0.50$, at approximately one-half and at full nonsingleton-subset coverage.

| | | $L1$ | | $HD$ | | $CW$ | |
|---|---|---|---|---|---|---|---|
| $\lvert\Omega\rvert$ | $\rho$ | mean $\lvert S\rvert$ | mean dim. | mean $\lvert S\rvert$ | mean dim. | mean $\lvert S\rvert$ | mean dim. |
| 4 | 54.5% | 5.38 | 2.86 | 3.67 | 1.91 | 1.22 | 0.20 |
| 4 | 100.0% | 1.00 | 0.00 | 1.00 | 0.00 | 1.00 | 0.00 |
| 5 | 53.8% | 5.62 | 2.44 | 2.76 | 1.20 | 1.27 | 0.23 |
| 5 | 100.0% | 1.82 | 0.78 | 1.02 | 0.02 | 1.00 | 0.00 |
| 6 | 54.4% | 209.00 | 5.40 | 2.53 | 0.83 | 3.17 | 0.67 |
| 6 | 100.0% | 43.73 | 3.97 | 2.50 | 1.03 | 1.10 | 0.10 |

Table 4: Mean number of optimal vertices and mean affine dimension for $q = 0.50$, at approximately one-half and full nonsingleton-subset coverage.

For the settings shown in the table, the $L1$-optimal face is typically larger than the $HD$- and $CW$-optimal faces. The difference is particularly pronounced for $|\Omega| = 6$. At the intermediate coverage level, the $L1$-optimal face contains on average 209 vertices, compared with 2.53 for $HD$ and 3.17 for $CW$. Even at full coverage, $L1$ has on average 43.73 optimal vertices, whereas the corresponding averages are 2.50 and 1.10 for $HD$ and $CW$.

The same difference appears when uniqueness is evaluated over the complete controlled

experiment. For $|\Omega| = 4, 5$, and 6, respectively, $L1$ has a unique optimal vertex in 34.3%, 30.5%, and 11.0% of the runs. The corresponding percentages are 34.3%, 32.8%, and 41.4% for $HD$, and 70.7%, 80.3%, and 76.7% for $CW$.

For $|\Omega| = 6$, the median numbers of optimal vertices over the complete experiment are 10, 2, and 1 for $L1$, $HD$, and $CW$, respectively. Thus, the criteria differ not only in which belief functions they prefer, but also in the degree to which they identify a particular solution. In these experiments, $CW$ most frequently produces a unique optimal vertex, whereas $L1$ can leave a substantially larger set of equally optimal belief functions.

### 3.5 Precise observations

The preceding experiments investigated the role of ambiguity in the observations. To separate this source of uncertainty from the statistical uncertainty involved in estimating the lower confidence bounds, we now consider a control regime in which every observation is precise. Setting $\rho = 0$ implies $q = 0$, so all observations are singletons. This case should therefore not be interpreted as the left endpoint of the preceding curves, which were obtained for fixed positive values of $q$.

We next ask whether $L1$ and $HD$ can still select different belief functions in the absence of observational ambiguity, and whether their difference changes as the sample size increases. For uniform precise-data cases, we repeated the construction for

$$N \in 50, 100, 200, 500, 1000, 5000.$$

Figure 3 shows the $L_1$ distance between the $L1$- and $HD$-optimal BPAs. For $|\Omega| = 4$, the two criteria have the same optimum for every tested $N$. For $|\Omega| = 5$ and 6, the optima remain distinct unique vertices throughout the tested range, while their numerical distance decreases.

The $L_1$ distance used in the figure is

$$\sum_{\emptyset \neq A \subseteq \Omega} |m_{L1}(A) - m_{HD}(A)| .$$

For $|\Omega| = 5$, this distance decreases from 0.1124 at $N = 50$ to 0.0194 at $N = 5000$. For $|\Omega| = 6$, the corresponding distance decreases from 0.0390 to 0.0086.

Thus, observational ambiguity is not necessary for $L1$ and $HD$ to select different belief functions. Distinct optima can remain even when every observation is precise, showing that the construction of the data-derived confidence bounds provides an additional statistical source of uncertainty. In the uniform cases studied here, the numerical difference between the two optima decreases as $N$ increases. This empirical behaviour does not, however, establish a convergence result.

## 4 Discussion and conclusions

This study was motivated by a simple fact: a single solution returned by linear optimization does not necessarily represent the complete optimum. A linear criterion may attain

# Comparison of Parametric Models for Dominance-based Rough Set Approach

**Yoshifumi Kusunoki**

Graduate School of Informatics
Osaka Metropolitan University
yoshifumi.kusunoki@omu.ac.jp

**Abstract**

The dominance-based rough set approach (DRSA) is a framework for analyzing inconsistency in preference data. To tolerate inconsistency, several parametric models of DRSA have been proposed, such as variable-precision DRSA (VP-DRSA) and isotonic regression. In this paper, we extend to DRSA a probabilistic model for rough sets based on Bayesian learning, which was previously proposed for the classical rough set approach. We then compare the maximum likelihood estimation of this model with VP-DRSA and with isotonic regression. The three models coincide when the labels are consistent with the dominance relation. For VP-DRSA, we give a sufficient condition under which the optimal solution of the likelihood problem is expressed by the rough membership function. For isotonic regression, we show by a counterexample that the two models differ in general, and prove that they coincide when the dominance relation is a total order.

**Keywords:** Dominance-based Rough Set Approach; Variable-precision model; Isotonic regression; Bayesian learning

## 1 Introduction

Extracting the classification rules inherent in data is a central research topic in machine learning, and it is also an important theme in decision analysis. Whereas machine learning methods aim at objective predictive accuracy under the assumption of a probabilistic model, decision analysis requires describing the characteristics of the data. Therefore, transparency and explainability of data analysis methods are emphasized.

The rough set approach has attracted attention in decision analysis. It is a mathematical framework for handling logical uncertainty arising from inconsistency between *relations* (binary relations) and data. Through the definition of a relation, users can flexibly incorporate their knowledge. It provides transparent methods based on relatively simple principles, which make the analysis process easy to understand.

Recently, in order to improve the prediction accuracy of the rough set approach, we have studied the incorporation of Bayesian learning [5], a machine learning approach based on probabilistic inference. In that study, Bayesian learning was introduced into the classical rough set model, and a probabilistic model reflecting the indiscernibility relation was defined. In this paper, we extend this approach to the dominance-based rough set approach (DRSA) [2], an extension of the rough set approach to preference datasets. Because the dominance relation lacks symmetry, the probabilistic model must be modified.

The probabilistic model for DRSA can be regarded as a parametric rough set model. Several parametric models for DRSA exist. The best-known is variable-consistency DRSA (VC-DRSA) [1]. VC-DRSA tolerates a certain amount of inconsistency by using a rough membership function and a threshold. Variable-precision DRSA (VP-DRSA) [3] is similar to VC-DRSA except that it uses a different membership function. Kusunoki et al. [6] provided a statistical interpretation of VP-DRSA. Isotonic regression [4] is also a well-known parametric model for DRSA, although it arises in a different context. It gives a membership function via a regression problem with order constraints.

Another objective of this study is to compare the probabilistic model for DRSA with existing parametric models. The comparison is made with VP-DRSA and isotonic regression, since both are naturally aligned with statistical error minimization. These three models are generally different; however, we propose sufficient conditions under which the probabilistic model becomes equivalent to each of the other two.

This paper is organized as follows. Section 2 introduces the parametric models for DRSA compared in this study, and ends with the proposed probabilistic model for DRSA. Section 3 compares the probabilistic model with VP-DRSA and isotonic regression, and gives sufficient conditions under which the probabilistic model coincides with the other models. Finally, Section 4 concludes the paper.

# 2 Parametric Models for Dominance-based Rough Set Approach

## 2.1 Dominance-based Rough Set Approach

DRSA (Dominance-based Rough Set Approach) is a mathematical model for dealing with inconsistency in preference data. We consider multicriteria classification (sorting) problems. Let $A = \{a_1, a_2, \ldots, a_n\}$ be a set of criteria (attributes), and $U = \{u_1, u_2, \ldots, u_m\}$ be a set of objects. Each object $u_i$ is evaluated by the criteria. For each criterion $a_j$, the value of $u_i$ is denoted by $a_j(u_i)$. The range of each criterion $a_j$ is equipped with a total order. These orders induce a binary relation called the dominance relation. The dominance relation with respect to $B \subseteq A$ is defined as follows:

$$D_B = \{(u, u') \in U \times U \mid a(u) \geq a(u') \text{ for all } a \in B\}. \tag{1}$$

For each object $u \in U$, we define the set of objects dominating $u$ and the set of objects dominated by $u$ as follows:

$$D_B^+(u) = \{u' \in U \mid (u', u) \in D_B\}, \quad D_B^-(u) = \{u' \in U \mid (u, u') \in D_B\}. \tag{2}$$

Let $d$ be a decision attribute, which is a function of objects. It takes finitely many values $d_1, d_2, \ldots, d_p$. We call them labels (or decision classes); they are the targets to be estimated in a classification problem. The set of labels is also equipped with a total order: $d_1 \leq d_2 \leq \cdots \leq d_p$. We assume a monotone relationship between the criteria and the decision attribute, called the dominance principle: for a given set of criteria $B$,

> If $a(u) \geq a(u')$ holds for every $a \in B$ then $d(u) \geq d(u')$ is necessarily satisfied.

Let $Y_1, Y_2, \ldots, Y_p$ be the partition of $U$ induced by the decision attribute, that is, $Y_k = \{u \in U \mid d(u) = d_k\}$. Each $Y_k$ is called a decision class. The upward union of $Y_k$, denoted by $Y_k^{\geq}$, is the union of $Y_k, Y_{k+1}, \ldots, Y_p$. Similarly, the downward union $Y_k^{\leq}$ is the union of $Y_1, \ldots, Y_{k-1}, Y_k$. In practice, a decision class may be inconsistent with the dominance principle for a given set of criteria. Let $B \subseteq A$. $Y_k^{\geq}$ is expressed by a pair of object subsets, called the lower and upper approximations, which are defined respectively as follows:

$$\underline{B}(Y_k^{\geq}) = \{u \in U \mid D_B^+(u) \subseteq Y_k\}, \quad \overline{B}(Y_k^{\geq}) = \{u \in U \mid D_B^-(u) \cap Y_k \neq \emptyset\}. \tag{3}$$

The lower and upper approximations of $Y_k^{\leq}$ are defined in the same way except that $D_B^+$ and $D_B^-$ are swapped.

Using the lower and upper approximations, attribute reduction is performed in order to generalize the classification rules induced by the dominance relation. For example, using the dominance relation $D_B$ with respect to $B \subseteq A$, an unseen object $u_*$ is classified into $Y_k^{\geq}$ or $Y_{k-1}^{\leq}$ by the following rules:

$$(u_*, u) \in D_B \text{ for } \exists u \in \underline{B}(Y_k^{\geq}) \implies u_* \in Y_k^{\geq},$$
$$(u, u_*) \in D_B \text{ for } \exists u \in \underline{B}(Y_{k-1}^{\leq}) \implies u_* \in Y_{k-1}^{\leq}.$$

The original DRSA strictly follows the dominance principle. Hence, the approximations deteriorate when the dataset is highly inconsistent. For this reason, many authors have studied parametric versions of DRSA.

In the remainder of this paper, we consider binary classification problems, that is, the case of $p = 2$. In this case, the upward and downward unions reduce to two classes, $Y_2^{\geq}$ and $Y_1^{\leq}$, which we denote by $Y^{\geq}$ and $Y^{<}$ for simplicity. Moreover, since the attribute subset is fixed throughout the discussion, the symbol $B$ is omitted from the dominance relation and the approximations. The lower and upper approximations of $Y^{\geq}$ (resp. $Y^{<}$) are denoted by $\underline{Y}^{\geq}$ and $\overline{Y}^{\geq}$ (resp. $\underline{Y}^{<}$ and $\overline{Y}^{<}$), respectively.

## 2.2 Variable-precision DRSA

VP-DRSA (Variable-precision DRSA) [3] is a parametric extension of DRSA. It follows the variable precision rough set model: in the definition of the approximations, a certain degree of inconsistency is tolerated by introducing a rough membership function and a threshold. For each object $u \in U$, the rough membership function of $u$ for $Y^{\geq}$ is defined as follows:

$$\mu^{\geq}(u) = \frac{|Y^{\geq} \cap D^{-}(u)|}{|Y^{\geq} \cap D^{-}(u)| + |Y^{<} \cap D^{+}(u)|}. \tag{4}$$

The rough membership function for $Y^{<}$ is defined by $\mu^{<}(u) = 1 - \mu^{\geq}(u)$. The objects in $Y^{\geq}$ that are dominated by $u$ provide evidence for $u \in Y^{\geq}$. Conversely, the objects in $Y^{<}$ that dominate $u$ provide evidence against $u \in Y^{\geq}$.

$\mu^{\geq}$ (and also $\mu^{<}$) is monotone with respect to the dominance relation. That is, $\mu^{\geq}(u) \geq \mu^{\geq}(u')$ ($\mu^{<}(u) \leq \mu^{<}(u')$) if $(u, u') \in D$. This property is desirable in the context of classification.

Given the rough membership function and a threshold $\alpha \in [0, 0.5)$, we define the lower and upper approximations of $X^{\geq}$ in VP-DRSA as follows:

$$\underline{X}^{\geq}_{\alpha} = \{u \in U \mid \mu^{\geq}(u) \geq 1 - \alpha\}, \quad \overline{X}^{\geq}_{\alpha} = \{u \in U \mid \mu^{\geq}(u) > \alpha\}. \tag{5}$$

The lower and upper approximations of $X^{<}$ are defined in the same manner. We have $\underline{X}^{\geq}_{\alpha} = U \setminus \overline{X}^{<}_{\alpha}$.

Kusunoki et al. [6] proposed a statistical perspective on VP-DRSA. A subset of objects $W \subseteq U$ is called a classifier if it is consistent with the dominance relation, that is, if $(u, u') \in D$ implies that $u \notin W$ and $u' \in W$ cannot hold simultaneously. Given a classifier $W$ and moreover positive values $\lambda_W$ and $\lambda_{\bar{W}}$, we define a score function of $W$ as follows:

$$f_W(u) = \begin{cases} \lambda_W |D^{-}(u) \cap W| & u \in W, \\ -\lambda_{\bar{W}} |D^{+}(u) \setminus W| & u \notin W. \end{cases} \tag{6}$$

$f_W(u)$ can be regarded as the signed distance from the classification boundary to $u$. $\lambda_W$ and $\lambda_{\bar{W}}$ are the magnitudes of their respective slopes. Additionally, let $y : U \to \{0, 1\}$ be the support function of $Y^{\geq}$, that is, $y(u) = 1$ iff $u \in Y^{\geq}$.

Combining the hinge loss with the score function, we formulate a minimization problem of the loss function:

$$\begin{aligned} \underset{W}{\text{minimize}} \quad & \sum_{u \in U} \max\{0, -y(u) f_W(u)\} \\ \text{subject to} \quad & W \text{ is consistent with } D, \end{aligned} \tag{7}$$

Considering the cases in the definition of $f_W$, the above optimization problem is reformulated as follows:

$$\begin{aligned} \underset{W}{\text{minimize}} \quad & \sum_{u \in Y^{\geq} \setminus W} \lambda_{\bar{W}} |D^{+}(u) \setminus W| + \sum_{u \in Y^{<} \cap W} \lambda_W |D^{-}(u) \cap W| \\ \text{subject to} \quad & W \text{ is consistent with } D. \end{aligned} \tag{8}$$

With the rough membership function of VP-DRSA, this minimization problem has the following closed-form optimal solution:

$$W = \{u \in U \mid \mu^{\geq}(u) \geq \lambda_{\bar{W}}/(\lambda_{\bar{W}} + \lambda_W)\}.$$

## 2.3 Isotonic Regression

Let $y$ be the support function of $Y^{\geq}$. Isotonic regression is another parametric model for DRSA. A function $\pi^\star : U \to \mathbb{R}$ is called an isotonic regression of $y$ if it is an optimal solution of the following minimization problem:

$$\begin{array}{ll} \underset{\pi}{\text{minimize}} & \displaystyle\sum_{u \in U} (\pi(u) - y(u))^2 \\ \text{subject to} & \pi(u) \geq \pi(u') \text{ for } (u, u') \in D. \end{array} \tag{9}$$

As discussed in [4], when $y(U) \subseteq [0, 1]$, the above minimization problem is equivalent to the following one:

$$\begin{array}{ll} \underset{\pi}{\text{minimize}} & \displaystyle -\sum_{u \in U} (y(u) \log \pi(u) + (1 - y(u)) \log(1 - \pi(u))) \\ \text{subject to} & \pi(u) \geq \pi(u') \text{ for } (u, u') \in D, \\ & \pi(u) \in [0, 1],\ u \in U. \end{array} \tag{10}$$

Only the objective function has changed; the latter is called the cross-entropy.

The isotonic regression $\pi^\star$ has the following property. Let $V$ be the range of $\pi^\star$. For each $v \in V$, consider the level set of $\pi^\star$ at $v$, namely, $(\pi^\star)^{-1}(v)$. Then, the average of $y(u)$ over $u \in (\pi^\star)^{-1}(v)$ coincides with $v$.

## 2.4 Probabilistic Model for DRSA

Recently, the author of [5] proposed a probabilistic model for classical rough sets. In this paper, we extend the above probabilistic model to DRSA. Let $\boldsymbol{y} \in \{0, 1\}^m$ be the vector corresponding to the support function of $Y^{\geq}$, that is, $y_i = 1$ iff $u_i \in Y^{\geq}$. Let $\boldsymbol{D} \in \{0, 1\}^{m \times m}$ be the matrix corresponding to the dominance relation $D$, that is, its $(i, j)$ component, denoted by $d_{i,j}$, is 1 iff $(u_i, u_j) \in D$. The $i$-th row vector of $\boldsymbol{D}$ is denoted by $\boldsymbol{d}_i^-$, and the $i$-th column vector of $\boldsymbol{D}$ is denoted by $\boldsymbol{d}_i^+$.

The probability of $y_i = 1$ is defined as follows:

$$\rho_i = \phi(\boldsymbol{d}_i^{-\top} \boldsymbol{w}^+ - \boldsymbol{d}_i^+ \boldsymbol{w}^-) = \frac{1}{1 + \exp(-(\boldsymbol{d}_i^{-\top} \boldsymbol{w}^+ - \boldsymbol{d}_i^+ \boldsymbol{w}^-))}, \tag{11}$$

where $\phi$ is the logistic function, and $\boldsymbol{w}^+$ and $\boldsymbol{w}^-$ are vectors of size $m$, and their components are defined by $w_i^+ = \max\{0, \boldsymbol{w}\}$ and $w_i^- = \max\{0, -w_i\}$. Hence, $p(y_i | \boldsymbol{w}, \boldsymbol{R})$ is defined by

$$p(y_i | \boldsymbol{w}, \boldsymbol{d}_i^-, \boldsymbol{d}_i^+) = \rho_i^{y_i} (1 - \rho_i)^{1 - y_i}. \tag{12}$$

The label $y_i$ tends to be 1 when the weights of the objects dominated by $u_i$ are likely to be positive, and it tends to be 0 when the weights of the objects dominating $u_i$ are likely to be negative.

Given a prior probability of $\boldsymbol{w}$, the joint probability of $\boldsymbol{y}$ and $\boldsymbol{w}$ is defined as follows:

$$p(\boldsymbol{y}, \boldsymbol{w}|\boldsymbol{D}) = \prod_{i \in U} p(y_i|\boldsymbol{w}, \boldsymbol{d}_i^-, \boldsymbol{d}_i^+) p(\boldsymbol{w}). \tag{13}$$

Using Bayes' theorem, we obtain the posterior probability of $\boldsymbol{w}$:

$$p(\boldsymbol{w}|\boldsymbol{y}, \boldsymbol{D}) = \frac{p(\boldsymbol{y}, \boldsymbol{w}|\boldsymbol{D})}{p(\boldsymbol{y}|\boldsymbol{D})} = \frac{p(\boldsymbol{y}|\boldsymbol{w}, \boldsymbol{D}) p(\boldsymbol{w})}{p(\boldsymbol{y}|\boldsymbol{D})}. \tag{14}$$

In the previous work, we estimate the weight vector $\boldsymbol{w}$ by MAP (maximum a posteriori). On the other hand, in the following subsections, we compare the likelihood estimation of (12) with VP-DRSA and the isotonic regression.

$$\begin{aligned} \underset{\boldsymbol{w}}{\text{minimize}} \quad & -\sum_{i \in U} (y_i \log \rho_i + (1 - y_i) \log(1 - \rho_i) \\ \text{subject to} \quad & \rho_i = \phi(\boldsymbol{d}_i^{-\top} \boldsymbol{w}^+ - \boldsymbol{d}_i^{+\top} \boldsymbol{w}^-),\ i \in U, \\ & w_i^+ = \max\{0, w_i\},\ w_i^- = \max\{0, -w_i\},\ i \in U. \end{aligned} \tag{15}$$

Let $\boldsymbol{\mu} = [\mu_1, \mu_2, \ldots, \mu_m]^\top$ be the vector corresponding to the rough membership function (4), that is, $\mu_i = \mu^{\geq}(u_i)$. Let $\boldsymbol{\pi}^\star = [\pi_1^\star, \pi_2^\star, \ldots, \pi_m^\star]^\top$ be the vector corresponding to the optimal solution of the isotonic regression problem (10), that is, $\pi_i^\star = \pi^\star(u_i)$. Let $\boldsymbol{\rho}^\star = [\rho_1^\star, \rho_2^\star, \ldots, \rho_m^\star]^\top$ be the optimal solution of the likelihood problem (15).

First, the three models coincide when the labels are consistent with the dominance relation.

**Proposition 1.** *When* $(u_i, u_j) \in D \implies y_i \geq y_j$ *for all* $i, j \in U$*, we have*

$$\mu_i = \pi_i^\star = \rho_i^\star = y_i \text{ for all } i \in U.$$

Note that in this case, $|\boldsymbol{d}_i^{-\top} \boldsymbol{w}^+ - \boldsymbol{d}_i^{+\top} \boldsymbol{w}^-| \to \infty$, and hence $\boldsymbol{w}$ diverges.

# 3 Comparison of Parametric Models for DRSA

## 3.1 Comparison with VP-DRSA

We compare the likelihood model (15) with the membership function of VP-DRSA (4). We redefine the probability $\boldsymbol{\rho}$ in (11) with a fixed positive parameter $\alpha$, and express it in the last form below.

$$\rho_i^\alpha = \frac{1}{1 + \exp(-\alpha(\boldsymbol{r}^{-\top} \boldsymbol{w}^+ - \boldsymbol{r}_i^{+\top} \boldsymbol{w}^-))} = \frac{\exp(-\alpha \boldsymbol{r}_i^{+\top} \boldsymbol{w}^-)}{\exp(-\alpha \boldsymbol{r}_i^{+\top} \boldsymbol{w}^-) + \exp(-\alpha \boldsymbol{r}_i^{-\top} \boldsymbol{w}^+)}.$$

Then, the probabilistic model is expressed as follows:

$$p(\boldsymbol{y}|\boldsymbol{w},\boldsymbol{D}) = \prod_{i\in U}(\rho_i^{\alpha})^{y_i}(1-\rho_i^{\alpha})^{1-y_i} = \prod_{i\in U}\frac{\exp(-\alpha \boldsymbol{r}_i^{+\top}\boldsymbol{w}^-)^{y_i}\exp(-\alpha \boldsymbol{r}_i^{-\top}\boldsymbol{w}^+)^{1-y_i}}{\exp(-\alpha \boldsymbol{r}_i^{+\top}\boldsymbol{w}^-)+\exp(-\alpha \boldsymbol{r}_i^{-\top}\boldsymbol{w}^+)}.$$

We consider the negative log-likelihood $-\frac{1}{\alpha}\log p(\boldsymbol{y}|\boldsymbol{w},\boldsymbol{R})$, which is reformulated as follows:

$$\begin{aligned}
&-\frac{1}{\alpha}\log p(\boldsymbol{y}|\boldsymbol{w},\boldsymbol{D})\\
&=\sum_{i\in U}\left(y_i \boldsymbol{d}_i^{+\top}\boldsymbol{w}^- + (1-y_i)\boldsymbol{d}_i^{-\top}\boldsymbol{w}^+\right)\\
&\qquad\qquad +\frac{1}{\alpha}\log\prod_{i\in U}\Big(\exp(-\alpha \boldsymbol{d}_i^{+\top}\boldsymbol{w}^-)+\exp(-\alpha \boldsymbol{d}_i^{-\top}\boldsymbol{w}^+)\Big)\\
&=\sum_{i\in U}\left(y_i \boldsymbol{d}_i^{+\top}\boldsymbol{w}^- + (1-y_i)\boldsymbol{d}_i^{-\top}\boldsymbol{w}^+\right)\\
&\qquad\qquad +\frac{1}{\alpha}\log\sum_{\boldsymbol{s}\in\{0,1\}^m}\exp\left(-\alpha\sum_{i\in U}\Big(s_i \boldsymbol{d}_i^{+\top}\boldsymbol{w}^- + (1-s_i)\boldsymbol{d}_i^{-\top}\boldsymbol{w}^+\Big)\right)
\end{aligned} \tag{16}$$

Assume that $\boldsymbol{w}$ is a $\{-1,1\}$ vector consistent with the dominance relation $D$, that is, $d_{i,j}=1 \implies w_i \geq w_j$. Then, identifying $\boldsymbol{w}$ with $W$, the first term coincides with the objective function of (8), for the following reason:

$$\boldsymbol{d}_i^{+\top}\boldsymbol{w}^- = |D^+(u_i)\setminus W|, \quad \boldsymbol{d}_i^{-\top}\boldsymbol{w}^+ = |D^-(u_i)\cap W|. \tag{17}$$

Here, we set $\lambda_W = \lambda_{\bar{W}} = 1$.

If the second term of (16) is close to 0, the maximum likelihood estimator coincides with the minimizer of the empirical risk (8). The following proposition is useful for deriving a sufficient condition.

**Proposition 2.** *Suppose that $\boldsymbol{w}$ satisfies the following condition:*

$$d_{i,j}=1 \implies w_i \geq w_j \text{ for every } i,j\in U.$$

*Then, we have*

$$0 \leq \frac{1}{\alpha}\log\sum_{\boldsymbol{s}\in\{0,1\}^m}\exp\left(-\alpha\sum_{j\in U}(s_i \boldsymbol{d}_i^{+\top}\boldsymbol{w}^- + (1-s_i)\boldsymbol{d}_i^{-\top}\boldsymbol{w}^+)\right) \leq \frac{m\log 2}{\alpha}.$$

*Proof.* Let $L(\boldsymbol{s}) = \sum_{i\in U}(s_i \boldsymbol{d}_i^{+\top}\boldsymbol{w}^- + (1-s_i)\boldsymbol{d}_i^{-\top}\boldsymbol{w}^+)$. In general, we have the following inequality.

$$\max_{\boldsymbol{s}\in\{0,1\}^m} -L(\boldsymbol{s}) \leq \frac{1}{\alpha}\log\sum_{\boldsymbol{s}\in\{0,1\}^m}\exp(-\alpha L(\boldsymbol{s})) \leq \max_{\boldsymbol{s}\in\{0,1\}^m} -L(\boldsymbol{s}) + \frac{m\log 2}{\alpha}$$

Because all terms in the summation are nonnegative, we have $L(\boldsymbol{s}) \geq 0$. We obtain $L(\boldsymbol{s}) = 0$ when $s_i = 1$ iff $w_i > 0$ for each $i = 1, \ldots, m$. In this case, the following equation holds.

$$\begin{aligned}
L(\boldsymbol{s}) &= \sum_{i \in U} (s_i \boldsymbol{d}_i^{+\top} \boldsymbol{w}^- + (1 - s_i) \boldsymbol{d}_i^{-\top} \boldsymbol{w}^+) \\
&= \sum_{i \in U} s_i \sum_{j \in U} d_{j,i} w_j^- + \sum_{i \in U} (1 - s_i) \sum_{j \in U} d_{i,j} w_j^+ \\
&= \sum_{i \in U} \sum_{j \in U} d_{j,i} s_i (s_j - 1) w_j + \sum_{i \in U} \sum_{j \in U} d_{i,j} (1 - s_i) s_j w_j \\
&= - \sum_{i \in U} \sum_{j \in U} d_{i,j} s_j (1 - s_i) w_i + \sum_{i \in U} \sum_{j \in U} d_{i,j} (1 - s_i) s_j w_j \\
&= \sum_{i \in U} \sum_{j \in U} d_{i,j} s_j (1 - s_i)(w_j - w_i).
\end{aligned}$$

$d_{i,j} s_j (1 - s_i) > 0$ only if $d_{i,j} = 1$ and $w_j > 0 \geq w_i$, which contradicts the assumption. □

If $w_i \in \{-1, 1\}$ and $\alpha$ is sufficiently large, the second term of (16) can be ignored.

**Proposition 3.** *Suppose that* $d_{i,j} = 1 \implies w_i \geq w_j$ *and* $w_i \in \{-1, 1\}$ *for every* $i \in U$. *Moreover, we assume*

$$\alpha > m \log 2.$$

*Then, we have*

$$\operatorname*{argmax}_{\boldsymbol{w}} \log p(\boldsymbol{y} | \boldsymbol{w}, \boldsymbol{D}) \subseteq \operatorname*{argmin}_{\boldsymbol{w}} \sum_{i \in U} (y_i \boldsymbol{d}_i^{+\top} \boldsymbol{w}^- + (1 - y_i) \boldsymbol{d}_i^{-\top} \boldsymbol{w}^+).$$

*Proof.* $L_1(\boldsymbol{w})$ and $L_2(\boldsymbol{w})$ denotes the first and second term of (16), respectively, that is

$$L_1(\boldsymbol{w}) = \sum_{i \in U} (y_i \boldsymbol{d}_i^{+\top} \boldsymbol{w}^- + (1 - y_i) \boldsymbol{d}_i^{-\top} \boldsymbol{w}^+),$$

$$L_2(\boldsymbol{w}) = \frac{1}{\alpha} \log \sum_{\boldsymbol{s} \in \{0,1\}^m} \exp \left( -\alpha \sum_{i \in U} (s_i \boldsymbol{d}_i^{+\top} \boldsymbol{w}^- + (1 - s_i) \boldsymbol{d}_i^{-\top} \boldsymbol{w}^+) \right).$$

Let $\boldsymbol{w}^\star$ be one of the optima of $L_1(\boldsymbol{w})$, and let $L_1^\star = L_1(\boldsymbol{w}^\star)$. Since $L_1(\boldsymbol{w})$ takes only integer values, if $\boldsymbol{w}$ is not optimal for $L_1(\boldsymbol{w})$, then we have

$$L_1(\boldsymbol{w}) \geq L_1(\boldsymbol{w}^\star) + 1 > L_1(\boldsymbol{w}^\star) + \frac{m \log 2}{\alpha}.$$

Since $0 \leq L_2(\boldsymbol{w}) \leq m \log 2 / \alpha$, we have

$$L_1(\boldsymbol{w}) + L_2(\boldsymbol{w}) \geq L_1(\boldsymbol{w}) > L_1(\boldsymbol{w}^\star) + \frac{m \log 2}{\alpha} \geq L_1(\boldsymbol{w}^\star) + L_2(\boldsymbol{w}^\star).$$

Therefore, if $\boldsymbol{w}$ is not a minimizer for $L_1(\boldsymbol{w})$, then it is not a maximizer for $\log p(\boldsymbol{y} | \boldsymbol{w}, \boldsymbol{D})$ either.

□

Using the above proposition, we show the connection between the probabilistic model and VP-DRSA.

**Corollary 1.** *Let $\mu_i = \mu^{\geq}(u_i)$ be the membership values in VP-DRSA, where $\mu^{\geq}$ is defined in* (4)*, and suppose $\mu_i \neq 1/2$ for all $i = 1, \ldots, m$ and $\alpha > m \log 2$. Consider the minimization of* (16) *under the conditions that $d_{i,j} = 1 \implies w_i \geq w_j$ and $w_i \in \{-1, 1\}$. Then, the optimum of* (16) *is given as follows:*

$$w_i = \begin{cases} -1 & \mu_i < 1/2, \\ 1 & \mu_i > 1/2. \end{cases}$$

Note that when $\mu_i \neq 1/2$ for all $i \in U$, the first term of (16) has a unique minimizer.

## 3.2 Comparison with Isotonic Regression

Here, we compare the isotonic regression (10) with the likelihood estimation (15). We use the above-mentioned notation $y_i = y(u_i)$ and $\pi_i = \pi(u_i)$ in (10).

In general, they do not coincide. Consider three objects $u_1, u_2, u_3$ whose dominance relation is given as follows:

$$\boldsymbol{D} = \begin{bmatrix} 1 & 1 & 1 \\ 0 & 1 & 0 \\ 0 & 0 & 1 \end{bmatrix}.$$

The labels are $y_1 = 0$ and $y_2 = y_3 = 1$.

Consider the KKT conditions of (10). Assuming $\pi = \pi_1 = \pi_2 = \pi_3 \in (0, 1)$, we have

$$\frac{1}{\pi} - \alpha_1 - \alpha_2 = 0, \quad -\frac{1}{1-\pi} + \alpha_1 = 0, \quad -\frac{1}{1-\pi} + \alpha_2 = 0, \quad \alpha_1 > 0,\ \alpha_2 > 0,$$

where $\alpha_1$ and $\alpha_2$ are the multipliers for $\pi_1 \geq \pi_2$ and $\pi_1 \geq \pi_3$. As a result, we obtain $\pi = 2/3$.

Let $b = \phi^{-1}(2/3)$. On the other hand, we show that $\boldsymbol{d}_i^{-\top} \boldsymbol{w}^+ - \boldsymbol{d}_i^{+\top} \boldsymbol{w}^- = b$ cannot hold for all $u_i \in U$. We use Farkas' lemma. The above system of equations is written in matrix form as $\boldsymbol{D}\boldsymbol{w}^+ - \boldsymbol{D}^\top \boldsymbol{w}^- = \boldsymbol{b}$, where $\boldsymbol{b}$ is a vector of size $m$ all of whose elements equal $b$. We assume $\boldsymbol{w}^+$ and $\boldsymbol{w}^-$ are independent. Let $\boldsymbol{A} = [\boldsymbol{D} \ -\boldsymbol{D}^\top]$, and $\boldsymbol{z} = [1, -1, -1]^\top$. Then, $\boldsymbol{z}^\top \boldsymbol{A} \geq 0$ and $\boldsymbol{z}^\top \boldsymbol{b} = -\phi^{-1}(2/3) < 0$. Therefore, there does not exist a nonnegative vector $\boldsymbol{w}' = [\boldsymbol{w}^+; \boldsymbol{w}^-]$ such that $\boldsymbol{A}\boldsymbol{w}' = \boldsymbol{b}$. Hence, the optimum of (15) does not produce $\rho_1 = \rho_2 = \rho_3 = 2/3$.

On the other hand, when $\boldsymbol{D}$ represents a total order, the optimal solutions of both problems coincide.

**Proposition 4.** *Assume that $\boldsymbol{D}$ represents a total order, that is, with a suitable ordering of the objects, it is an upper triangular matrix whose upper-triangular entries are all one. Then, the optimal solutions* (10) *and* (15) *coincide, that is, $\boldsymbol{\pi}^\star = \boldsymbol{\rho}^\star$.*

*Proof.* Let $\boldsymbol{\pi}$ be a feasible solution of (10). Assume that its elements are arranged in descending order. Let $b_i = \phi^{-1}(\pi_i)$, and define the vector $\boldsymbol{b} = [b_1, \ldots, b_m]^\top$.

Let $k$ be the index such that $b_k$ is the minimum positive value. We define $w_k, w_{k+1}, \ldots, w_m$ as follows: $w_k = b_k$ and $w_i = b_i - b_{i-1}$ for every $i = k+1, \ldots, m$. As a result, we have $\sum_{j=k}^{i} w_j = b_i$ and $w_i \geq 0$ for all $i = k \ldots, m$. On the other hand, we define $w_{k-1}, w_{k-2}, \ldots, w_1$ as follows: $w_{k-1} = b_{k-1}$ and $w_i = b_i - b_{i+1}$ for every $i = k-2, \ldots, 1$. As a result, we have $\sum_{j=i}^{k-1} w_j = b_i$ and $w_i \leq 0$ for all $i = k-1, \ldots, 1$. We arrange the above elements into a vector $\boldsymbol{w}$. Then, we have $\boldsymbol{D}\boldsymbol{w}^+ - \boldsymbol{D}^\top \boldsymbol{w}^- = \boldsymbol{b}$.

Therefore, any feasible solution of (10) is also feasible in (15). This implies that the optima of both problems coincide.

□

# 4 Conclusions

In this study, we compared a probabilistic model for DRSA with VP-DRSA and isotonic regression. First, we extended to DRSA the probabilistic model that was proposed for the classical rough set approach. Then, we compared its maximum likelihood estimation with the rough membership function of VP-DRSA and with the isotonic regression. The three models are identical when the labels are consistent with the dominance relation: $d_{i,j} = 1 \implies y_i \geq y_j$ for all $u_i, u_j \in U$. For the comparison with VP-DRSA, we established a connection between the maximum likelihood estimation and VP-DRSA. We showed a sufficient condition under which the optimal solution of the maximum likelihood problem is expressed by the rough membership function. For the comparison with the isotonic regression, we showed that, in general, the probabilistic model cannot produce the same solution as the isotonic regression. On the other hand, when the dominance relation is a total order, they produce the same solution.

As future work, we will examine the MAP estimation of the probabilistic model for DRSA on synthetic and benchmark datasets.

# References

[1] Jerzy Błaszczyński, Salvatore Greco, Roman Słowiński, and Marcin Szeląg. Monotonic variable consistency rough set approaches. *International Journal of Approximate Reasoning*, 50(7):979–999, 2009.

[2] Salvatore Greco, Benedetto Matarazzo, and Roman Słowiński. Rough sets theory for multicriteria decision analysis. *European Journal of Operational Research*, 129(1):1–47, 2001.

[3] Masahiro Inuiguchi, Yukihiro Yoshioka, and Yoshifumi Kusunoki. Variable-precision dominance-based rough set approach and attribute reduction. *International Journal of Approximate Reasoning*, 50(8):1199–1214, 2009.

[4] Wojciech Kotłowski, Krzysztof Dembczyński, Salvatore Greco, and Roman Słowiński. Stochastic dominance-based rough set model for ordinal classification. *Information Sciences*, 178(21):4019–4037, 2008.

[5] Yoshifumi Kusunoki. A study on application of Bayesian learning in rough set approaches to data analysis. In *Proceedings of the 23rd Czech-Japan Seminar on Data Analysis and Decision Making under Uncertainty*, 2023.

[6] Yoshifumi Kusunoki, Jerzy Błaszczyński, Masahiro Inuiguchi, and Roman Słowiński. Empirical risk minimization for dominance-based rough set approaches. *Information Sciences*, 567:395–417, 2021.

# Shared Verifiable Local Policies for Multi-Agent Pathfinding

**Jakub Mestek**

Department of Theoretical Computer Science and Mathematical Logic
Charles University, Faculty of Mathematics and Physics
jakub.mestek@mff.cuni.cz

**Keywords:** multi-agent pathfinding, rule-based system

## 1 Introduction

The classical Multi-Agent Pathfinding [2] is the problem of navigating agents to their destinations in a grid-based environment. Time is discrete; each agent simultaneously performs one action per time step – move to a neighboring cell (4-neighborhood) or wait (stay). Agents have to avoid collisions – vertex conflicts (two agents at the same location in same time) and swap conflicts (two neighboring agents switching locations). In this work, we consider the disappear-at-goal setting – once the agent reaches its destination, it disappears from the environment.

Most of the existing algorithms are based on a centralized approach – the solver computes plans (action sequences) for all agents at once, then the agents just execute them. However, in large or non-deterministic environments, decentralized online approaches (at each timestep, each agent decides what to do next) provide better scalability.

## 2 Social Laws Framework

In our decentralized online framework [1], agents share a predefined ordered list of rules (a so-called social law), where each rule maps an agent's neighborhood ($5 \times 5$) to an action. At each timestep, the agent checks if any of the rules matches its current situation. If it does, the agent executes the action prescribed by the first such rule; otherwise, the agent follows the shortest path to its goal. Figure 1 shows an example of this procedure.

The structure of the rules (a list of literals "there is/is not an obstacle/agent at this relative location") makes the correctness (prescription of non-conflicting actions for nearby agents) of the laws easily verifiable. We can restrict the check to mini-scenarios involving just two main agents (whose actions we check) and their neighborhood – one can build

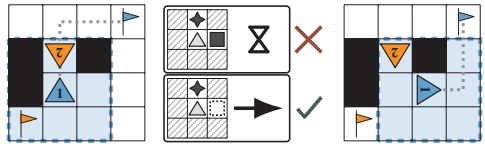


Figure 1: Illustrative toy example of the social laws framework, using only a $3 \times 3$ neighborhood. A conflicting situation (left) is resolved by a social law (center). The first rule (*if there is an agent ahead, regardless of its orientation, and an obstacle on the right, then wait*) does not apply to agent 1. The second rule (*if there is an agent ahead and no obstacle on the right, then move to the right*) applies, so agent 1 moves to the right (right), instead of following the shortest path to its goal (gray dotted line). The shortest path is then replanned, which also determines the agent's updated orientation. Regarding agent 2, the first rule applies, so agent 2 waits.

a QBF formula that checks non-conflictness of the prescribed actions for each possible mini-scenario:

$$\text{Given } L : \bigwedge_{C} (\forall S) \bigwedge_{(A_1,A_2)\in Conf(C)} \neg Performs(C\,[1]\,, A_1, S, L) \vee \neg Performs(C\,[2]\,, A_2, S, L)$$

where $C$ is the (relative) position of the two agents, $Conf(C)$ is the set of conflicting action-pairs in configuration $C$, $S$ represents the states (free/obstacle/other agent) of the cells in their neighborhoods, $Performs(C\,[i]\,, A_i, S)$ is a subformula computing whether agent $i$ located at $C\,[i]$ performs action $A_i$ in situation $S$, given the social law $L$ (encoding of the actual rules).

# 3 Learning the Social Law

The original paper [1] presents two manually designed social laws, deterministic and stochastic (to resolve possible deadlocks/livelocks in situations symmetrical for involved agents, the rules prescribe a distribution of actions from which the action is sampled). Both laws are correct (guarantee no collisions) but we are interested in finding better performing laws (reaching the goal earlier, better deadlock/livelock prevention).

One possible approach would be to convert the law-checking formula into a law-finding one – by existential quantification of the law-related variables and seeking a satisfying assignment. However, it is necessary to add some optimization of the law performance (e.g., requiring some amount of "forward" actions on a given set of scenarios); otherwise, the solver will produce a trivial law (such as "always wait"). However, after the modification, we were not able to solve the QBF problem in reasonable time.

Hence, our approach is to use imitation learning and learn the rules from plans created by an (optimal) centralized solver. The method works as follows: from the plans, we extract interesting situations (agent neighborhood + action) which forms our dataset. The neighborhood is represented as a vector of boolean features saying whether there is

an agent and whether there is an obstacle at each cell in the neighborhood. Then, we train a decision tree on this dataset. Note, that the splitting criteria in nodes exactly corresponds to the literals in our social law formalization. Finally, we may transform the decision tree into rules, simply by listing all branches – each branch corresponds to one rule.

## Acknowledgments

Research is supported by Charles University, project GA UK No. 36124 and SVV project number 260 821.

## References

[1] Jan Slezák, Jakub Mestek, and Roman Barták. Social Laws for Multi-Agent Pathfinding. In *Proc. ICAART 2025*, pages 463–470. INSTICC, SciTePress, 2025.

[2] Roni Stern, Nathan Sturtevant, Ariel Felner, Sven Koenig, Hang Ma, Thayne Walker, Jiaoyang Li, Dor Atzmon, Liron Cohen, T. K. Satish Kumar, Eli Boyarski, and Roman Barták. Multi-Agent Pathfinding: Definitions, Variants, and Benchmarks. In *Symposium on Combinatorial Search (SoCS)*, pages 151–158, 2019.

# Human–AI Collaboration in Mathematical Problem Solving: Capabilities, Limitations, and a Worked Example

**Karel Mls**

Department of Information Technologies
Faculty of Informatics and Management
University of Hradec Kralove
karel.mls@uhk.cz

**Abstract**

Recent advances in generative AI raise the question of how such systems can contribute to mathematical problem solving while preserving transparency, verifiability, and human methodological control. This paper presents an exploratory case study of human–AI collaboration centred on rank reversal in the Analytic Hierarchy Process (AHP), and develops the initial example into a more general analysis of susceptibility to ranking changes.

A general-purpose reasoning model was used to construct numerical examples, derive candidate explanations, and suggest generalizations. The resulting claims were subsequently challenged, re-derived, and computationally checked, with a second AI system used in an adversarial reviewer role. The mathematical analysis shifts attention from the binary question of whether rank reversal is possible to where and how easily it occurs. For distributive normalization, we define a rank-reversal region in the space of newly introduced alternatives. For two criteria, its boundary is affine; for multiple criteria, it becomes linear after transformation to reciprocal normalization coordinates. This leads to a directional reversal threshold and, after specifying an admissible domain and probability model, to a probabilistic measure of rank-reversal susceptibility.

The study does not propose a new feasibility theory of rank reversal. Its contribution lies in extending the analysis toward geometric and probabilistic measures of susceptibility while documenting a human-controlled workflow for generating, challenging, and verifying AI-assisted mathematical reasoning.

**Keywords:** human–AI collaboration; mathematical reasoning; Analytic Hierarchy Process; rank reversal; susceptibility analysis; decision making

# 1 Motivation and scope

Large language models were initially surprisingly weak at mathematical reasoning, particularly when several logically dependent steps or exact calculations were required [10]. Their capabilities have since progressed rapidly. Systems combining language models with search, symbolic reasoning, reinforcement learning, and formal proof environments have reached olympiad-level performance [18, 7].

More recently, the boundary between mathematical assistance and mathematical research has become less clear. In October 2026, OpenAI released a large collection of mathematical manuscripts and proof artifacts reported as outputs of an unreleased internal model evaluated on open research problems [14, 13]. These results should be interpreted with appropriate caution: the producing model is not publicly available, not all results have been formally verified, and several released manuscripts required subsequent correction or withdrawal. Nevertheless, such developments make the practical question increasingly relevant: *how should researchers work with AI-generated mathematical reasoning so that useful exploration is combined with effective verification?*

The present contribution does not attempt a statistical evaluation of AI mathematical capability. Instead, it reports a single exploratory and reproducible case study in a domain closely related to decision analysis.

# 2 Case study: AHP rank reversal

Rank reversal in the Analytic Hierarchy Process has been discussed since the classical example of Belton and Gear [4] and remains part of a broader methodological debate about normalization, aggregation, and the meaning of rank preservation [15, 5, 3]. We therefore treat rank reversal here as a phenomenon to be analysed, rather than a priori as a defect of AHP.

The interaction was conducted in ChatGPT using GPT-5.6 Sol with high reasoning effort in October 2026. The problem was introduced conversationally by suggesting rank reversal in AHP as a possible worked example; no numerical instance was supplied by the human participant. The AI model proposed two equally weighted criteria and the ratio-scale scores

$$A = (9, 4), \qquad B = (1, 9), \qquad C = (8, 1).$$

These scores are equivalent to perfectly consistent pairwise-comparison matrices. This removes inconsistency as a possible explanation, while also making clear that the example primarily examines the effects of normalization rather than the estimation of priorities from inconsistent AHP judgements.

For distributive synthesis,

$$p_i^{(d)} = \frac{1}{2}\frac{x_{i1}}{\sum_k x_{k1}} + \frac{1}{2}\frac{x_{i2}}{\sum_k x_{k2}}. \tag{1}$$

The original priorities are

$$p_A = 0.3929, \qquad p_B = 0.3492, \qquad p_C = 0.2579,$$

so that $A > B > C$. Adding an exact duplicate $D = (8, 1)$ gives

$$p_A = 0.3064, \qquad p_B = 0.3192, \qquad p_C = p_D = 0.1872,$$

and the order of the unchanged alternatives reverses to $B > A$.

The model initially noted that using ideal normalization,

$$p_i^{(i)} = \frac{1}{2}\frac{x_{i1}}{\max_k x_{k1}} + \frac{1}{2}\frac{x_{i2}}{\max_k x_{k2}}, \tag{2}$$

preserves $A > B$ when the exact duplicate is added. Taken alone, this observation can invite an overly broad interpretation of the robustness of ideal normalization. An independent human review challenged this interpretation and proposed the alternative $D = (15, 1)$. Recalculation gives

$$p_A^{(i)} = 0.5222, \qquad p_B^{(i)} = 0.5333,$$

and hence $B > A$ also under ideal normalization. The counterexample shows that the absence of reversal for the duplicate was a property of that particular construction, not a general immunity of ideal-mode synthesis.

Table 1: Effect of adding a duplicate alternative on AHP priorities.

| Scenario | $p_A$ | $p_B$ | Order of $A, B$ |
|---|---|---|---|
| Original, distributive | 0.3929 | 0.3492 | $A > B$ |
| Add $D = (8, 1)$, distributive | 0.3064 | 0.3192 | $B > A$ |
| Add $D = (8, 1)$, ideal | 0.7222 | 0.5556 | $A > B$ |
| Add $D = (15, 1)$, ideal | 0.5222 | 0.5333 | $B > A$ |

# 3 Lessons for human–AI mathematical work

The example is deliberately simple and is not presented as evidence of novel mathematical discovery. The duplicate-alternative construction is closely related to the classical rank-reversal literature, and a compact instance can also be found computationally. Its value lies instead in making the human–AI process inspectable.

In this interaction, AI contributed to formulation of the numerical instance, calculation, comparison of synthesis modes, and explanation. Human review was essential in challenging an attractive generalization, constructing a counterexample, and determining what additional verification was required. The resulting sequence can be summarized as

$$\text{generation} \longrightarrow \text{verification} \longrightarrow \text{falsification} \longrightarrow \text{revision}.$$

This small example supports a broader methodological point. As AI systems become capable of producing increasingly sophisticated mathematical arguments, plausibility should not be confused with validity. Reproducible computation, explicit disclosure of the model and interaction, active search for counterexamples, and independent human or formal verification become part of the research method itself. These principles are consistent with recent calls for transparency and accountability in AI-assisted mathematics [9].

The case study does not establish how frequently current reasoning models succeed or fail on such tasks; repeated independent runs and systematic comparisons between models remain natural extensions. Its more modest conclusion is that useful human–AI mathematical collaboration is possible, but its scientific value depends at least as much on the quality of the verification process as on the quality of the generated solution.

# 4 Mathematical Perspectives on Rank Reversal

Rank reversal is not a single mathematical phenomenon with a unique interpretation. More than four decades of research have related it to normalization, aggregation, inconsistency of pairwise comparisons, priority-derivation methods, measurement scales, and the interpretation of preferences themselves [1, 11]. Recent results have also provided explicit feasibility and geometric characterizations of rank reversal in AHP [20, 21]. For the purposes of the present study, five complementary mathematical perspectives are particularly relevant.

## 4.1 Geometric perspective

A natural way to study rank reversal is to represent alternatives as points in a criterion space and to ask how the introduction of a new alternative changes the relative position of the existing alternatives. Earlier work has already shown that regions associated with rank preservation and reversal can be characterized geometrically [6], while recent analyses provide geometric conditions for the feasibility or infeasibility of rank reversal in the Saaty and Belton–Gear frameworks [20, 21].

A related but more operational viewpoint is to regard the newly introduced alternative itself as a point

$$D = (d_1, \ldots, d_m) \in \mathbb{R}_+^m$$

and to partition this space into regions in which the ordering of two original alternatives is preserved or reversed. Such a representation does not merely answer whether rank reversal is possible; it shows *which* additional alternatives can produce it and how close a given decision problem is to such a change.

## 4.2 Probabilistic perspective

A deterministic statement that rank reversal is possible does not indicate how likely it is to occur. A probabilistic formulation can therefore be introduced by treating either the judgments or the newly introduced alternative as random quantities.

Stam and Duarte Silva [17] studied rank reversal probabilities arising from stochastic pairwise judgments. More recently, Jiang, Liao, and De Baets [8] used simulation to compare the probabilities of rank reversal, tie making, and tie breaking across a broad range of MCDM methods.

In the setting considered here, the random quantity can instead be the new alternative $D$. Once a probability distribution over admissible alternatives is specified, the probability of rank reversal becomes the probability mass of the corresponding reversal region. This connects the geometric and probabilistic interpretations directly.

## 4.3 Perturbation and spectral perspective

The case study in Section 3 deliberately uses perfectly consistent pairwise-comparison matrices. Consequently, the corresponding priority vectors are equivalent to normalized ratio-scale values and the observed rank reversal can be isolated from inconsistency effects.

For general AHP matrices, however, the problem is substantially richer. The principal eigenvector of a positive reciprocal matrix depends on the entire matrix, and changes in the set of alternatives may interact with inconsistency, intransitivity, and the method used to derive priorities. Perturbation theory and spectral properties of pairwise-comparison matrices therefore provide another mathematical route to the problem.

Alvarez et al. [2] relate stability properties of AHP to matrix conditioning and rank deficiency. Tu and Wu [19] distinguish several causes of rank reversal associated with inconsistent preferences, prioritization procedures, and aggregation rules. Extending the present analysis from consistent ratio-scale matrices to inconsistent matrices, and comparing the eigenvector and geometric-mean methods, is therefore a natural subsequent step.

## 4.4 Measurement-theoretic and compositional perspective

Rank reversal can also be interpreted as a consequence of the mathematical representation used for priorities. Under distributive normalization, the value assigned to every existing alternative changes when the reference set changes. Thus, an unchanged alternative does not retain an unchanged numerical representation after another alternative is introduced.

Barzilai and Golany [3] connected rank reversal with normalization and aggregation rules and argued for preserving the underlying ratio structure. More recently, Mohammadi and Rezaei [12] approached MCDM priorities from the perspective of compositional data and proposed a normalization-agnostic ratio-product model. From this viewpoint, rank reversal raises a more fundamental question: which transformations and aggregation operations preserve the meaning encoded in ratio-scale priorities?

## 4.5 Choice-theoretic perspective

Finally, rank reversal has a normative interpretation. If an alternative that is irrelevant to a comparison between $A$ and $B$ is introduced, should the ordering between $A$ and $B$ necessarily remain unchanged?

Dyer [5] regarded rank reversal as evidence of a fundamental problem in the AHP ranking procedure. In contrast, Saaty and Vargas [16], and later Saaty [15], argued that rank reversal can be legitimate in relative measurement because the introduction of a new alternative may change the context in which the original alternatives are evaluated.

This distinction is important for the present work. We do not assume that every rank reversal is necessarily an error. Instead, we analyse the mathematical conditions under which it occurs. Whether such a change is meaningful or undesirable remains partly a modelling and decision-theoretic question.

### 4.6 Selected direction

The remainder of this paper concentrates on the first two perspectives. Existing research provides important results on the *feasibility* of rank reversal [20, 21]. We complement this viewpoint by considering the space of possible newly introduced alternatives and asking four progressively stronger questions:

$$\boxed{\text{feasibility} \longrightarrow \text{location} \longrightarrow \text{threshold} \longrightarrow \text{probability}}$$

That is, once rank reversal is feasible, we seek to determine which additional alternatives cause it, how strong a perturbation is needed, and how susceptible the original ranking is under a specified model of possible new alternatives.

## 5 Reversal Regions and Susceptibility to Rank Reversal

### 5.1 General formulation

To separate the effect of normalization from the effects of inconsistent judgments, we first retain the consistent ratio-scale formulation used in the case study.

Consider $n$ original alternatives evaluated with respect to $m$ criteria. Let

$$x_{ij} > 0, \qquad i = 1, \dots, n, \quad j = 1, \dots, m,$$

denote the ratio-scale performance of alternative $i$ with respect to criterion $j$. The criterion weights satisfy

$$w_j > 0, \qquad \sum_{j=1}^{m} w_j = 1.$$

For each criterion, define

$$S_j = \sum_{i=1}^{n} x_{ij}.$$

Under distributive normalization, the global priority of alternative $i$ is

$$p_i^{(d)} = \sum_{j=1}^{m} w_j \frac{x_{ij}}{S_j}. \tag{3}$$

We focus on two original alternatives $A$ and $B$, whose criterion-wise performances are denoted by $a_j$ and $b_j$, respectively. Define

$$\delta_j = a_j - b_j.$$

Suppose that initially

$$p_A^{(d)} > p_B^{(d)}.$$

Now introduce a new alternative

$$D = (d_1, \ldots, d_m), \qquad d_j \geq 0.$$

The priorities of the original alternatives become

$$p_i^{(d)}(D) = \sum_{j=1}^{m} w_j \frac{x_{ij}}{S_j + d_j},$$

and the difference between the priorities of $A$ and $B$ is

$$F_{AB}(D) = p_A^{(d)}(D) - p_B^{(d)}(D) = \sum_{j=1}^{m} w_j \frac{\delta_j}{S_j + d_j}. \tag{4}$$

Because $F_{AB}(0) > 0$, rank reversal between $A$ and $B$ occurs precisely when

$$F_{AB}(D) < 0.$$

This motivates the following definition.

**Definition 1 (rank-reversal region).** For the ordered pair $(A, B)$, the distributive rank-reversal region is

$$\mathcal{R}_{AB}^{(d)} = \left\{ D \in \mathbb{R}_+^m : F_{AB}(D) < 0 \right\}. \tag{5}$$

Its boundary is the level set

$$F_{AB}(D) = 0.$$

A simple observation already follows from Eq. (4). If $A$ is at least as good as $B$ with respect to every criterion, i.e.

$$\delta_j \geq 0 \qquad \text{for all } j,$$

then $\mathcal{R}_{AB}^{(d)}$ is empty. Thus, conflicting criterion-wise preferences are necessary for rank reversal in this formulation.

Conversely, if $F_{AB}(0) > 0$ but $\delta_j < 0$ for at least one criterion, then a rank reversal can be produced in the unrestricted non-negative space by sufficiently increasing the denominators associated with the criteria favouring $A$, while leaving the criteria favouring $B$ unchanged. This provides a simple feasibility interpretation for the consistent distributive case.

## 5.2 Two criteria: an affine reversal boundary

For two criteria, Eq. (4) becomes

$$F_{AB}(d_1, d_2) = w_1 \frac{\delta_1}{S_1 + d_1} + w_2 \frac{\delta_2}{S_2 + d_2}. \tag{6}$$

Since both denominators are positive, the boundary $F_{AB}(d_1, d_2) = 0$ is equivalent to

$$w_1\delta_1(S_2 + d_2) + w_2\delta_2(S_1 + d_1) = 0. \tag{7}$$

Thus, although the normalized priorities are rational functions of the new alternative, the boundary separating rank preservation from rank reversal is an affine line in the $(d_1, d_2)$ plane.

For the example introduced in Section 3,

$$A = (9, 4), \qquad B = (1, 9), \qquad C = (8, 1),$$

with $w_1 = w_2 = 1/2$, we have

$$S_1 = 18, \qquad S_2 = 14, \qquad \delta_1 = 8, \qquad \delta_2 = -5.$$

Equation (7) therefore reduces to

$$5d_1 - 8d_2 = 22. \tag{8}$$

Because the original ranking is $A > B$, the reversal region is

$$\mathcal{R}_{AB}^{(d)} = \left\{(d_1, d_2) \in \mathbb{R}_+^2 : 5d_1 - 8d_2 > 22\right\}. \tag{9}$$

The previously used duplicate alternative $D = (8, 1)$ lies inside this region because

$$5 \cdot 8 - 8 \cdot 1 = 32 > 22.$$

The numerical example can therefore be interpreted not as an isolated construction but as one point in an entire half-plane of alternatives producing the same reversal.

## 5.3 Multiple criteria and a reciprocal-coordinate representation

For $m > 2$, the reversal boundary

$$\sum_{j=1}^{m} w_j \frac{\delta_j}{S_j + d_j} = 0$$

is generally nonlinear in the original coordinates $d_j$. Multiplying by the strictly positive product

$$\prod_{k=1}^{m} (S_k + d_k)$$

gives the equivalent polynomial equation

$$G_{AB}(D) = \sum_{j=1}^{m} w_j \delta_j \prod_{\substack{k=1 \\ k \neq j}}^{m} (S_k + d_k) = 0. \tag{10}$$

The resulting boundary is a multilinear algebraic hypersurface of total degree at most $m - 1$.

A simpler representation is obtained by introducing reciprocal normalization coordinates

$$y_j = \frac{1}{S_j + d_j}. \tag{11}$$

Because $d_j \geq 0$,

$$0 < y_j \leq \frac{1}{S_j}.$$

In the transformed coordinates, Eq. (4) becomes

$$F_{AB}(y) = \sum_{j=1}^{m} w_j \delta_j y_j. \tag{12}$$

Consequently, the reversal boundary is a hyperplane,

$$\sum_{j=1}^{m} w_j \delta_j y_j = 0, \tag{13}$$

intersected with the admissible box

$$0 < y_j \leq \frac{1}{S_j}.$$

This transformation reveals that the apparent nonlinearity of the rank-reversal boundary is caused by the normalization denominators. In reciprocal normalization space, rank preservation and rank reversal are separated by a linear decision boundary.

## 5.4 Directional reversal threshold

The reversal region describes where a reversal occurs but not how large a change is required to reach it. To quantify this notion, consider a family of possible new alternatives lying along a fixed direction

$$D(t) = tq, \qquad q = (q_1, \ldots, q_m) \in \mathbb{R}_+^m, \qquad t \geq 0.$$

The vector $q$ describes the performance profile of the additional alternative, while $t$ controls its magnitude. We define the *directional reversal threshold* as

$$t^*(q) = \inf \{ t \geq 0 : F_{AB}(tq) \leq 0 \}, \tag{14}$$

whenever such a value exists.

For two criteria, the sign of $F_{AB}(tq)$ is the same as the sign of

$$C_0 + tC_1(q), \tag{15}$$

where

$$C_0 = w_1\delta_1 S_2 + w_2\delta_2 S_1$$

and

$$C_1(q) = w_1\delta_1 q_2 + w_2\delta_2 q_1.$$

Since the original ranking is $A > B$, $C_0 > 0$. If

$$C_1(q) < 0,$$

there is a unique reversal threshold

$$t^*(q) = -\frac{C_0}{C_1(q)}. \tag{16}$$

If $C_1(q) \geq 0$, no rank reversal can occur along that direction.

For the running example,

$$C_0 = 11, \qquad C_1(q) = 4q_2 - 2.5q_1.$$

Hence

$$t^*(q) = \frac{22}{5q_1 - 8q_2}, \qquad 5q_1 > 8q_2. \tag{17}$$

This expression quantifies how strongly an alternative of a given criterion profile must enter the decision problem before the ranking of $A$ and $B$ changes.

## 5.5 Probabilistic susceptibility

The geometric formulation naturally leads to a probabilistic measure of susceptibility. Let the newly introduced alternative $D$ be a random vector with density $f_D(d)$ over an admissible domain $\Omega \subseteq \mathbb{R}^m_+$. The probability of rank reversal between $A$ and $B$ is

$$P_{\mathrm{RR}}(A, B) = \Pr(D \in \mathcal{R}^{(d)}_{AB}) = \int_{\mathcal{R}^{(d)}_{AB} \cap \Omega} f_D(d)\,\mathrm{d}d. \tag{18}$$

If $D$ is uniformly distributed over a bounded domain $\Omega$, this reduces to the relative volume

$$P_{\mathrm{RR}}(A, B) = \frac{\mathrm{Vol}\left(\mathcal{R}^{(d)}_{AB} \cap \Omega\right)}{\mathrm{Vol}(\Omega)}. \tag{19}$$

For the two-criterion example, suppose

$$D \sim \mathcal{U}\left([0, U_1] \times [0, U_2]\right).$$

Using Eq. (9), define

$$h = \min\left\{U_2,\ \max\left(0,\ \frac{5U_1 - 22}{8}\right)\right\}.$$

The area of the reversal region within the rectangle is

$$A_{\mathrm{RR}} = h\left(U_1 - \frac{22}{5}\right) - \frac{4}{5}h^2,$$

and therefore

$$P_{\mathrm{RR}} = \frac{h\left(U_1 - \frac{22}{5}\right) - \frac{4}{5}h^2}{U_1 U_2}. \tag{20}$$

Importantly, $P_{\mathrm{RR}}$ is not an intrinsic property of the AHP instance alone. It depends on the assumed domain and probability model for plausible new alternatives. The probability should therefore be interpreted as a conditional susceptibility measure rather than as an absolute characteristic of the decision problem.

## 5.6 Comparison with ideal normalization

The same geometric approach can be applied to ideal normalization. Let

$$M_j = \max_{i=1,\dots,n} x_{ij}$$

denote the original maximum performance under criterion $j$. After the addition of alternative $D$, the difference between $A$ and $B$ becomes

$$F_{AB}^{(i)}(D) = \sum_{j=1}^{m} w_j \frac{\delta_j}{\max(M_j, d_j)}. \tag{21}$$

Unlike distributive normalization, this function is piecewise defined. The mathematical form changes whenever $d_j$ crosses the existing maximum $M_j$. Consequently, the ideal-mode reversal region consists of pieces corresponding to different active sets of criteria for which the new alternative establishes a new maximum.

For the running example,

$$M_1 = M_2 = 9,$$

and

$$F_{AB}^{(i)}(D) = \frac{4}{\max(9, d_1)} - \frac{2.5}{\max(9, d_2)}. \tag{22}$$

Rank reversal occurs when

$$\frac{\max(9, d_1)}{\max(9, d_2)} > \frac{8}{5}. \tag{23}$$

For the duplicate $D = (8, 1)$, the ratio on the left-hand side equals one and the original ordering is preserved. In contrast, for $D = (15, 1)$,

$$\frac{\max(9, 15)}{\max(9, 1)} = \frac{15}{9} > \frac{8}{5},$$

and rank reversal occurs.

This makes explicit why the absence of reversal for the duplicate alternative cannot be generalized into a claim that ideal normalization is immune to rank reversal.

### 5.7 From feasibility to susceptibility

The proposed formulation distinguishes several levels of analysis. Feasibility asks whether any newly introduced alternative can reverse the order of $A$ and $B$. The reversal region identifies the alternatives that do so. The directional threshold measures how far the system is from reversal along a specified performance profile, and the probabilistic formulation quantifies susceptibility under an explicit model of possible new alternatives.

Thus, rather than describing rank reversal only as a binary property, the framework suggests a sequence

$$\boxed{\text{possible?} \longrightarrow \text{where?} \longrightarrow \text{how far?} \longrightarrow \text{how likely?}}$$

The present analysis is restricted deliberately to consistent ratio-scale priorities so that the effects of normalization can be studied in isolation. The spectral and perturbation perspective discussed in Section 4.3 provides a natural direction for extending the framework to inconsistent pairwise-comparison matrices.

## 6 Conclusions and Methodological Reflection

This study started from a deliberately simple question: whether a general-purpose reasoning model could assist in analysing a familiar mathematical phenomenon in decision making and, more importantly, how such assistance should be verified. The initial AHP rank-reversal example gradually developed into a broader investigation of the geometry and susceptibility of ranking changes caused by the introduction of a new alternative.

The resulting mathematical contribution should be interpreted accordingly. We do not claim a new feasibility theory of rank reversal; conditions under which rank reversal is possible or impossible have already been studied extensively. Instead, the analysis shifts the emphasis from the binary question of existence toward a quantitative description of susceptibility. For distributive normalization, the newly introduced alternative is treated as a point in criterion space, which leads naturally to the definition of a rank-reversal region. For two criteria, its boundary is affine; for multiple criteria, the boundary becomes nonlinear in the original coordinates but linear in reciprocal normalization coordinates. This representation then enables the definition of a directional reversal threshold and, after specifying an admissible domain and probability model for new alternatives, a probabilistic measure of rank-reversal susceptibility. The corresponding analysis of ideal normalization shows that its reversal regions are piecewise defined and that the absence of reversal in a particular example must not be interpreted as general immunity.

Equally important is the way in which these results were obtained. The manuscript was developed iteratively through human–AI interaction. The human author selected the

research problem, evaluated the relevance of intermediate results, challenged interpretations, and decided which claims required further verification. A general-purpose reasoning model contributed candidate formulations, symbolic derivations, numerical examples, generalizations, and possible interpretations. A separate AI system was subsequently used in an adversarial reviewer role to identify weak assumptions, overgeneralizations, and possible counterexamples. Suggestions produced by either system were not treated as evidence by themselves; mathematical claims were re-derived, recalculated, and, where appropriate, checked computationally.

This distinction is methodologically important. An interaction with a generative model is not reproducible in the same sense as a deterministic algorithm, even when the same prompt and model configuration are used. The interaction can instead be made *inspectable*: the model, configuration, prompts, relevant transcript, and provenance of individual ideas can be disclosed. The mathematical results derived during that interaction must then satisfy the usual stronger requirement of independent reproducibility through explicit derivations and executable computational checks.

From this perspective, the role of AI in the present work is neither that of an autonomous discoverer nor merely that of a numerical calculator. Its principal value lies in accelerating the cycle of

$$\text{formulation} \longrightarrow \text{generation} \longrightarrow \text{challenge} \longrightarrow \text{verification} \longrightarrow \text{revision}.$$

The case study suggests that this cycle may be a useful model for human–AI mathematical research more generally. Increased generative capacity does not reduce the need for mathematical judgement; rather, it increases the importance of provenance, adversarial testing, counterexample search, and independent verification. In this sense, the most significant contribution of human–AI collaboration may not be the production of more candidate results, but the ability to explore a larger space of hypotheses while retaining a transparent path from conjecture to validated conclusion.

# References

[1] Renan Felinto de Farias Aires and Luciano Ferreira. The rank reversal problem in multi-criteria decision making: A literature review. *Pesquisa Operacional*, 38(2):331–362, 2018.

[2] G. B. Alvarez, R. G. de Almeida, C. T. Hernández, and P. A. P. de Sousa. Some mathematical comments about the analytic hierarchy process: Part i – theoretical analysis. *Journal of Multi-Criteria Decision Analysis*, 28(5–6):296–310, 2021.

[3] Jonathan Barzilai and Boaz Golany. Ahp rank reversal, normalization and aggregation rules. *INFOR: Information Systems and Operational Research*, 32(2):57–64, 1994.

[4] Valerie Belton and Tony Gear. On a short-coming of saaty's method of analytic hierarchies. *Omega*, 11(3):228–230, 1983.

[5] James S. Dyer. Remarks on the analytic hierarchy process. *Management Science*, 36(3):249–258, 1990.

[6] András Farkas and Pál Rózsa. An analysis of rank preservation and reversal in the analytic hierarchy process. *Periodica Polytechnica Social and Management Sciences*, 4(1):63–78, 1996.

[7] Thomas Hubert, Rishabh Mehta, Laurent Sartran, et al. Olympiad-level formal mathematical reasoning with reinforcement learning. *Nature*, 651:607–613, 2026.

[8] Lisheng Jiang, Huchang Liao, and Bernard De Baets. A simulation study on the probabilities of rank reversal, tie making, and tie breaking for multiple criteria decision making methods. *Omega*, 125:103033, 2024.

[9] Leiden Declaration on Artificial Intelligence and Mathematics. Leiden declaration on artificial intelligence and mathematics. `https://leidendeclaration.ai/`, June 2026.

[10] Aitor Lewkowycz, Anders Andreassen, David Dohan, et al. Solving quantitative reasoning problems with language models. volume 35, pages 3843–3857, 2022.

[11] Bitong Li and Ali Abbas. A trend analysis of rank reversal in widely used decision-making methods. *Journal of Multi-Criteria Decision Analysis*, 33(1):e70027, 2026.

[12] Majid Mohammadi and Jafar Rezaei. Ratio product model: A rank-preserving normalization-agnostic multi-criteria decision-making method. *Journal of Multi-Criteria Decision Analysis*, 30(5–6):163–172, 2023.

[13] OpenAI. Mathematical manuscripts and supporting proof artifacts produced by an internal openai model. `https://github.com/openai/math`, 2026. GitHub repository, accessed 20 October 2026.

[14] OpenAI. Sharing ai progress in mathematics. `https://openai.com/index/sharing-ai-progress-in-mathematics/`, October 2026. Accessed 20 October 2026.

[15] Thomas L. Saaty. Rank generation, preservation, and reversal in the analytic hierarchy decision process. *Decision Sciences*, 18(2):157–177, 1987.

[16] Thomas L. Saaty and Luis G. Vargas. The legitimacy of rank reversal. *Omega*, 12(5):513–516, 1984.

[17] A. Stam and A. P. Duarte Silva. Stochastic judgments in the AHP: The measurement of rank reversal probabilities. *Decision Sciences*, 28(3):655–688, 1997.

[18] Trieu H. Trinh, Yuhuai Wu, Quoc V. Le, He He, and Thang Luong. Solving olympiad geometry without human demonstrations. *Nature*, 625:476–482, 2024.

[19] Jiancheng Tu and Zhibin Wu. Analytic hierarchy process rank reversals: Causes and solutions. *Annals of Operations Research*, 346(2):1785–1809, 2025.

[20] Junpeng Yan and Changxuan Mao. An infeasibility condition for rank reversal in the analytic hierarchy process. *Axioms*, 14(12):860, 2025.

[21] Junpeng Yan and Changxuan Mao. Geometric and algebraic characterizations of infeasibility of rank reversal in the saaty and belton–gear frameworks. *Axioms*, 15(5):311, 2026.

# On the Convergence of Relaxed Core Dynamics in Simple Symmetric Fractional Hedonic Games

**Shao-Chin Sung***

Department of Industrial and Systems Engineering
Aoyama Gakuin University
son@ise.aoyama.ac.jp

**Abstract**

In fractional hedonic games, the utility of an agent for a coalition is the average value she assigns to its members. For simple symmetric fractional hedonic games (SS-FHG), Fanelli, Monaco and Moscardelli proved that every $q$-size core dynamics—a sequence of deviations by blocking coalitions of at most $q$ agents—converges whenever $q \leq 3$, and left open the largest $q$ for which convergence is guaranteed. To address this question, we reformulate convergence as acyclicity of a directed graph on the partitions of the agents, which we call the *deviation graph*, and exhaustively examine the deviation graphs of instances of SS-FHG with up to ten agents. This search reveals an instance of SS-FHG with six agents admitting a cyclic 4-size core dynamics, whose cycle can be verified by hand. Since the cycle remains admissible for every larger $q$, $q = 3$ is exactly the largest $q$ for which convergence is guaranteed. The search further shows that six agents are necessary and that non-convergence becomes typical as the number of agents grows. Finally, a welfare argument shows that, for every $k > 2$, every $k$-improvement core dynamics has $O(n)$ deviations, where $n$ is the number of agents.

**Keywords:** hedonic games; fractional hedonic games; coalition formation; relaxed core stability; dynamics; convergence

## 1 Introduction

Hedonic games [13, 6, 4] model coalition formation in which every agent cares only about the members of her own coalition; see Aziz and Savani [3] for a survey and our earlier work [18] for a unified treatment of myopic stability concepts. Under *core stability*, no

*Shao-Chin Sung is currently known as So Akiyama.

group of agents can jointly leave their coalitions and form a new coalition in which all of them are strictly better off. In fractional hedonic games (FHG) [1], the utility of an agent for a coalition is the average value she assigns to its members; they are closely related to network clustering [2]. Even in *simple symmetric* FHG (SS-FHG), where the valuations of an instance are given by an undirected unweighted graph, the core may be empty and deciding its non-emptiness is computationally hard [1]; related stability notions are studied in [5, 7, 11].

Motivated by these negative results and by the difficulty of coordinating large groups, Fanelli, Monaco and Moscardelli [14, 15] introduced *$q$-size core stability*, in which only blocking coalitions of at most $q$ agents are admissible (see also [12]). They studied the convergence of *$q$-size core dynamics*, in which admissible blocking coalitions deviate one after another from an arbitrary partition. Convergence guarantees that myopic agents eventually reach a stable outcome; similar questions have been studied for single-agent deviations [9, 8]. They showed that every instance of symmetric FHG (S-FHG) is 2-size core convergent, whereas for every $q \geq 3$ some instance of S-FHG is not $q$-size core convergent [15, Thm. 3, Ex. 6], and that every instance of SS-FHG is 3-size core convergent within a polynomial number of deviations [15, Thm. 4]. They asked for the largest $q$ for which convergence is guaranteed [15, Sec. 6]; for S-FHG their results give $q = 2$, whereas for SS-FHG the question remained open. Their experiments on random instances did not examine 4-size core dynamics [15, Sec. 5].

**Methodology.** Convergence results are usually obtained by mathematical arguments such as potential functions, as for $q \leq 3$ in [15]. A negative answer for $q \geq 4$, however, requires an explicit counterexample, which is hard to construct by hand. We therefore take a *computational approach*, in line with computational approaches to impossibility theorems in computational social choice [19, 16, 10]. We reformulate convergence as acyclicity of a finite directed graph, the deviation graph, which applies to any notion of stability defined by coalitional deviations, and exhaustively examine all instances of SS-FHG with few agents. Unlike simulations of random dynamics on random instances [15, Sec. 5], this also shows that no smaller counterexample exists, and the counterexample found is small enough to be verified by hand, so the non-convergence result does not rely on our implementation. Such an exhaustive examination is possible only for SS-FHG: since valuations are 0 or 1, an instance with $n$ agents is a graph on $n$ vertices, of which there are finitely many up to isomorphism, whereas FHG and S-FHG have infinitely many instances for each $n$. Even so, with a carefully tuned implementation, the experiments for ten agents required about 79 days of total CPU time, run in parallel over several days.

**Our contribution.** We answer the convergence part of the above open problem.

- We give an instance of SS-FHG with six agents and a cyclic 4-size core dynamics (Theorem 5). Hence, for every $q \geq 4$ and $n \geq 6$, some instance of SS-FHG with $n$ agents is not $q$-size core convergent, and $q = 3$ is the largest $q$ for which convergence is guaranteed (Corollary 6).

- Our exhaustive experiments (Section 4) show that six agents are necessary, and that for ten agents more than 90% of the instances are not 4-size core convergent.
- For $k$-improvement core dynamics, a welfare inequality underlying [15, Thm. 5] shows that, for every $k > 2$, every $k$-improvement core dynamics in an instance of SS-FHG has fewer than $\frac{k}{k-2}(n-1)$ deviations (Theorem 8).

# 2 Preliminaries

We follow the notation of our earlier work [18].

**Hedonic games.** Let $N = \{1, 2, \dots, n\}$ be a finite set of agents. A *coalition* is a non-empty subset of $N$. A *partition* $\Pi$ of $N$ is a set of pairwise disjoint coalitions whose union is $N$; partitions are also called *coalition structures* in the literature (e.g., [18, 15]). For each $i \in N$, we denote by $\Pi(i)$ the coalition of $\Pi$ containing $i$. Let $\mathcal{P}(N)$ denote the set of all partitions of $N$; its cardinality is the Bell number $B_n$. Each agent $i$ has a preference $\succeq_i$ (a complete and transitive binary relation) over the coalitions containing $i$, with strict part $\succ_i$. An *instance of hedonic games* is a pair $(N, \succeq)$ with $\succeq = (\succeq_1, \dots, \succeq_n)$.

**Simple symmetric fractional hedonic games.** SS-FHG is a subclass of hedonic games each of whose instances is induced by an undirected graph. Let $G = (N, E)$ be an undirected graph. The instance $(N, \succeq)$ of SS-FHG induced by $G$ is defined as follows. Each agent $i$ assigns value 1 to every other agent $j$ with $\{i, j\} \in E$ and value 0 to all other agents. For an agent $i \in N$ and a set $C \subseteq N$, let $\delta_i(C) = |\{j \in C : \{i, j\} \in E\}|$ denote the number of neighbours of $i$ in $C$; we do not require $i \in C$. If $i \in C$, then $\delta_i(C)$ is the degree of $i$ in the subgraph $G[C]$ induced by $C$. The utility of $i$ for a coalition $C$ with $i \in C$ is

$$u_i(C) = \frac{\delta_i(C)}{|C|},$$

and the preference $\succeq_i$ is defined by $C \succeq_i D$ if and only if $u_i(C) \geq u_i(D)$. Since this instance is completely determined by $G$, we refer to it simply as $G$. Note that

$$u_i(C) \leq \frac{|C| - 1}{|C|} \qquad \text{for all } i \in C, \tag{1}$$

with equality if and only if $i$ is adjacent to all other members of $C$.

**Core and $q$-size core.** Let $\Pi$ be a partition. A coalition $X$ is a *blocking coalition* for $\Pi$ (with respect to core stability) if $X \succ_i \Pi(i)$ for every $i \in X$, that is, every member of $X$ strictly prefers $X$ to her current coalition. Note that a blocking coalition $X$ satisfies $X \notin \Pi$. The partition $\Pi$ is *core stable* if there is no blocking coalition for $\Pi$. In SS-FHG, every blocking coalition has at least two members, since $u_i(\{i\}) = 0$. The relaxed notions below restrict the admissible blocking coalitions. For an integer $q \geq 2$, a blocking coalition $X$ for $\Pi$ with $|X| \leq q$ is called a *$q$-size blocking coalition* for $\Pi$, and $\Pi$ is *$q$-size*

*core stable* if there is no $q$-size blocking coalition for $\Pi$ [15]. Clearly, for $q \leq q'$, every $q$-size blocking coalition is also a $q'$-size blocking coalition, and the $n$-size blocking coalitions are exactly the blocking coalitions. Similarly, for a real number $k \geq 1$, a coalition $X$ is a *$k$-improvement blocking coalition* for $\Pi$ if $u_i(X) > k\, u_i(\Pi(i))$ for every $i \in X$, and $\Pi$ is *$k$-improvement core stable* if there is no $k$-improvement blocking coalition for $\Pi$ [15]. Since $k \geq 1$, every $k$-improvement blocking coalition is a blocking coalition with respect to core stability, and the 1-improvement blocking coalitions are exactly the blocking coalitions.

**Dynamics and convergence.** When the members of a coalition $X$ deviate from $\Pi$, they leave their coalitions and form $X$, while all other agents stay where they are. The resulting partition is

$$\Pi[X] = \{\, Y \setminus X \mid Y \in \Pi,\ Y \not\subseteq X \,\} \cup \{X\}.$$

A *$q$-size core dynamics* is a finite or infinite sequence $\langle \Pi^0, \Pi^1, \Pi^2, \dots \rangle$ of partitions such that, for every $t \geq 1$, there is a $q$-size blocking coalition $X^t$ for $\Pi^{t-1}$ with $\Pi^t = \Pi^{t-1}[X^t]$. An instance of SS-FHG is *$q$-size core convergent* if every $q$-size core dynamics, starting from any partition, is finite; in that case every maximal dynamics ends in a $q$-size core stable partition. For $q = n$ we simply speak of *core dynamics*. A *$k$-improvement core dynamics* and *$k$-improvement core convergence* are defined analogously, using $k$-improvement blocking coalitions.

**Theorem 1** (Fanelli et al. [15])**.** *Every instance of SS-FHG is* 2*-size and* 3*-size core convergent. Moreover, every* 3*-size core dynamics has polynomial length.*

# 3 Approach: the deviation graph

Instead of searching for a potential, we look for a counterexample. A partition of $N$ represents a state of cooperation among the agents, and each deviation moves the agents from one such state to another, so that a dynamics is a process of transitions between states of cooperation. We therefore encode all dynamics of a given instance in a single finite object, the *deviation graph*, which represents the transition relation between states of cooperation induced by the notion of stability under consideration. The construction does not depend on the particular notion of stability, so we describe it for an arbitrary notion defined by coalitional deviations. Let $H = (N, \succeq)$ be an instance of hedonic games, and consider a notion of stability $\mathcal{S}$ that specifies, for each partition $\Pi$, a set $\mathcal{A}_\mathcal{S}(\Pi)$ of *admissible* coalitions, where every $X \in \mathcal{A}_\mathcal{S}(\Pi)$ satisfies $X \notin \Pi$; for example, $\mathcal{A}_\mathcal{S}(\Pi)$ may be the set of blocking coalitions or of $q$-size blocking coalitions for $\Pi$, or, for instances of SS-FHG, the set of $k$-improvement blocking coalitions for $\Pi$. Note that $\mathcal{A}_\mathcal{S}(\Pi)$ depends not only on $\mathcal{S}$ but also on $H$; we omit $H$ from the notation, as the instance under consideration will always be clear from the context. We say that $\Pi$ is *$\mathcal{S}$-stable* if $\mathcal{A}_\mathcal{S}(\Pi) = \emptyset$. A *$\mathcal{S}$-dynamics* is a finite or infinite sequence $\langle \Pi^0, \Pi^1, \dots \rangle$ of partitions such that $\Pi^t = \Pi^{t-1}[X^t]$ for some $X^t \in \mathcal{A}_\mathcal{S}(\Pi^{t-1})$ for every $t \geq 1$, and $H$ is *$\mathcal{S}$-convergent* if every $\mathcal{S}$-dynamics is finite. For the three examples above, these notions coincide with those of Section 2.

**Definition 2** (deviation graph)**.** The *deviation graph* of $H$ with respect to $\mathcal{S}$ is the directed graph $\mathcal{D}_{\mathcal{S}}(H) = (\mathcal{P}(N), R_{\mathcal{S}})$ with

$$R_{\mathcal{S}} = \left\{ (\Pi, \Pi[X]) \;\middle|\; \Pi \in \mathcal{P}(N),\ X \in \mathcal{A}_{\mathcal{S}}(\Pi) \right\}.$$

Depending on the preferences, an arc may correspond to several admissible coalitions; for example, if $\Pi = \{N\}$ and both $X$ and $N \setminus X$ are admissible, then $\Pi[X] = \Pi[N \setminus X]$. The results of this paper depend only on which transitions exist, so we do not distinguish such coalitions in our analysis. In an implementation, however, it can be convenient to regard $\mathcal{D}_{\mathcal{S}}(H)$ as a multigraph with one arc per admissible coalition, so that each arc corresponds to a unique deviating coalition.

Since every $X \in \mathcal{A}_{\mathcal{S}}(\Pi)$ satisfies $X \notin \Pi$ but $X \in \Pi[X]$, the deviation graph has no self-loops. By definition, every $\mathcal{S}$-dynamics is a directed walk in $\mathcal{D}_{\mathcal{S}}(H)$, and every directed walk in $\mathcal{D}_{\mathcal{S}}(H)$ is a $\mathcal{S}$-dynamics; note that a walk may visit the same partition more than once. Because $\mathcal{P}(N)$ is finite, we obtain the following reformulation.

**Proposition 3.** *Let $H$ be an instance of hedonic games and $\mathcal{S}$ as above.*

*(i) A partition $\Pi$ is $\mathcal{S}$-stable if and only if $\Pi$ is a sink (a vertex of out-degree 0) of $\mathcal{D}_{\mathcal{S}}(H)$.*

*(ii) $H$ is $\mathcal{S}$-convergent if and only if $\mathcal{D}_{\mathcal{S}}(H)$ is acyclic.*

*Proof.* (i) is immediate from the definitions. For (ii), a directed cycle $\Pi^0 \to \Pi^1 \to \cdots \to \Pi^\ell = \Pi^0$ yields the infinite dynamics obtained by repeating it. Conversely, an infinite dynamics is an infinite walk in a finite digraph, so some vertex appears twice, and the walk between these two appearances contains a directed cycle. □

Although we focus on $q$-size core stability in SS-FHG, the framework applies equally to the core and to $k$-improvement core stability (Section 5), and more generally to any notion of stability defined by coalitional deviations.

For the analysis of $q$-size core dynamics in an instance $G$ of SS-FHG, we use the deviation graph of $G$ with respect to $q$-size blocking coalitions, i.e., $\mathcal{A}_{\mathcal{S}}(\Pi)$ is the set of $q$-size blocking coalitions for $\Pi$. We denote it by $\mathcal{D}_q(G)$ and call it the *$q$-size deviation graph* of $G$. The $q$-size deviation graph behaves monotonically under increasing $q$ and adding agents.

**Lemma 4.** *Let $G = (N, E)$ be an instance of SS-FHG.*

*(i) If $2 \le q \le q'$, then $\mathcal{D}_q(G)$ is a spanning subgraph of $\mathcal{D}_{q'}(G)$. In particular, if $G$ is not $q$-size core convergent, then it is not $q'$-size core convergent.*

*(ii) Let $G'$ be obtained from $G$ by adding an isolated agent $z \notin N$. If $\mathcal{D}_q(G)$ contains a cycle, so does $\mathcal{D}_q(G')$.*

*Proof.* (i) holds because every $q$-size blocking coalition is also a $q'$-size blocking coalition. For (ii), map every $\Pi \in \mathcal{P}(N)$ to $\Pi' = \Pi \cup \{\{z\}\} \in \mathcal{P}(N \cup \{z\})$. For $X \subseteq N$ and $i \in X$, we have $\Pi'(i) = \Pi(i)$, so the utilities of the members of $X$ are the same in $G$ and $G'$. Hence, if $X$ is a $q$-size blocking coalition for $\Pi$, it is also one for $\Pi'$, and $\Pi'[X] = \Pi[X] \cup \{\{z\}\}$. Therefore the image of a cycle of $\mathcal{D}_q(G)$ is a cycle of $\mathcal{D}_q(G')$. □

**Why $q = 4$ is the critical size.** Inequality (1) gives a simple reason why small deviations cannot cycle forever in SS-FHG, and why this argument stops working at $q = 4$. If $|X| \leq 3$, then $u_i(X) \leq 2/3$ for every $i \in X$. Hence an agent sitting in a triangle (a coalition inducing $K_3$, where every member has utility $2/3$) never takes part in a 3-size deviation. The potential of Fanelli et al. [15, Thm. 4] exploits exactly this: its first component, the number of triangle coalitions, never decreases. With $|X| = 4$, however, the centre of a star $K_{1,3}$ obtains utility $3/4 > 2/3$. A 4-size deviation can therefore break a triangle, after which the triangle may be re-created by smaller deviations. The cycle of Theorem 5 follows exactly this pattern: agent 6 leaves the triangle $\{4, 5, 6\}$ to become the centre of the star $\{1, 2, 3, 6\}$ (Table 2).

# 4 Computational experiments

## 4.1 Setup

For a graph $G$ on $n$ vertices, let $q^*(G)$ be the largest $q \leq n$ such that $G$ is $q$-size core convergent. By Lemma 4(i) and Theorem 1, $G$ is $q$-size core convergent exactly for $q \leq q^*(G)$, and $q^*(G) \geq \min\{3, n\}$. For every graph on $n \leq 10$ vertices up to isomorphism, connected or disconnected, we determined $q^*(G)$ and the maximum length of a $q^*(G)$-size core dynamics, i.e., of a longest directed path in $\mathcal{D}_{q^*(G)}(G)$. The graphs were taken from the lists of all graphs up to isomorphism, in graph6 format, provided by McKay [17].

For a fixed $q$, we construct a separate deviation graph $\mathcal{D}_q(G)$ with $B_n$ vertices for each graph $G$ (Table 1) and test its acyclicity with Kahn's topological sorting algorithm. We find $q^*(G)$ by binary search over $q \in \{3, \ldots, n\}$, and longest paths by dynamic programming over a topological order. Two observations make the computation feasible. First, the partitions, the candidate deviations $X$ and the resulting partitions $\Pi[X]$ do not depend on the graph, so they are precomputed once for each $n$. Second, for each graph we precompute $u_i(C)$ for every coalition $C$ and every $i \in C$, and test coalition by coalition whether a candidate $X$ with $|X| \leq q$ is a $q$-size blocking coalition for $\Pi$: this is the case if and only if, for every $Y \in \Pi$ with $X \cap Y \neq \emptyset$, all agents in $X \cap Y$ strictly prefer $X$ to $Y$. This condition depends only on $(X, Y)$, so it is evaluated once per graph and shared by all partitions containing $Y$. Utilities are compared in exact integer arithmetic as $\delta_i(X)\,|Y| > \delta_i(Y)\,|X|$. As a cross-check, the results for $n \leq 7$ were reproduced by an independent implementation, and the cycle reported below was recomputed in rational arithmetic. All experiments were run on several machines of the same specification, each with a 14-core Apple M4 Pro processor and 64 GB of memory. The implementation is single-threaded; we ran up to eight processes in parallel on each machine, and all reported computation times are total CPU times.

## 4.2 Results

Table 1 summarises the results. We make the following observations.

- As a sanity check, $\mathcal{D}_3(G)$ was acyclic for every graph, as predicted by Theorem 1; this also confirms the lower end of the binary search.

Table 1: Results of the experiment on all graphs (connected and disconnected) on $n$ vertices up to isomorphism: the number of graphs, the number $B_n$ of partitions (the number of vertices of each $\mathcal{D}_q(G)$), the number of graphs with each value of $q^*(G)$, the maximum length $\ell^*(n)$ of a $q^*(G)$-size core dynamics, and the computation time (total CPU time for all graphs).

| $n$ | #graphs | $B_n$ | $q^*=3$ | $q^*=4$ | $5 \le q^* < n$ | $q^*=n$ | $\ell^*(n)$ | time |
|---|---|---|---|---|---|---|---|---|
| 2 | 2 | 2 | – | – | – | 2 | 1 | < 0.01 ms |
| 3 | 4 | 5 | – | – | – | 4 | 2 | 0.011 ms |
| 4 | 11 | 15 | 0 | – | – | 11 | 4 | 0.035 ms |
| 5 | 34 | 52 | 0 | 0 | – | 34 | 6 | 0.54 ms |
| 6 | 156 | 203 | 10 | 3 | 0 | 143 | 14 | 11 ms |
| 7 | 1,044 | 877 | 239 | 182 | 0 | 623 | 24 | 0.43 s |
| 8 | 12,346 | 4,140 | 6,028 | 3,685 | 1 | 2,632 | 41 | 65 s |
| 9 | 274,668 | 21,147 | 204,092 | 58,507 | 343 | 11,726 | 59 | 4.3 h |
| 10 | 12,005,168 | 115,975 | 10,927,592 | 1,013,500 | 7,821 | 56,255 | 96 | 79 d |

- For $n \le 5$, $q^*(G) = n$ for all graphs. Hence at least six agents are needed for non-convergence, and Theorem 5 below is minimal.
- For $n = 6$, ten graphs (with 9 to 13 edges) have $q^*(G) = 3$ and three (the sparsest with 7 edges) have $q^*(G) = 4$; all of them are connected.
- Non-convergence quickly becomes typical: the fraction of graphs with $q^*(G) = 3$ is 6.4%, 22.9%, 48.8%, 74.3% and 91.0% for $n = 6, \dots, 10$.
- For $n \le 7$, $q^*(G) \in \{3, 4, n\}$; from $n = 8$ on, intermediate values occur (for $n = 10$: 974, 5,525, 1,319 and 3 graphs with $q^*(G) = 5, 6, 7, 8$). However, $q^*(G) = n - 1$ does not occur for any $n \le 10$.

## 4.3 A non-convergent instance

Among the ten six-agent instances that are not 4-size core convergent (those with $q^*(G) = 3$), the graph shown in Figure 1 has the fewest edges, and it is the only one with nine edges. It consists of a clique $K_4$ on $\{1, 4, 5, 6\}$, an agent 2 adjacent to 5 and 6, and an agent 3 adjacent only to 6:

$$E = \big\{\{1,4\},\{1,5\},\{1,6\},\{2,5\},\{2,6\},\{3,6\},\{4,5\},\{4,6\},\{5,6\}\big\}.$$

**Theorem 5.** *The instance $G^*$ of SS-FHG shown in Figure 1 is not $q$-size core convergent for any $q \ge 4$.*

*Proof.* By Lemma 4(i) it suffices to exhibit a cycle in $\mathcal{D}_4(G^*)$. Consider

$$\Pi^0 = \{\{1\},\{2\},\{3\},\{4,5,6\}\}, \qquad \Pi^1 = \Pi^0[X^1] = \{\{1,2,3,6\},\{4,5\}\},$$
$$\Pi^2 = \Pi^1[X^2] = \{\{1,2,5\},\{3,6\},\{4\}\}, \qquad \Pi^3 = \Pi^2[X^3] = \{\{1,4\},\{2,5\},\{3,6\}\},$$

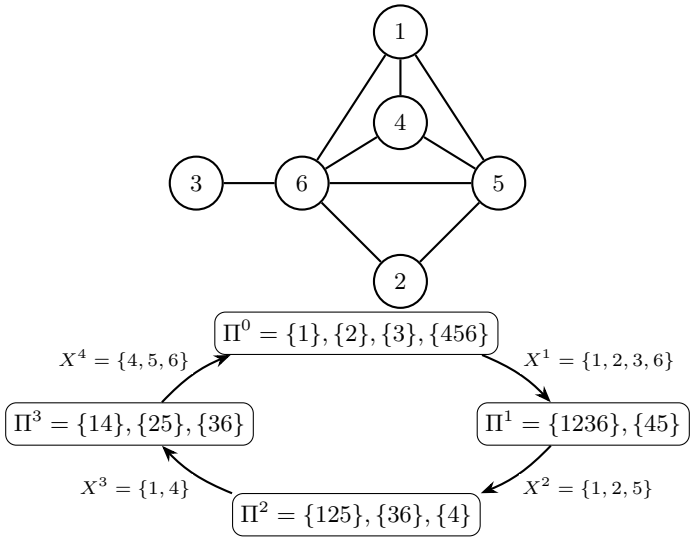



Figure 1: Left: the instance $G^*$ of SS-FHG used in Theorem 5. Right: a cycle of length four in $\mathcal{D}_4(G^*)$; coalitions are written without commas (e.g., $\{456\} = \{4,5,6\}$).

Table 2: Verification of the cycle of Theorem 5. For each deviation $X^t$, the utility $u_i(\Pi^{t-1}(i))$ of every $i \in X^t$ before the deviation and $u_i(X^t)$ after it.

| $t$ | $X^t$ | $\lvert X^t\rvert$ | agent: $u_i(\Pi^{t-1}(i)) \to u_i(X^t)$ | $G^*[X^t]$ |
|---|---|---|---|---|
| 1 | $\{1,2,3,6\}$ | 4 | 6: $\frac{2}{3} \to \frac{3}{4}$; 1, 2, 3: $0 \to \frac{1}{4}$ | star $K_{1,3}$ |
| 2 | $\{1,2,5\}$ | 3 | 5: $\frac{1}{2} \to \frac{2}{3}$; 1, 2: $\frac{1}{4} \to \frac{1}{3}$ | path $P_3$ |
| 3 | $\{1,4\}$ | 2 | 1: $\frac{1}{3} \to \frac{1}{2}$; 4: $0 \to \frac{1}{2}$ | edge $K_2$ |
| 4 | $\{4,5,6\}$ | 3 | 4, 5, 6: $\frac{1}{2} \to \frac{2}{3}$ | triangle $K_3$ |

with $X^1 = \{1,2,3,6\}$, $X^2 = \{1,2,5\}$, $X^3 = \{1,4\}$, $X^4 = \{4,5,6\}$. One checks directly that $\Pi^3[X^4] = \Pi^0$. Table 2 lists, for every deviation, the utility of each deviating agent before and after the deviation. In every row the utility increases strictly, so $X^t$ is a 4-size blocking coalition for $\Pi^{t-1}$ for $t = 1,2,3,4$ (with $\Pi^4 = \Pi^0$). Hence $\langle \Pi^0, \Pi^1, \Pi^2, \Pi^3, \Pi^0, \Pi^1, \dots \rangle$ is an infinite 4-size core dynamics. □

Combining Theorem 5, Lemma 4 and Theorem 1 yields our main conclusion.

**Corollary 6.** *For every $q \geq 4$ and every $n \geq 6$, there is an instance of SS-FHG with $n$ agents that is not $q$-size core convergent. Consequently, the largest $q$ such that every instance of SS-FHG is $q$-size core convergent is $q = 3$. In particular, core dynamics in SS-FHG need not converge, even with six agents.*

*Proof.* For $n \geq 6$, add $n-6$ isolated agents to $G^*$ and apply Lemma 4(ii) and Theorem 5.

The threshold statement follows from Theorem 1. □

# 5 $k$-improvement core dynamics

Fanelli et al. [15, Thm. 5] showed that $k$-improvement core dynamics converge for every $k \geq 2$, using the social welfare as a potential function, and asked whether they converge after a polynomial number of deviations [15, Sec. 6]. We show that, in SS-FHG, the answer is affirmative for every $k > 2$.

Let $G = (N, E)$ be an instance of SS-FHG. For $C, D \subseteq N$, let $\delta_C(D) = \sum_{i \in C} \delta_i(D)$; then $\delta_C(D) \geq 0$, $\delta_C(D)$ is additive in each argument with respect to disjoint unions, and $\delta_C(D) = \delta_D(C)$ by symmetry. The *social welfare* of a coalition $C$ is $\mathrm{sw}(C) = \sum_{i \in C} u_i(C) = \delta_C(C)/|C|$, with $\mathrm{sw}(\emptyset) = 0$, and that of a partition $\Pi$ is $\mathrm{sw}(\Pi) = \sum_{Y \in \Pi} \mathrm{sw}(Y)$. By (1), $0 \leq \mathrm{sw}(\Pi) \leq n - 1$. Moreover, if $X$ is a blocking coalition with respect to core stability for some partition (in particular, if $X$ is a $k$-improvement blocking coalition with $k \geq 1$), then every member of $X$ has a neighbour in $X$, so that $\delta_X(X) \geq |X|$ and

$$\mathrm{sw}(X) \geq 1. \tag{2}$$

**Lemma 7.** *Let $\Pi$ be a partition and $X$ a coalition. Then*

$$\mathrm{sw}(\Pi[X]) - \mathrm{sw}(\Pi) \;\geq\; \mathrm{sw}(X) - 2\sum_{i \in X} u_i(\Pi(i)).$$

*Proof.* Let $\mathcal{Y} = \{Y \in \Pi \mid Y \cap X \neq \emptyset\}$, and for $Y \in \mathcal{Y}$ let $P_Y = Y \cap X$ and $Q_Y = Y \setminus X$. Then $\Pi[X] = (\Pi \setminus \mathcal{Y}) \cup \{X\} \cup \{Q_Y \mid Y \in \mathcal{Y},\ Q_Y \neq \emptyset\}$, so

$$\mathrm{sw}(\Pi[X]) = \mathrm{sw}(\Pi) + \mathrm{sw}(X) + \sum_{Y \in \mathcal{Y}} \big(\mathrm{sw}(Q_Y) - \mathrm{sw}(Y)\big).$$

Since $\sum_{Y \in \mathcal{Y}} \delta_{P_Y}(Y)/|Y| = \sum_{i \in X} u_i(\Pi(i))$, it suffices to show $2\delta_P(Y)/|Y| + \mathrm{sw}(Q) - \mathrm{sw}(Y) \geq 0$ for every $Y \in \mathcal{Y}$, where $P = P_Y$ and $Q = Q_Y$. If $Q = \emptyset$, the left-hand side equals $\delta_Y(Y)/|Y| \geq 0$. Otherwise, by additivity and symmetry, $\delta_Y(Y) = 2\delta_P(Y) - \delta_P(P) + \delta_Q(Q)$, and the left-hand side equals $\delta_P(P)/|Y| + (1/|Q| - 1/|Y|)\,\delta_Q(Q) \geq 0$. □

For $k \geq 2$, a $k$-improvement blocking coalition $X$ for $\Pi$ satisfies $\mathrm{sw}(X) > k \sum_{i \in X} u_i(\Pi(i)) \geq 2\sum_{i \in X} u_i(\Pi(i))$, so by Lemma 7 the social welfare strictly increases, which yields the convergence result of [15, Thm. 5]; in terms of Section 3, the deviation graph for $k$-improvement blocking coalitions is acyclic by Proposition 3. For $k > 2$, combining Lemma 7 with (2) gives a linear bound.

**Theorem 8.** *Let $k > 2$ and let $G$ be an instance of SS-FHG with $n$ agents. If $X$ is a $k$-improvement blocking coalition for a partition $\Pi$, then $\mathrm{sw}(\Pi[X]) - \mathrm{sw}(\Pi) > (k-2)/k$. Consequently, every $k$-improvement core dynamics has fewer than $\frac{k}{k-2}(n-1)$ deviations.*

*Proof.* Let $U = \sum_{i \in X} u_i(\Pi(i))$. Then $kU < \mathrm{sw}(X)$, and by Lemma 7 and (2),

$$\mathrm{sw}(\Pi[X]) - \mathrm{sw}(\Pi) \;\geq\; \mathrm{sw}(X) - 2U \;>\; \Big(1 - \frac{2}{k}\Big)\mathrm{sw}(X) \;\geq\; \frac{k-2}{k}.$$

Since $0 \leq \mathrm{SW}(\Pi) \leq n-1$, a $k$-improvement core dynamics with $t \geq 1$ deviations satisfies $t\,(k-2)/k < n-1$. □

For $k = 2$, since utilities are ratios of integers, each member $i$ of a 2-improvement blocking coalition $X$ satisfies $u_i(X) - 2u_i(\Pi(i)) \geq 1/(|X|\,n)$, so the social welfare increases by at least $1/n$ and every 2-improvement core dynamics has at most $n(n-1)$ deviations. Whether this $O(n^2)$ bound can be improved remains open.

# 6 Conclusion

We have shown that $q$-size core dynamics in SS-FHG are not guaranteed to converge for any $q \geq 4$. Together with the result of Fanelli, Monaco and Moscardelli for $q \leq 3$, this determines the exact convergence threshold $q = 3$, answering part (iii) of their open problem for SS-FHG. The witness was obtained by a computational approach—an exhaustive search of deviation graphs—and can be verified by hand. We believe that such computational approaches complement mathematical arguments for questions on dynamics in hedonic games, where counterexamples are hard to construct by hand. On the positive side, $k$-improvement core dynamics have fewer than $\frac{k}{k-2}(n-1)$ deviations for every $k > 2$. Moreover, a slight refinement of the potential argument of [15, Thm. 4] shows that every 3-size core dynamics has at most $\lfloor 10n/3 \rfloor$ deviations, consistent with their experiments; this result, together with exhaustive computations of the maximum length of 3-size core dynamics, will be presented in a full version of this paper.

Several questions remain open. First, the other parts of the open problem of [15] remain unresolved for SS-FHG: the largest $q$ for which $q$-size core stable outcomes are guaranteed to exist (they exist for $q \leq 3$ [15, Thm. 4], but not necessarily for $q \geq 11$ [15, Sec. 6], based on the 40-agent instance of SS-FHG with an empty core [1, Thm. 4.1]) and can be computed efficiently. Second, it is open whether 4-size core dynamics in SS-FHG are *weakly acyclic*, i.e., whether from every partition some dynamics reaches a stable outcome. Third, whether the $O(n^2)$ bound for 2-improvement core dynamics can be improved remains open. Finally, it would be interesting to characterise the graphs whose deviation graph contains a cycle, and to exploit the structure of the deviation graph to search larger instances without enumerating all $B_n$ partitions.

# References

[1] Haris Aziz, Florian Brandl, Felix Brandt, Paul Harrenstein, Martin Olsen, and Dominik Peters. Fractional hedonic games. *ACM Transactions on Economics and Computation*, 7(2):6:1–6:29, 2019.

[2] Haris Aziz, Serge Gaspers, Joachim Gudmundsson, Julián Mestre, and Hanjo Täubig. Welfare maximization in fractional hedonic games. In *Proceedings of the 24th International Joint Conference on Artificial Intelligence (IJCAI)*, pages 461–467, 2015.

[3] Haris Aziz and Rahul Savani. Hedonic games. In *Handbook of Computational Social Choice*, pages 356–376. Cambridge University Press, 2016.

[4] Suryapratim Banerjee, Hideo Konishi, and Tayfun Sönmez. Core in a simple coalition formation game. *Social Choice and Welfare*, 18(1):135–153, 2001.

[5] Vittorio Bilò, Angelo Fanelli, Michele Flammini, Gianpiero Monaco, and Luca Moscardelli. Nash stable outcomes in fractional hedonic games: existence, efficiency and computation. *Journal of Artificial Intelligence Research*, 62:315–371, 2018.

[6] Anna Bogomolnaia and Matthew O. Jackson. The stability of hedonic coalition structures. *Games and Economic Behavior*, 38(2):201–230, 2002.

[7] Florian Brandl, Felix Brandt, and Martin Strobel. Fractional hedonic games: individual and group stability. In *Proceedings of the 14th International Conference on Autonomous Agents and Multiagent Systems (AAMAS)*, pages 1219–1227, 2015.

[8] Felix Brandt, Martin Bullinger, and Leo Tappe. Stability based on single-agent deviations in additively separable hedonic games. *Artificial Intelligence*, 334:104160, 2024.

[9] Felix Brandt, Martin Bullinger, and Anaëlle Wilczynski. Reaching individually stable coalition structures in hedonic games. In *Proceedings of the 35th AAAI Conference on Artificial Intelligence (AAAI)*, pages 5211–5218, 2021.

[10] Felix Brandt and Christian Geist. Finding strategyproof social choice functions via SAT solving. *Journal of Artificial Intelligence Research*, 55:565–602, 2016.

[11] Raffaello Carosi, Gianpiero Monaco, and Luca Moscardelli. Local core stability in simple symmetric fractional hedonic games. In *Proceedings of the 18th International Conference on Autonomous Agents and MultiAgent Systems (AAMAS)*, pages 574–582, 2019.

[12] Tom Demeulemeester and Jannik Peters. Relaxed core stability for hedonic games with size-dependent utilities. In *Proceedings of the 48th International Symposium on Mathematical Foundations of Computer Science (MFCS)*, volume 272 of *LIPIcs*, pages 41:1–41:14, 2023.

[13] Jacques H. Drèze and Joseph Greenberg. Hedonic coalitions: optimality and stability. *Econometrica*, 48(4):987–1003, 1980.

[14] Angelo Fanelli, Gianpiero Monaco, and Luca Moscardelli. Relaxed core stability in fractional hedonic games. In *Proceedings of the 30th International Joint Conference on Artificial Intelligence (IJCAI)*, pages 182–188, 2021.

[15] Angelo Fanelli, Gianpiero Monaco, and Luca Moscardelli. Relaxed core stability in hedonic games. *Artificial Intelligence*, 348:104394, 2025.

[16] Christian Geist and Ulle Endriss. Automated search for impossibility theorems in social choice theory: ranking sets of objects. *Journal of Artificial Intelligence Research*, 40:143–174, 2011.

[17] Brendan D. McKay. Combinatorial Data: Graphs. `https://users.cecs.anu.edu.au/~bdm/data/graphs.html`. Accessed April 2026.

[18] Shao Chin Sung and Dinko Dimitrov. On myopic stability concepts for hedonic games. *Theory and Decision*, 62(1):31–45, 2007.

[19] Pingzhong Tang and Fangzhen Lin. Computer-aided proofs of Arrow's and other impossibility theorems. *Artificial Intelligence*, 173:1041–1053, 2009.

# Minimizing the Number of Late Jobs with Non-Renewable Resources

**Xiaowen Zhao** and **Shao-Chin Sung***

Department of Industrial and Systems Engineering
Aoyama Gakuin University
zhao@ise.aoyama.ac.jp, son@ise.aoyama.ac.jp

**Abstract**

We study single-machine scheduling with a non-renewable resource that is supplied at known dates and consumed by each job when it starts, with the objective of minimizing the number of late jobs, denoted by $1|rm = 1|\sum U_j$. If the whole resource is available at time zero, the problem is solved by the Moore–Hodgson algorithm, but the due-date property on which this algorithm relies fails as soon as the resource arrives in two portions. The problem is known to be strongly NP-hard when the number of supply dates is part of the input, and it is NP-hard already for two supply dates by a classical result for the makespan. We show that it can nevertheless be solved in pseudo-polynomial time for any fixed number of supply dates, which completes the complexity classification with respect to this number. We further prove that the due-date rule can be imposed within each phase of the resource supply, and we use this property in an exact branch-and-bound algorithm. Computational experiments show that the algorithm efficiently obtains optimal schedules for a wide range of test instances.

**Keywords:** single-machine scheduling; non-renewable resources; number of late jobs; pseudo-polynomial algorithm; branch-and-bound

## 1 Introduction

In many production and project environments, a job cannot be started merely because the machine is idle: it also needs a certain amount of a consumable input, such as raw material, purchased components, energy, or money. Such inputs are typically not available in full at the beginning of the planning horizon but are delivered at known dates in known quantities, and every job uses up its share at the moment it starts. Scheduling under these *non-renewable resource* constraints was introduced by Carlier and Rinnooy Kan [3] and

*Shao-Chin Sung is currently known as So Akiyama.

Carlier [2], and problems of this kind are also called financial scheduling problems when the resource is a budget [4].

Most of the literature on single-machine scheduling with a non-renewable resource concerns the makespan [2, 16, 7, 8] and the total weighted completion time [9, 1]. In particular, minimizing the makespan is NP-hard already for two supply dates [2] and admits a pseudo-polynomial time algorithm for a constant number of supply dates [8]. Minimizing the number of late jobs is a classical objective: $1||\sum U_j$ is solved by the Moore–Hodgson algorithm [14] in $O(n \log n)$ time [15], while the weighted version [10, 12] and the version with release dates [13, 11] are NP-hard. With a non-renewable resource, the problem is strongly NP-hard when the number of supply dates is part of the input [4], and NP-hardness for two supply dates follows from [2] by introducing a common due date. To the best of our knowledge, it has not been known whether the problem can be solved in pseudo-polynomial time for a fixed number of supply dates, and exact solution methods have not been studied.

In this paper, we consider the single-machine problem with one non-renewable resource and the objective of minimizing the number of late jobs, denoted by $1|rm = 1|\sum U_j$. A natural starting point is the Moore–Hodgson algorithm, which applies to the special case in which the whole resource is available at time zero. Its correctness rests on the fact that a set of jobs can be completed on time if and only if this is the case under the due-date rule. We show that this fact fails as soon as the resource arrives in two portions: a job with an earlier due date may have to wait for a delivery, while a job with a later due date could have used the waiting time. Thus, the interplay between due dates and the cumulative resource supply makes the problem substantially different from its classical counterpart. Our contributions are as follows.

- We show that there is always an optimal schedule in which the on-time jobs precede the late ones, and we give an instance in which the due-date rule fails for the on-time jobs (Section 2).
- We show that the problem can be solved in pseudo-polynomial time for every fixed number $q$ of supply dates (Section 3). We first present a dynamic programming algorithm for $q = 2$ and then extend it to any fixed $q$; it assigns the on-time jobs to blocks associated with the supply dates, in the spirit of the algorithm of Györgyi and Kis [8] for the makespan. Together with the NP-hardness for $q = 2$, which follows from [2], and the strong NP-hardness when $q$ is part of the input [4], this yields a complete classification of the complexity with respect to $q$.
- We prove a dominance property stating that the due-date rule can be imposed within each phase, i.e., among the jobs that use the stock available after a resource arrival, and we use it, together with ideas from the Moore–Hodgson algorithm, in an exact branch-and-bound algorithm (Section 4). Computational experiments on instances with up to 30 jobs and up to 45 supply dates show that the algorithm solves each instance in less than 2 milliseconds on average, and that its running time depends only weakly on the number of supply dates (Section 5).

## 2 Problem Definition

An instance of the problem consists of $n$ jobs, indexed by $J = [n] = \{1, \dots, n\}$, and a single non-renewable resource. For each job $j \in J$, three non-negative integers are specified: its *processing time* $p_j$, its *due date* $d_j$, and its *resource requirement* $a_j$. The resource is not available all at once; instead, it is replenished at $q$ known *supply dates* $t_1 < t_2 < \cdots < t_q$, where $b_i$ units become available at $t_i$ for $i = 1, \dots, q$. Without loss of generality, we let $t_1 = 0$ and assume $\sum_{i=1}^{q} b_i = \sum_{j \in J} a_j$; that is, the resource supplied over the whole horizon exactly covers the total demand. Being non-renewable, the resource is used up by the job that takes it, while any amount not yet taken remains available for later jobs.

A single machine processes the jobs one at a time, and no job may be interrupted once started. Starting job $j$ removes $a_j$ units from the current stock, so job $j$ may start at time $t$ only if the total amount supplied up to $t$, minus the total amount taken by the jobs started before $j$, is at least $a_j$.

A *schedule* is a permutation $\sigma = (\sigma(1), \sigma(2), \dots, \sigma(n))$ of $[n]$, where $\sigma(k)$ is the job in the $k$th position on the machine. Following [1], we identify a permutation with the schedule in which every job is started as early as possible, i.e., as soon as the machine is free and enough resource is in stock; delaying a job beyond this time can never reduce the number of late jobs. The start time $S_j^\sigma$ and the *completion time* $C_j^\sigma$ of every job are then fixed by $\sigma$ and the supply data. Explicitly, setting $C_{\sigma(0)}^\sigma := 0$, we have

$$S_{\sigma(k)}^\sigma = \max\Big\{ C_{\sigma(k-1)}^\sigma,\ \min\Big\{ t_i : \sum_{l=1}^{i} b_l \geq \sum_{h=1}^{k} a_{\sigma(h)} \Big\} \Big\}, \tag{1}$$

$$C_{\sigma(k)}^\sigma = S_{\sigma(k)}^\sigma + p_{\sigma(k)}, \qquad k = 1, \dots, n. \tag{2}$$

The inner minimum in (1) is the earliest resource arrival time at which the cumulative supply covers the cumulative requirement of the first $k$ jobs; it is well defined because $\sum_{i=1}^{q} b_i = \sum_{j \in J} a_j$. Where no confusion can arise, the superscript $\sigma$ is omitted.

**Late jobs.** A job $j$ is *late* in schedule $\sigma$ if it is completed after its due date, i.e., $C_j^\sigma > d_j$; otherwise, it is *on time*. We write

$$U_j^\sigma = \begin{cases} 1 & \text{if } C_j^\sigma > d_j \quad (\text{job } j \text{ is late}), \\ 0 & \text{if } C_j^\sigma \leq d_j \quad (\text{job } j \text{ is on time}). \end{cases}$$

Note that a late job is not rejected: it must still be processed and must still consume its resource requirement; it merely counts as a unit penalty in the objective. The goal is to find a schedule $\sigma$ minimizing the number of late jobs $\sum_{j \in J} U_j^\sigma$.

**Notation.** Following the three-field classification of Graham et al. [6], together with the field $rm = r$ introduced by Grigoriev et al. [7] to indicate $r$ types of non-renewable resources ("raw materials"), we denote our problem by $1|rm = 1|\sum U_j$. Recall that $q$

is the number of supply dates, i.e., the number of times the resource is replenished. If $q = 1$, the resource is delivered only once, at $t_1 = 0$, so the whole supply is in stock from the beginning and the resource never delays any job. In this case, we recover the classical problem $1||\sum U_j$, which is solvable efficiently: the Moore–Hodgson algorithm [14] finds an optimal schedule, and it can be implemented to run in $O(n \log n)$ time [15, Section 3.3]. In contrast, the case $q \geq 2$ is the subject of this paper.

**On-time jobs first.**

**Lemma 1.** *For every instance of* $1|rm = 1|\sum U_j$*, there exists an optimal schedule in which all on-time jobs precede all late jobs.*

Indeed, if the late jobs of an optimal schedule are moved to the end while the on-time jobs keep their relative order, then no on-time job is delayed, since each of them faces no more preceding resource demand than before and finds the machine free no later than before, and the moved jobs can still be processed because the total supply equals the total requirement.

By Lemma 1, the order of the late jobs is irrelevant, and $1|rm = 1|\sum U_j$ can be restated as the problem of finding a maximum-cardinality subset $E \subseteq J$ of jobs that can be sequenced so that every job in $E$ is completed on time, where the jobs of $E$ are scheduled first and only the resource supply $b_1, \ldots, b_q$ is taken into account.

**The due-date rule.** In the classical setting, Moore [14, Lemma 2] further showed, by a lemma of Jackson, that the on-time jobs can be reordered according to the due-date rule (i.e., in non-decreasing order of due dates) without making any of them late. Thus, for $1||\sum U_j$, a set of jobs can be completed on time if and only if no job is late when they are sequenced by the due-date rule. This property does not carry over to $1|rm = 1|\sum U_j$. Note that any counterexample must have $q \geq 2$, since for $q = 1$ the problem coincides with the one treated in [14], and clearly $n \geq 2$.

**Example 1.** Let $q = 2$ with $(t_1, b_1) = (0, 1)$ and $(t_2, b_2) = (2, 2)$, and let $n = 2$ with

$$p_1 = 2,\ d_1 = 4,\ a_1 = 2, \qquad p_2 = 2,\ d_2 = 5,\ a_2 = 1.$$

The due-date rule gives the schedule $(1, 2)$. Job 1 requires two units of the resource, which are not available until $t_2 = 2$; hence $S_1 = 2$ and $C_1 = 4 \leq d_1$. Job 2 then starts at $S_2 = 4$ and completes at $C_2 = 6 > d_2$, so it is late. In contrast, in the schedule $(2, 1)$, job 2 starts at time 0 using the unit arriving at $t_1$ and completes at $C_2 = 2 \leq d_2$, and job 1 starts at $S_1 = \max\{2, t_2\} = 2$ and completes at $C_1 = 4 \leq d_1$. Thus both jobs are on time in $(2, 1)$, whereas the due-date rule yields one late job; see Figure 1.

Example 1 shows that, under non-renewable resource constraints, even deciding the order of a given set of on-time jobs is no longer straightforward, since a job with an earlier due date may have to wait for a resource arrival while another job could use the waiting time.

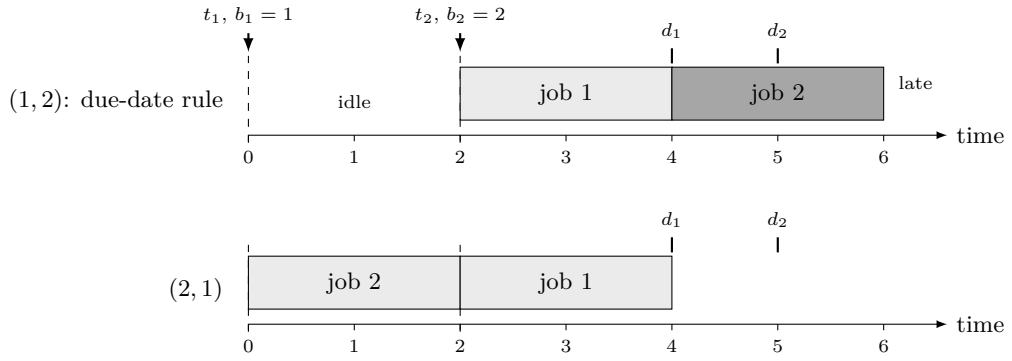



Figure 1: The two schedules of Example 1. Dashed lines mark the resource arrivals $t_1 = 0$ and $t_2 = 2$, and the ticks above each row mark the due dates $d_1 = 4$ and $d_2 = 5$. Under the due-date rule (top), job 1 must wait for the second arrival, and job 2 (shaded) completes late at time 6. In the schedule $(2, 1)$ (bottom), job 2 uses the waiting time, and both jobs are on time.

# 3 Pseudo-Polynomial Time Algorithms

In this section, we show that $1|rm = 1|\sum U_j$ can be solved in pseudo-polynomial time for every fixed number $q$ of supply dates. We first recall the known hardness results that motivate this question.

## 3.1 Known hardness results

We consider the decision version of $1|rm = 1|\sum U_j$: given an instance and an integer $K$, is there a schedule with at most $K$ late jobs? It belongs to NP, since a permutation can serve as a certificate and the start and completion times can be computed by (1) and (2) in polynomial time. When the number of supply dates is part of the input, the problem is strongly NP-hard.

**Theorem 1** (Gafarov et al. [4])**.** *$1|rm = 1|\sum U_j$ is NP-hard in the strong sense if the number $q$ of resource arrivals is part of the input.*

This was shown in [4, Theorem 1] by a reduction from 3-Partition, which is NP-complete in the strong sense [5]; the number of resource arrivals in the constructed instance equals the number of triples and thus grows with the input. We describe this construction for a general number $m$ of resource arrivals, as its special case $m = 2$ also yields NP-hardness for two supply dates. Let $m \geq 2$ and let $s_1, \ldots, s_n$ be positive integers with $\sum_{j=1}^{n} s_j = mB$. We define the instance $I(s; m)$ of $1|rm = 1|\sum U_j$ as follows: the job set is $J = [n]$ with

$$p_j = s_j, \qquad a_j = s_j, \qquad d_j = mB \qquad (j \in J),$$

and there are $q = m$ resource arrivals with $(t_i, b_i) = ((i-1)B,\ B)$ for $i = 1, \ldots, m$. Thus, each job consumes as many units of the resource as its processing time, all jobs share the due date $mB$, and $B$ units arrive every $B$ time units. Clearly, $\sum_{i=1}^{m} b_i = mB = \sum_{j \in J} a_j$. For an instance of 3-PARTITION with $m$ triples, $I(s; m)$ is the instance constructed in [4].

**Lemma 2.** *In $I(s; m)$, there is a schedule without late jobs if and only if $J$ can be partitioned into $m$ sets $S_1, \ldots, S_m$ with $\sum_{j \in S_i} s_j = B$ for $i = 1, \ldots, m$.*

*Proof sketch.* If such a partition exists, processing $S_1, S_2, \ldots, S_m$ in this order fills $[0, mB]$ without idle time, since the jobs of $S_i$ need only the units supplied up to $t_i = (i-1)B$. Conversely, in a schedule without late jobs, the machine is busy throughout $[0, mB]$. The jobs that start before $iB$ require at most $iB$ units, so their total processing time is at most $iB$; since there is no idle time, it is exactly $iB$. Hence every multiple of $B$ is a job boundary, which yields the desired partition. □

For two supply dates, the following NP-hardness result is essentially known: Carlier [2] showed that minimizing the makespan is NP-hard for $q = 2$ (see also [8, Lemma 1]), and adding a common due date turns the makespan question into the question of whether all jobs can be on time. For completeness, we give a short proof based on Lemma 2 and the following problem, which is NP-complete [5].

**Partition:** Given positive integers $s_1, \ldots, s_n$ with $\sum_{j=1}^{n} s_j = 2B$, is there a subset $S \subseteq [n]$ with $\sum_{j \in S} s_j = B$?

**Proposition 1** (cf. [2])**.** *$1|rm = 1|\sum U_j$ is NP-hard even if $q = 2$.*

*Proof.* Given an instance $s_1, \ldots, s_n$ of PARTITION with $\sum_j s_j = 2B$, construct $I(s; 2)$, i.e., $p_j = a_j = s_j$ and $d_j = 2B$ for $j \in [n]$, and $(t_1, b_1) = (0, B)$, $(t_2, b_2) = (B, B)$. By Lemma 2, $I(s; 2)$ admits a schedule without late jobs if and only if the PARTITION instance is a yes-instance. □

Recall that the problem is solvable in $O(n \log n)$ time if $q = 1$; thus, a single additional resource arrival already makes the problem intractable. However, the known results leave open whether the problem with $q = 2$ is NP-hard in the ordinary sense or in the strong sense: Proposition 1 relies on PARTITION, which is solvable in pseudo-polynomial time, whereas Theorem 1 requires the number of resource arrivals to grow with the input. The same question arises for every fixed $q \geq 2$. We answer it by giving pseudo-polynomial time algorithms, first for $q = 2$ in Section 3.2 and then for any fixed $q$ in Section 3.3.

## 3.2 Two supply dates

**Theorem 2.** *If $q = 2$, then $1|rm = 1|\sum U_j$ can be solved in $O(nP^3 b_1)$ time, where $P = \sum_{j \in J} p_j$.*

*Proof sketch.* By Lemma 1, there is an optimal schedule in which the set $E$ of on-time jobs comes first. Let $X \subseteq E$ consist of the jobs whose cumulative requirement is at most $b_1$, and let $Y = E \setminus X$. The jobs of $X$ are processed without idle time from time 0, and those

of $Y$ without idle time from $T = \max\{p(X), t_2\}$, where $p(X) = \sum_{j\in X} p_j$; by Jackson's lemma (see [14]), each block may be assumed to be in non-decreasing order of due dates. Conversely, any disjoint $X$, $Y$ with $a(X) \le b_1$ and any $T \ge \max\{p(X), t_2\}$ such that no job is late when $X$ is sequenced from 0 and $Y$ from $T$ in this order give a schedule with at least $|X| + |Y|$ on-time jobs. The algorithm enumerates $T \in \{t_2, \ldots, \max\{t_2, P\}\}$, scans the jobs in non-decreasing order of due dates, and stores for every state $(p(X), a(X), p(Y))$ the maximum of $|X| + |Y|$; job $j$ is declared late, appended to $X$ if $p(X) + p_j \le d_j$ and $a(X) + a_j \le b_1$, or appended to $Y$ if $T + p(Y) + p_j \le d_j$. This gives $O(P)$ values of $T$, $n$ steps, and $O(P^2 b_1)$ states. □

### 3.3 A fixed number of supply dates

The approach of Theorem 2 extends from two blocks to any fixed number of blocks.

**Theorem 3.** *For every fixed $q$, $1|rm = 1|\sum U_j$ can be solved in time polynomial in $n$, $P = \sum_{j\in J} p_j$, and $\bar{A} = \sum_{j\in J} a_j$.*

*Proof sketch.* We generalize the proof of Theorem 2 from two blocks to $q$ blocks. In an optimal schedule with the on-time jobs first, let $X_i$ consist of the on-time jobs whose cumulative requirement exceeds $B_{i-1} = \sum_{l<i} b_l$ but not $B_i$. Then $X_1, \ldots, X_q$ form consecutive blocks, and $X_i$ is processed without idle time from $T_i = \max\{T_{i-1} + p(X_{i-1}), t_i\}$, with $T_1 = 0$. The algorithm enumerates $T_2, \ldots, T_q$ among the $O(qP)$ values $t_i$ and $t_l + v$ ($l < i$, $0 \le v \le P$), and runs the dynamic program of Theorem 2 with states $(x_1, \ldots, x_q, \alpha_1, \ldots, \alpha_q)$, where $x_i$ and $\alpha_i$ are the total processing time and total requirement of the jobs assigned to block $i$. This gives the running time $O\big((qP)^{q-1} \cdot nq \cdot (P+1)^q(\bar{A}+1)^q\big)$. Details are given in the full version of this paper. □

Together with Proposition 1 and Theorem 1, Theorem 3 completes the complexity classification of $1|rm = 1|\sum U_j$ with respect to the number $q$ of supply dates: the problem is solvable in $O(n \log n)$ time for $q = 1$, NP-hard in the ordinary sense for every fixed $q \ge 2$, and NP-hard in the strong sense if $q$ is part of the input.

## 4 Branch-and-Bound Algorithm

In this section, we first establish a dominance property and then describe our branch-and-bound algorithm, which builds schedules job by job and uses this property together with a simple exclusion rule to discard unnecessary nodes.

### 4.1 Dominance within phases

By Lemma 1, we restrict attention to schedules in which all on-time jobs precede all late jobs. For $i = 1, \ldots, q$, let $B_i = \sum_{l=1}^{i} b_l$ be the cumulative supply up to $t_i$, and for a schedule $\sigma$ and $k \in [n]$, let $A_k^\sigma = \sum_{h=1}^{k} a_{\sigma(h)}$ be the cumulative requirement of the first $k$ jobs. We define the *ith phase* of $\sigma$ as the set

$$G_i^\sigma = \big\{\, \sigma(k) : S_{\sigma(k)}^\sigma \ge t_i \text{ and } A_k^\sigma \le B_i \,\big\}.$$

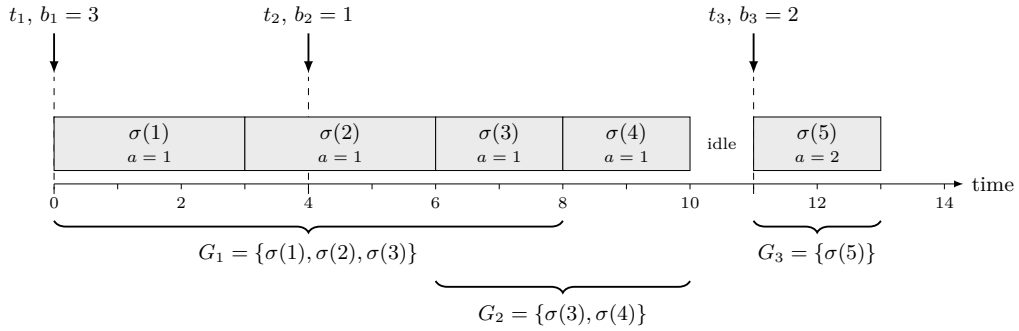



Figure 2: Phases of a schedule with $q = 3$ resource arrivals, where $B_1 = 3$, $B_2 = 4$, and $B_3 = 6$. The stock available at $t_1 = 0$ is used up only by $\sigma(3)$, which starts at time $6 > t_2$, so $G_1$ extends beyond $t_2$, and $\sigma(3)$ belongs to both $G_1$ and $G_2$. Job $\sigma(5)$ needs the units arriving at $t_3$ and has to wait. By Lemma 3, the on-time jobs within each phase may be assumed to follow the due-date rule.

In words, at time $t_i$, the jobs started before $t_i$ have consumed their requirements, and what is left in stock (possibly nothing) together with the newly arrived $b_i$ units is available for the jobs that follow; $G_i^\sigma$ consists of the jobs started from $t_i$ onwards until this stock is used up. Since $A_k^\sigma$ is non-decreasing and $S_{\sigma(k)}^\sigma$ is non-decreasing in $k$, each phase occupies consecutive positions of $\sigma$. Every job started in $[t_i, t_{i+1})$ belongs to $G_i^\sigma$, but a phase may extend beyond $t_{i+1}$ if the stock available at $t_i$ is not used up by then; consequently, consecutive phases may overlap; see Figure 2 for an example. The following lemma shows that the due-date rule can be imposed within each phase.

**Lemma 3.** *For every instance of* $1|rm = 1|\sum U_j$*, there exists an optimal schedule* $\sigma$ *in which all on-time jobs precede all late jobs and, for each* $i = 1, \ldots, q$*, the on-time jobs in* $G_i^\sigma$ *are sequenced in non-decreasing order of due dates.*

*Proof sketch.* Take an optimal schedule of the form in Lemma 1 that minimizes the number of pairs of on-time jobs violating the due-date rule. If some phase $G_i^\sigma$ contains such a pair, then, as phases occupy consecutive positions, it contains two consecutive on-time jobs $j = \sigma(m)$ and $k = \sigma(m + 1)$ with $d_j > d_k$. Since $k \in G_i^\sigma$, the resource needed by both jobs is available at $t_i \leq S_j^\sigma$. Interchanging $j$ and $k$ therefore lets $k$ complete by $S_j^\sigma + p_k \leq C_k^\sigma \leq d_k$ and $j$ by $C_k^\sigma \leq d_k < d_j$, while no other job is delayed. This yields an optimal schedule with fewer violating pairs, a contradiction. □

The start times and cumulative requirements of the jobs in a partial schedule, i.e., a prefix of a schedule, do not depend on how the schedule is completed, and hence neither does the membership of these jobs in the phases. Consequently, Lemma 3 yields the following pruning rule: if a partial schedule contains two on-time jobs in the same phase in an order that violates the due-date rule, then the corresponding node of the search tree can be discarded. In particular, this applies to on-time jobs started between two

consecutive resource arrivals, and it applies to a longer stretch of the schedule whenever the stock available at a resource arrival lasts beyond the next arrival. For $q = 1$, the only phase contains all jobs, and Lemma 3 reduces to the due-date property underlying the Moore–Hodgson algorithm. Example 1 is consistent with Lemma 3: in the schedule $(2, 1)$, job 2 belongs only to $G_1$ and job 1 only to $G_2$.

## 4.2 The algorithm

For $x \geq 0$, let $\tau(x) = \min\{t_i : B_i \geq x\}$ denote the earliest resource arrival at which the cumulative supply reaches $x$. By (1), if a job $j$ is appended to a partial schedule whose last job completes at time $C$ and whose jobs require $A$ units in total, then $j$ starts at

$$e_j = \max\{C,\ \tau(A + a_j)\}. \tag{3}$$

**Search tree.** By Lemma 1, it suffices to construct the sequence of on-time jobs; the late jobs can be appended at the end in any order. Each node of the search tree corresponds to a partial schedule $\pi$ consisting of on-time jobs, together with the set $R$ of jobs that are not in $\pi$ and have not yet been declared late. The root corresponds to the empty partial schedule with $R = J$. A node is branched by appending a job of $R$ to $\pi$, which creates one child per job that passes the tests below. The tree is explored by depth-first search, and the jobs of $R$ are tried in non-decreasing order of their *latest start times* $\ell_j = d_j - p_j$.

**Jobs bound to be late.** Let $C$ denote the completion time of the last job of $\pi$ ($C = 0$ if $\pi$ is empty). In any schedule extending $\pi$, a job $j \in R$ cannot start before $C$; hence, if $\ell_j < C$, then $j$ is late in every such schedule. These jobs are declared late and removed from $R$. Since $C$ does not decrease along a path of the search tree, they remain late at all descendants, and since the jobs are kept in non-decreasing order of $\ell_j$, they can be found at the beginning of this order. Moreover, a job $k \in R$ is not appended to $\pi$ if $e_k + p_k > d_k$, i.e., if it would be late even when started as early as possible; by (3), this test also takes the resource supply into account. Consequently, every job appended to $\pi$ starts at $e_k$ and is on time, so all partial schedules in the tree consist of on-time jobs.

**Pruning by Lemma 3.** Let $j$ be the last job of $\pi$, let $A = \sum_{h \in \pi} a_h$, and suppose that appending $k$ requires no resource arrival later than the one already needed by $j$, i.e., $\tau(A + a_k) = \tau(A) = t_i$ for some $i$. Then $A > B_{i-1}$, so $j$ starts no earlier than $t_i$, and $A + a_k \leq B_i$; hence $j$ and $k$ belong to the phase $G_i$ in the resulting partial schedule. Therefore, by Lemma 3, the child is not created if $d_j > d_k$. In words, consecutive jobs that are covered by the same resource arrival are sequenced according to the due-date rule. Note that this rule uses only a special case of Lemma 3: the lemma also applies, for instance, when $j$ was covered by an earlier arrival but could not start before $t_i$ because the machine was busy. Exploiting the lemma in full is left for future work.

**Bounding.** Let $\pi^*$ be the best partial schedule recorded so far, initially the empty one. Every leaf below a node $(\pi, R)$ is obtained by appending jobs of $R$ to $\pi$, so $|\pi| + |R|$ is

**Algorithm 1** Branch-and-bound algorithm for $1|rm = 1|\sum U_j$

**procedure** EXPLORE($\pi$, $R$)
  $j \leftarrow$ last job of $\pi$, $C \leftarrow C_j$, $A \leftarrow \sum_{h \in \pi} a_h$ ▷ $C = 0$, $d_j = -\infty$ if $\pi = ()$
  $R \leftarrow \{h \in R : C + p_h \leq d_h\}$ ▷ declare jobs with $\ell_h < C$ late
  **if** $|\pi| + |R| \leq |\pi^*|$ **then return** ▷ bounding
  **end if**
  *leaf* $\leftarrow$ **true**
  **for** each $k \in R$ in non-decreasing order of $\ell_k$ **do**
    **if** $\max\{C, \tau(A + a_k)\} + p_k > d_k$ **then continue** ▷ $k$ would be late
    **end if**
    **if** $\tau(A + a_k) = \tau(A)$ and $d_j > d_k$ **then continue** ▷ Lemma 3
    **end if**
    *leaf* $\leftarrow$ **false**; EXPLORE($\pi \oplus k$, $R \setminus \{k\}$)
  **end for**
  **if** *leaf* and $|\pi| > |\pi^*|$ **then** $\pi^* \leftarrow \pi$
  **end if**
**end procedure**

$\pi^* \leftarrow ()$; EXPLORE($()$, $J$)
**return** $\pi^*$ followed by the jobs of $J \setminus \pi^*$ in any order

an upper bound on the number of on-time jobs attainable in its subtree; equivalently, the number $n - |\pi| - |R|$ of jobs declared late so far is a lower bound on the number of late jobs. Hence, if $|\pi| + |R| \leq |\pi^*|$, the node is discarded. If no child of a node is created, the node is a leaf, and $\pi$ replaces $\pi^*$ if $|\pi| > |\pi^*|$; the corresponding schedule consists of $\pi$ followed by the remaining jobs and has $n - |\pi|$ late jobs.

No initial solution is computed in advance. Since the jobs are tried in non-decreasing order of $\ell_j$, the first leaf reached by the depth-first search corresponds to a greedy schedule, which repeatedly appends the first job in this order that can be appended, and it serves as the first incumbent. The procedure is summarized in Algorithm 1.

**Proposition 2.** *Algorithm 1 returns an optimal schedule.*

*Proof sketch.* Every recorded partial schedule yields a feasible schedule, and the bounding step discards only subtrees that cannot improve on $\pi^*$. Let $\sigma$ be an optimal schedule as in Lemma 3 with on-time set $E$. By induction on $k$, the prefix of length $k$ of its on-time part is generated: the remaining jobs of $E$ are not declared late, the next job starts at its earliest start time and is on time, and it is not pruned, since the pruning rule only concerns consecutive jobs in a common phase, which are in due-date order in $\sigma$. At the node of the whole on-time part, no child is created, since otherwise $|E| + 1$ jobs could be on time. Hence this node is recorded unless an equally good partial schedule has already been recorded. □

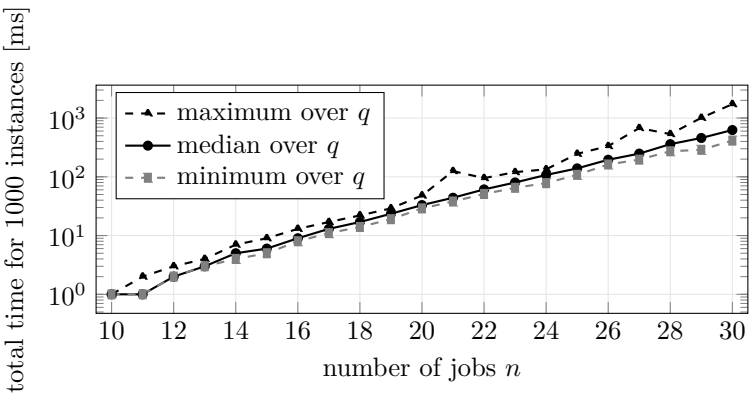



Figure 3: Total computation time of Algorithm 1 for 1000 instances per combination of $n$ and $q \in \{1, \ldots, \lfloor 3n/2 \rfloor\}$, summarized over $q$ for each $n$ (logarithmic scale).

# 5 Computational Experiments

We implemented Algorithm 1 in Rust, compiled it with `rustc` 1.99.1, and ran all experiments on a computer with an Apple M4 Max processor and 128 GB of memory.

**Instances.** For each $n \in \{3, \ldots, 30\}$ and $q \in \{1, \ldots, \lfloor 3n/2 \rfloor\}$, we generated 1000 instances with the generator `rand::thread_rng` of Rust (686 combinations in total). All values are integers drawn uniformly at random: $d_j \in [1, 500]$, $p_j \in [1, d_j]$, $a_j \in [1, 100]$, and supply dates in $[0, \max_j d_j]$, which involves no loss of generality since units arriving at $\max_j d_j$ or later cannot be used by on-time jobs. The amounts $b_i$ are drawn from $[1, \bar{A}]$ with $\bar{A} = \sum_j a_j$ and then adjusted until $\sum_i b_i = \bar{A}$ by repeatedly decreasing a random $b_i$ by a value in $[1, b_i - 1]$ or increasing it by a value in $[1, \bar{A} - \sum_i b_i]$.

**Results.** No time limit was imposed, and all instances were solved to optimality. Figure 3 shows the total time for the 1000 instances of each combination, summarized over $q$ for each $n \geq 10$ (for $n \leq 9$, at most 1 ms). Even for $n = 30$, it is 0.41 to 1.72 s, i.e., less than 2 ms per instance on average. The computation time grows exponentially with the number of jobs, as expected for an NP-hard problem: on a logarithmic scale, the median over $q$ increases almost linearly in $n$, by a factor of about 1.35 per additional job for $16 \leq n \leq 30$. In contrast, the dependence on the number of supply dates is weak. For $n \geq 16$, about 91% of the combinations lie within $\pm 30\%$ of the median for the same $n$, and $q = 2$ is not particularly difficult. For $n \geq 20$, a few combinations take up to about 2.8 times the median (e.g., $q = 35$, 36, 41 for $n = 30$), without a systematic pattern.

## Acknowledgment

The authors gratefully acknowledge the financial support provided by CAIR through its International Conference Presentation Support Program for Young Project Members (Phase II) for presenting this research at an international conference.

## References

[1] Kristóf Bérczi, Tamás Király, and Simon Omlor. Scheduling with non-renewable resources: minimizing the sum of completion times. *Journal of Scheduling*, 27:151–164, 2024.

[2] Jacques Carlier. *Problèmes d'ordonnancement à contraintes de ressources: algorithmes et complexité*. Thèse d'état, Université Paris VI – Pierre et Marie Curie, 1984.

[3] Jacques Carlier and Alexander H. G. Rinnooy Kan. Scheduling subject to nonrenewable-resource constraints. *Operations Research Letters*, 1(2):52–55, 1982.

[4] Evgeny R. Gafarov, Alexander A. Lazarev, and Frank Werner. Single machine scheduling problems with financial resource constraints: some complexity results and properties. *Mathematical Social Sciences*, 62(1):7–13, 2011.

[5] Michael R. Garey and David S. Johnson. *Computers and Intractability: A Guide to the Theory of NP-Completeness*. W. H. Freeman, San Francisco, 1979.

[6] Ronald L. Graham, Eugene L. Lawler, Jan Karel Lenstra, and Alexander H. G. Rinnooy Kan. Optimization and approximation in deterministic sequencing and scheduling: a survey. *Annals of Discrete Mathematics*, 5:287–326, 1979.

[7] Alexander Grigoriev, Martijn Holthuijsen, and Joris van de Klundert. Basic scheduling problems with raw material constraints. *Naval Research Logistics*, 52(6):527–535, 2005.

[8] Péter Györgyi and Tamás Kis. Approximation schemes for single machine scheduling with non-renewable resource constraints. *Journal of Scheduling*, 17(2):135–144, 2014.

[9] Péter Györgyi and Tamás Kis. New complexity and approximability results for minimizing the total weighted completion time on a single machine subject to non-renewable resource constraints. *Discrete Applied Mathematics*, 311:97–109, 2022.

[10] Richard M. Karp. Reducibility among combinatorial problems. In *Complexity of Computer Computations*, pages 85–103. Plenum Press, New York, 1972.

[11] Matthias Kaul, Matthias Mnich, and Hendrik Molter. Single-machine scheduling to minimize the number of tardy jobs with release dates. In *Proceedings of the 19th International Symposium on Parameterized and Exact Computation (IPEC 2024)*, LIPIcs, pages 19:1–19:15, 2024.

[12] Eugene L. Lawler and J. Michael Moore. A functional equation and its application to resource allocation and sequencing problems. *Management Science*, 16(1):77–84, 1969.

[13] Jan Karel Lenstra, Alexander H. G. Rinnooy Kan, and Peter Brucker. Complexity of machine scheduling problems. *Annals of Discrete Mathematics*, 1:343–362, 1977.

[14] J. Michael Moore. An $n$ job, one machine sequencing algorithm for minimizing the number of late jobs. *Management Science*, 15(1):102–109, 1968.

[15] Michael L. Pinedo. *Scheduling: Theory, Algorithms, and Systems*. Springer, Cham, 6th edition, 2022.

[16] Ahmet Toker, Suna Kondakci, and Nesim Erkip. Scheduling under a non-renewable resource constraint. *Journal of the Operational Research Society*, 42(9):811–814, 1991.

# List of Authors


Čepek, Ondřej, 1

Daniel, Milan, 14, 26

Hayashi, Toshitaka, 3

Innan, Shigeaki, 11
Inuiguchi, Masahiro, 11

Jiroušek, Radim, 14, 26

Kratochvíl, Václav, 14, 26
Kusunoki, Yoshifumi, 36

Mestek, Jakub, 47
Mls, Karel, 50

Sung, Shao-Chin, 65, 77

Zhao, Xiaowen, 77

26th Czech-Japan Seminar on Data Analysis and Decision Making
November 5 - 8, 2026
Nový Jičín, Czech Republic

**Editors:**
Masahiro Inuiguchi, Václav Kratochvíl, Yoshifumi Kusunoki, Karel Mls, Shao-Chin Sung

**Organized by:**
Institute for Research and Applications of Fuzzy Modeling, University of Ostrava
Faculty of Informatics and Management, University of Hradec Králové
ÚTIA - Institute of Information Theory and Automation, Czech Academy of Sciences

**Sponsors:**
Institute for Research and Applications of Fuzzy Modeling, University of Ostrava
Faculty of Informatics and Management, University of Hradec Králové
Institute of Information Theory and Automation, Czech Academy of Sciences

*ÚTIA*

ISBN: 978-80-905688-1-5